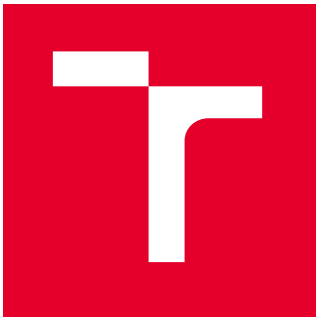

BRNO UNIVERSITY OF TECHNOLOGY

VYSOKÉ UČENÍ TECHNICKÉ V BRNĚ

FACULTY OF MECHANICAL ENGINEERING

FAKULTA STROJNÍHO INŽENÝRSTVÍ

INSTITUTE OF AUTOMOTIVE ENGINEERING

ÚSTAV AUTOMOBILNÍHO A DOPRAVNÍHO INŽENÝRSTVÍ

DESIGN OF A TORQUE VECTORING CONTROL SYSTEM FOR A FORMULA STUDENT VEHICLE

NÁVRH SYSTÉMU ŘÍZENÍ VEKTOROVÁNÍ TOČIVÉHO MOMENTU PRO VOZIDLO FORMULA STUDENT

MASTER'S THESIS

DIPLOMOVÁ PRÁCE

AUTHOR — Bc. Petr Gadas

AUTOR PRÁCE

SUPERVISOR — Ing. Jiří Míša

VEDOUCÍ PRÁCE

BRNO 2024

BRNO UNIVERSITY OF TECHNOLOGY
FACULTY OF MECHANICAL ENGINEERING

Assignment Master's Thesis

Institut:	Institute of Automotive Engineering
Student:	**Bc. Petr Gadas**
Degree programm:	Automotive and Material Handling Engineering
Branch:	no specialisation
Supervisor:	**Ing. Jiří Míša**
Academic year:	2023/24

As provided for by the Act No. 111/98 Coll. on higher education institutions and the BUT Study and Examination Regulations, the director of the Institute hereby assigns the following topic of Master's Thesis:

Design of a torque vectoring control system for a Formula student vehicle

Brief Description:

Vehicles equipped with an electric powertrain have the ability to regulate torque more smoothly at a given power and speed than vehicles with a conventional combustion engine. For this reason, this thesis was created to design a torque distribution system between the right and left wheels on the drive axle. In order to design a functional control system, advanced knowledge of vehicle dynamics and a basic understanding of the measurement chain on the vehicle is required. After defining the input parameters and creating the control system, simulations will be performed to clarify how much torque vectoring contributes to improving vehicle driving dynamics.

Master's Thesis goals:

Description of torque vectoring function.
Definition of input parameters and design of the algorithm.
Analysis and comparison of the required and available yaw moment.
Comparison of vehicles with and without torque vectoring control.

Recommended bibliography:

MILLIKEN, W. F. a D. L. MILLIKEN. Race car vehicle dynamics. Warrendale, PA, U.S.A.: SAE International, c1995. ISBN 15-609-1526-9.

GILLESPIE, T. D. Fundamentals of vehicle dynamics. Warrendale, PA: Society of Automotive Engineers, c1992. ISBN 15-609-1199-9.

RAJESH, R. Vehicle dynamics and control. 2. Boston: Springer-Verlag, 2012. ISBN 978-1-4614-1433-9.

Deadline for submission Master's Thesis is given by the Schedule of the Academic year 2023/24

In Brno,

L. S.

prof. Ing. Josef Štětina, Ph.D. Director of the Institute	doc. Ing. Jiří Hlinka, Ph.D. FME dean

ABSTRAKT

Tato diplomová práce se zabývá problematikou zvýšení výkonu vozidla při jízdě zatáčkou pomocí aktivního řízení hnacího momentu závodního vozu kategorie Formule Student. Náplní práce je návrh, simulace a následně testování algoritmu, který na základě zvolených parametrů řídí rozdělení momentu na hnané nápravě, aby bylo dosaženo optimálního stáčení vozidla pří zatáčení. Systém byl navržen na základě cíleného dynamického chování vozu při průjezdu zatáčkou. Pomocí virtuálního prostředí byly obdrženy simulační klíčové výsledky vlivu na chování vozidla, které byly následně validovány testováním na trati. Celkovým cílem práce bylo navýšení jízdní rychlosti a kontroly and vozidlem během zatáčení, s výsledkem snížení jízdního času na trati.

KLÍČOVÁ SLOVA

Formule Student, stáčivý pohyb, stáčivá rychlost, kontrola, vektorování točivého momentu, výkon, zatáčení, rozdělení točivého momentu

ABSTRACT

This master’s thesis deals with the challenges of increasing vehicle performance during cornering by implementing an active torque distribution system into a Formula Student racing vehicle. This paper will touch upon the design, simulation, and further testing of the algorithm which, based on selected parameters, distributes the driving torque on the driven axle in order to achieve optimal cornering performance. This system was designed based on targeted dynamic behaviour of a car when driving through a corner. Key results were obtained from simulating the system in a virtual environment and were further validated during physical track testing. The overall aim was to increase vehicle cornering performance and control in order to reduce lap time.

KEYWORDS

Formula Student, yawing motion, yaw rate, control, torque vectoring, performance, cornering, torque distribution

BIBLIOGRAPHIC CITATION

GADAS, Petr. *Návrh systému řízení vektorování točivého momentu pro vozidlo Formula student* [online]. Brno, 2024 [cit. 2024-05-24]. Dostupné z: https://www.vut.cz/studenti/zav-prace/detail/154026. Diplomová práce. Vysoké učení technické v Brně, Fakulta strojního inženýrství, Ústav automobilního a dopravního inženýrství. Vedoucí práce Jiří Míša.

DECLARATION

I declare this master's thesis to be my own work, I have elaborated this thesis independently under the supervision of Ing. Jiří Míša with the use of listed sources.

In Brno, May 24th, 2024 ……..……..……..

Bc. Petr Gadas

ACKNOWLEDGEMENT

I would like to express my deepest gratitude to my supervisor Ing Jiří Míša for his professional advice and guidance during the creation of this thesis, as well as his unending will in aiding me to accomplish this work. My deepest appreciation extends to the members of the Formula Student team TU Brno Racing, who gave me the opportunity to be one of their own and without whom this thesis would not exist. Finally, I would like to give my very special thanks to my girlfriend, my closest friends and my family, who supported me throughout my years of studying while taking part in Formula Student.

TABLE OF CONTENTS

INTRODUCTION

The increasing demand of electric vehicles provides the opportunity to develop new technologies. The availability of electric motors suited for propelling road and racing vehicles creates the option of powering each driven wheel separately, bringing new ways of improving the safety, handling and track performance. By implementing various control systems, which aid in different driving tasks it is possible to achieve a more reliable stable, and faster vehicle response and enable the driver to use the vehicle to its full potential.

The concept of creating a different behaviour at the driven wheels during cornering is not new. However, it is the electric vehicle structure that opens up the opportunity of introducing an active control algorithm. Torque vectoring is a control system which, in accordance with the chosen target behaviour, actively distributes different torques to the driven wheels to achieve the targeted vehicle response. In the case of road vehicles, road safety, ride comfort and control would be the top priorities. However, when considering race cars, the main objective would be improving the vehicle's responsivity to driver commands and the driver's control over the vehicle behaviour.

This thesis covers the design, simulation, and testing procedure of a newly developed torque vectoring algorithm for the 4th electric single seater made by members of the TU Brno Racing team, the Dragon e4.

The aim of this thesis is to design a control system focused on increasing the vehicle performance on track. As racetracks at Formula Student competitions are made mostly out of corners, control over cornering should bring the highest improvement in performance. A study of cornering behaviour and steering response is done at both transient and steady states of driving, in order to understand the key characteristics defining the optimal process of driving through each segment of a corner.

Based on the defined ideal vehicle behaviour, an algorithm in MATLAB Simulink has been designed. It compares the current and target vehicle characteristics and distributes the wheel torques accordingly to correct any error between those variables. The whole system underwent a large amount of simulation cycles in a virtual driving environment, in which the theoretical system and vehicle behaviour were analysed and tuned to achieve better cornering speeds, shorter lap times, and exploit the car to its maximum potential.

After achieving desired results from the simulation, the system was implemented in the latest single-seater and tested on a custom track, where the collected data together with the driver's feedback dictated several changes that needed to be done to make the car perform at the top of its capabilities.

1 FORMULA STUDENT

1.1 THE FORMULA STUDENT COMPETITION

Formula Student is a worldwide competition between university students, which challenges them to design, build, validate, and then race with a formula-type car. The purpose of the competition is to take an extra step in education and get hands on experience in engineering, through designing and manufacturing lightweight and high-performance parts. The success of a team is not merely defined by the fastest car, but by the best overall performance, good engineering practice and financial planning [1].

The competition divides the teams into three main classes based on the chosen type of vehicle. The Internal Combustion Engine Vehicles (CV) are the oldest category and includes prototypes with an internal combustion powertrain. The Electric Vehicles category (EV) is characterised by vehicles driven by one or more electric motors and is the most widespread in recent years, due to the increasing potential and demand of hybrid and electric cars in the automotive industry. Both class-type cars can take part in the Driverless Class (DC) cup which is gaining in popularity. It entails in designing a car that is capable of autonomous driving for some of the dynamic disciplines, like Acceleration or skidpad [1].

Figure 1 - Panoramic photo from FSG competition [2]

1.2 TU BRNO RACING

TU Brno Racing is a Formula Student team from the Brno University of Technology, located in the Czech Republic. It has been participating in the Formula Student competition for over 13 years in both Combustion and Electric categories and has a history of building a total of 13 unique single seaters. Among those, 10 cars were made for the Combustion category, before the team switched to EV and built 3 successful vehicles powered by electric motors.

Throughout the years, the team has managed to compete amongst the highest-ranking teams in the world. In the last season of 2022/2023, the team claimed 1st place among the teams in the Czech Republic in the EV category with the most recent single-seater Dragon E3. It has competed at FS Czech, claiming several podiums, including the overall 2nd place, at FS East, where the team claimed a podium for Engineering Design the second year in a row. On top of that, for the first time in history, the team competed at FS Germany with an electric vehicle, claiming an overall 10th place out of 70. The team is currently designing a 4th electric vehicle, still aiming to reach the top of the scoreboard [4].

Figure 2 - Dragon E3 and the 2023 season's achievements [3]

2 CORNERING DYNAMICS

To understand how implementing a torque vectoring system can be beneficial for a racing car's cornering potential, the knowledge of some vehicle dynamics principles is necessary. As the goal of this thesis is to design an algorithm for a formula student car, in which increasing its performance is the main objective, this chapter will be focusing primarily on the principles and effects in that area.

2.1 SETTING THE FOUNDATION

To demonstrate cornering behaviour in an understandable way, a coordinate system together with a vehicle model are defined.

2.1.1 COORDINATE SYSTEM

A coordinate system is placed in the vehicle's centre of gravity, as shown in Figure 3. To properly explain the workings of torque vectoring, this will be the reference system for forces, moments and other physical quantities discussed in this chapter [13].

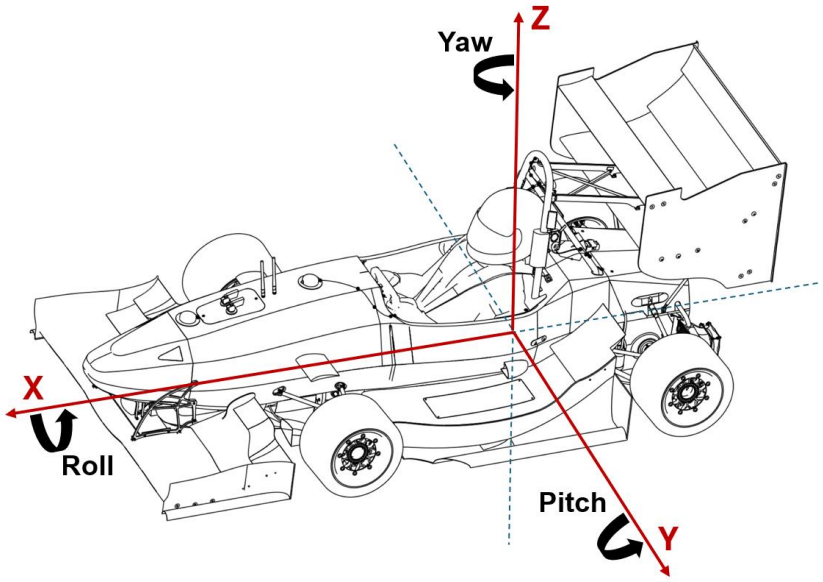

Figure 3 - Vehicle's coordinate system

2.1.2 VEHICLE MODEL

A vehicle model is defined in Figure 4, which represents a simplified version of the real single seater, for which the system will be designed. As this will be the first generation of a torque vectoring algorithm, the decision was made to first use a bicycle model to represent the real vehicle, and therefore simplify the defining equations to develop a solid foundation first, which could be made more accurate in the future. Said model is also a simpler way to explain the necessary vehicle dynamics principles [8].

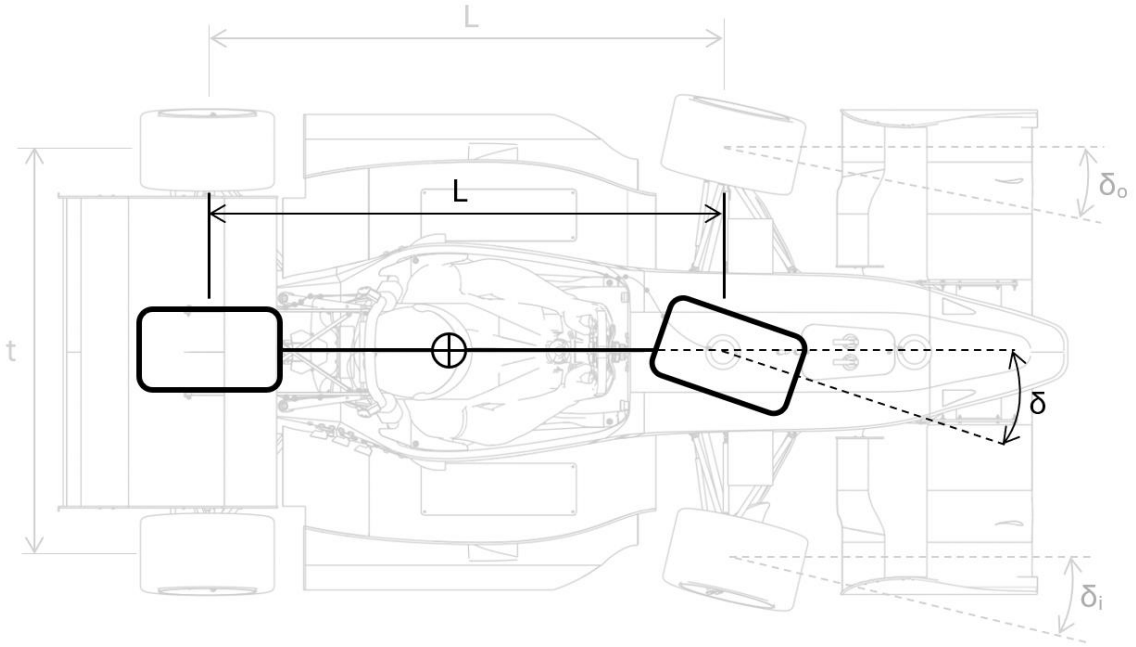

Figure 4 - bicycle model of the original single seater

By using the above illustrated model, a few points of influence on vehicle behaviour during cornering are erased, for further idealisation of the model [9].

The vehicle is compressed to a single-track model, therefore there is no lateral load transfer and no rolling or pitching motions. The longitudinal load transfer is not considered to give the tires a linear range of behaviour and the effects of aerodynamics, compliance of chassis and suspension, are neglected as well [9].

2.2 OVERALL CORNERING BEHAVIOUR

On a Formula Student racetrack, the car is in a cornering state approximately 80% of the time, and so exploiting the car's potential cornering performance to its maximum has arguably the biggest influence on lap time.

Cornering brings together forward velocity and the vehicle's rotation about its vertical Z axis, also known as yaw [10]. It can be divided into two main categories – steady state and transient state cornering, where both vary depending on if the car is experiencing a high-speed or low-speed turn [8].

When a vehicle is turning, it goes through three stages, as shown on Figure 5. First, it must execute a "transient turn-entry" (Stage B), where the yaw velocity and lateral acceleration build up from zero (straight line speed) to their steady state values. The second stage is steady state cornering, where yaw velocity, vehicle speed and turning radius are constant, the vehicle is in an equilibrium (Stage C). Third and final phase is the "transient turn-exit", where the vehicle is behaving similarly as in corner entry, except the yawing and lateral velocities are dropping from steady state values to zero, resulting in a straight-line exit (Stage D) [9].

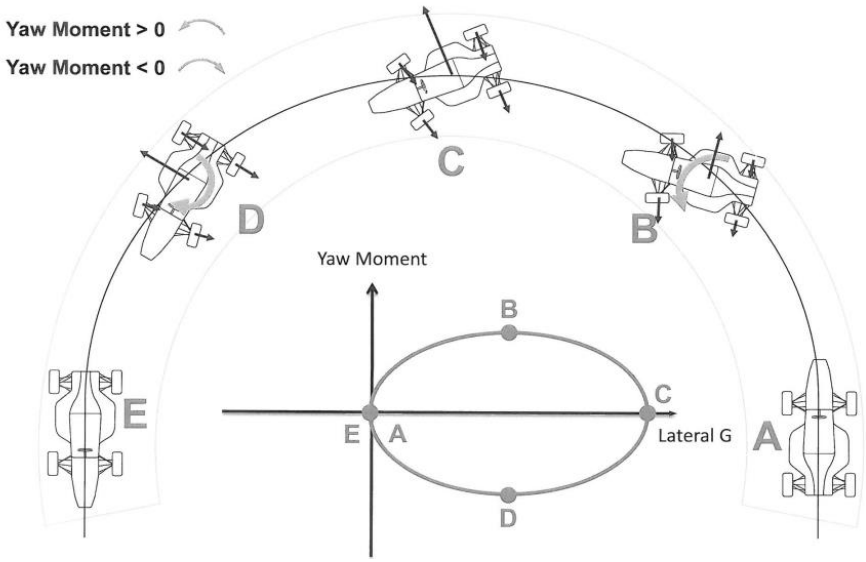

Figure 5 - Cornering states of a turning vehicle [11]

2.2.1 STEADY STATE

The form of steady state cornering is a vehicle's equilibrium driving state, in which the sum of lateral forces under all four tires equals the vehicle's centrifugal force, and the sum of moments around the car's Z axis is zero. Further, the sum of longitudinal forces under the tire equals the vehicles longitudinal force, and so the forward and yawing velocities are constant [12].

During a low-speed turn, the tires do not need to generate any lateral forces, and therefore the tires do not generate any slip angles. As a result, the vehicle is under no lateral forces during cornering, which means that the turn radius lies at the intersection of the projection of the rear axle and a perpendicular line drawn from the front wheels. The direction of travel is oriented clockwise, as the rear wheel follows a path that is inboard of the front wheel. From the forward and lateral velocities, the sideslip angle β is defined as the angle between the longitudinal axis, and the direction of travel (see Figure 6) [8].

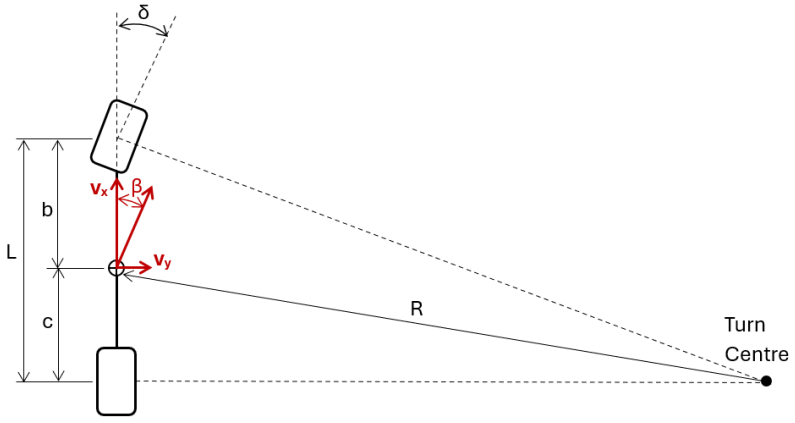

Figure 6 - Geometry of a turning vehicle in a low-speed corner

At high speeds, a lateral acceleration will act on the vehicle. The tires must develop lateral forces and therefore slip angles – the angles between the tire's pointing direction and its actual direction of travel. This results in a different turning geometry compared to low speed, where the rear wheels are an active part of defining a turn radius. At the same time, the increasing lateral acceleration makes the rear wheel drift outboard of the front wheel path to develop the needed slip angles, causing a shift in the direction of travel to the opposite side of the vehicle, then during a low-speed turn [8].

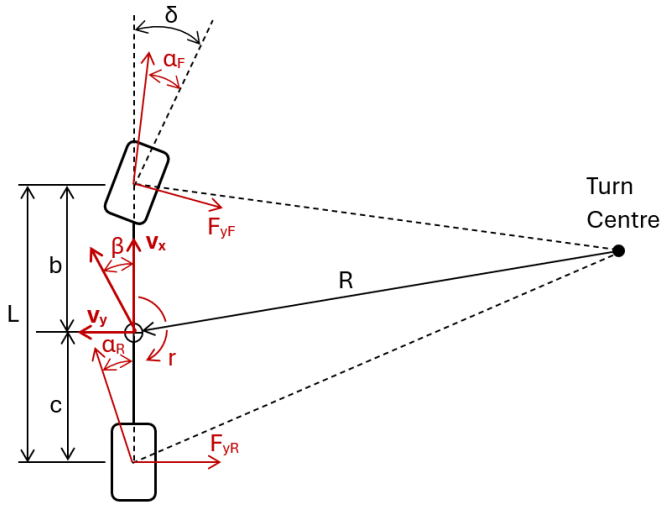

Figure 7 - Geometry of a turning vehicle in a high-speed corner

The developed lateral forces, known as cornering forces, are defined as [8]:

$$F_y = C_\alpha \cdot \alpha \tag{1}$$

Variable F_y is the lateral force, C_α the tire's cornering stiffness and α the slip angle. Such forces have a linear growth with the increasing slip angle when its values are low, and can be calculated from the vehicle geometry represented in Figure 7 and the equations below [9]:

$$\alpha_F = \beta + \frac{b \cdot r}{V} - \delta \qquad \alpha_R = \beta - \frac{c \cdot r}{V} \tag{2}$$

Where β is the chassis slip angle, b and c the distance between wheel centres and CoG, r represents yaw rate, V vehicle velocity and δ the wheel angle. The cornering behaviour is then defined by equations combining Newton's Second Law and the vehicle's geometry. As stated at the beginning of this chapter, a vehicle in a steady state is in an equilibrium around its centre of gravity, meaning the moments from the front and rear lateral forces are equal to zero [8]:

$$\Sigma M_z = F_{yF} \cdot b - F_{yR} \cdot c = 0 \tag{3}$$

$$\Sigma F_y = F_{yF} + F_{yR} \tag{4}$$

These equations – where M_z is the yaw moment and F_{yR} with F_{yF} lateral forces at the rear and front axles – will be the starting point of defining the state-space equations, that will describe the vehicle's mathematical model and its cornering behaviour. To have a complete understanding of such model, the transient turning behaviour needs to be considered as well.

2.2.2 TRANSIENT STATE

The transient behaviour of a car can be described by detailed and complex equations using Laplace transform mathematics and advanced understanding of vehicle dynamics, some of which are beyond the scope of this thesis [9]. This chapter will mainly focus on the overall behaviour which will help define the form of the torque vectoring algorithm, as that is the main goal of this thesis.

As stated earlier, the vehicle is in a transient state during corner entry and exit (view Figure 5). Unlike in steady state, it is characterised by the presence of a yaw moment and time varying values of yaw rate, lateral velocity, and path curvature. During corner entry, the vehicle passes from driving on a path with an infinite radius, to trying to reach a fixed-radius path of a steady state. To transition from the former to the latter, a yaw moment and lateral force are created by steering the front wheels, which results in a time varying behaviour. This analysis assumes a fixed position of the steering wheel, where the driver doesn't react to the outside forces and torques [9] [10].

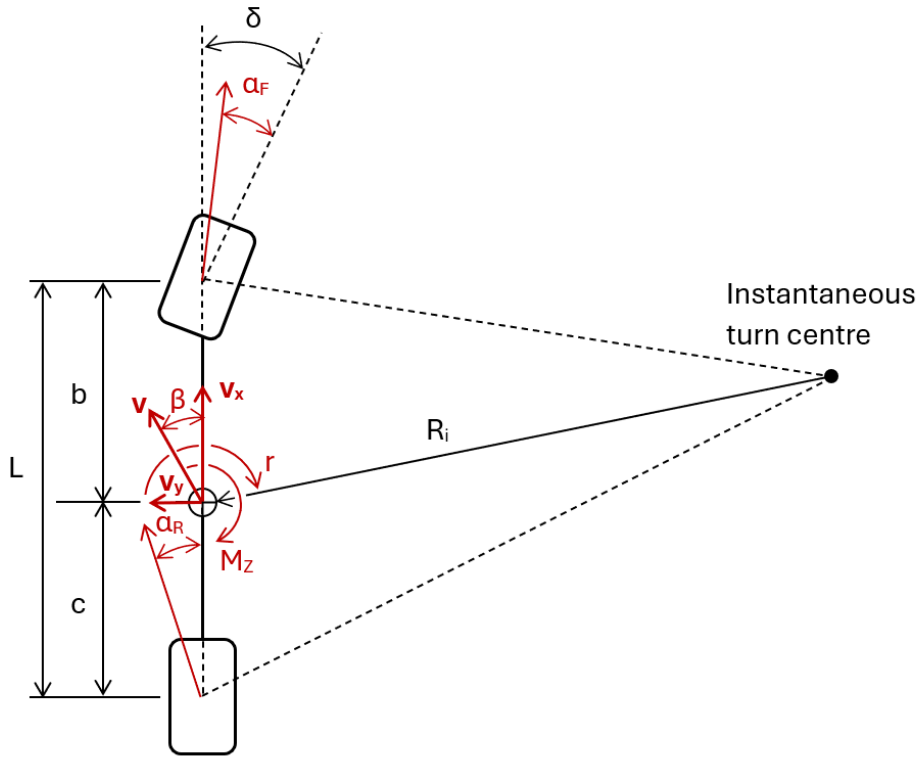

Figure 8 - Geometry of a vehicle in a transient state

The transient behaviour can be described by the equations of motion as well, however the yaw moment around the car's Z axis is no longer zero, the vehicle's total yawing moment is the product of the vehicle's moment of inertia and yaw acceleration [12].

$$\Sigma M_z = F_{yF} \cdot b - F_{yR} \cdot c = I_{zz} \cdot \dot{r} \tag{5}$$

$$\Sigma F_y = F_{yF} + F_{yR} \tag{6}$$

Where I_{zz} is the car's moment of inertial around Z axis and $\dot{r}$ the yaw acceleration.

2.3 TURNING RESPONSE

Whether a vehicle is in a steady or transient state during cornering, its behaviour through the turn is further defined by its response to a steering input. The steering angle of the front wheels, known as the Ackermann angle, is tied directly to the vehicle geometry [8] :

$$\delta_A = \frac{L}{R} \tag{7}$$

Where L is the wheelbase and R the turn radius. By including the effect of slip angles, a fundamental equation for cornering is defined [10]:

$$\delta = \frac{L}{R} + \alpha_F - \alpha_R \tag{8}$$

Where α_F and α_R are front and rear wheel slip angles and δ the wheel angle. The equation above indicates that the vehicle's response to a steering input depends not only on the vehicle geometry, but also on the rate, at which the front and rear slip angles are generated. Those depend on the magnitude of the generated lateral forces of the front and rear axle. To further understand the turning response dynamics, the dependency of the steering angle on the front and rear slip angles – and what influences them – needs to be understood.

2.3.1 STEADY STATE TURNING

A vehicle in a steady state is considered in equilibrium (as explained earlier) and its equations are derived from the turning geometry and the use of Newton's Second Law [8]:

$$\Sigma F_y = \frac{m \cdot V^2}{R} = F_{yF} + F_{yR} \tag{9}$$

Where m is the vehicle's mass. The equilibrium state dictates that the yaw moment around the car's Z axis is zero [10]:

$$F_{yF} \cdot b - F_{yR} \cdot c = 0 \tag{10}$$

$$\rightarrow F_{yF} = \frac{F_{yR} \cdot c}{b} \tag{11}$$

Combining equations (5) and (7):

$$\frac{m \cdot V^2}{R} = F_{yR} \cdot \frac{c}{b} + F_{yR} = F_{yR} \cdot \left(\frac{c+b}{b}\right) = F_{yR} \cdot \frac{L}{b} \tag{12}$$

Resulting equation for the lateral force at the rear axle:

$$F_{yR} = \frac{m \cdot V^2}{R} \cdot \frac{b}{L} \tag{13}$$

If the same process is followed for the front axle:

$$F_{yF} = \frac{m \cdot V^2}{R} \cdot \frac{c}{L} \tag{14}$$

To further define the link between steering angle and forward velocity, the vertical equilibrium equations need to be used [10].

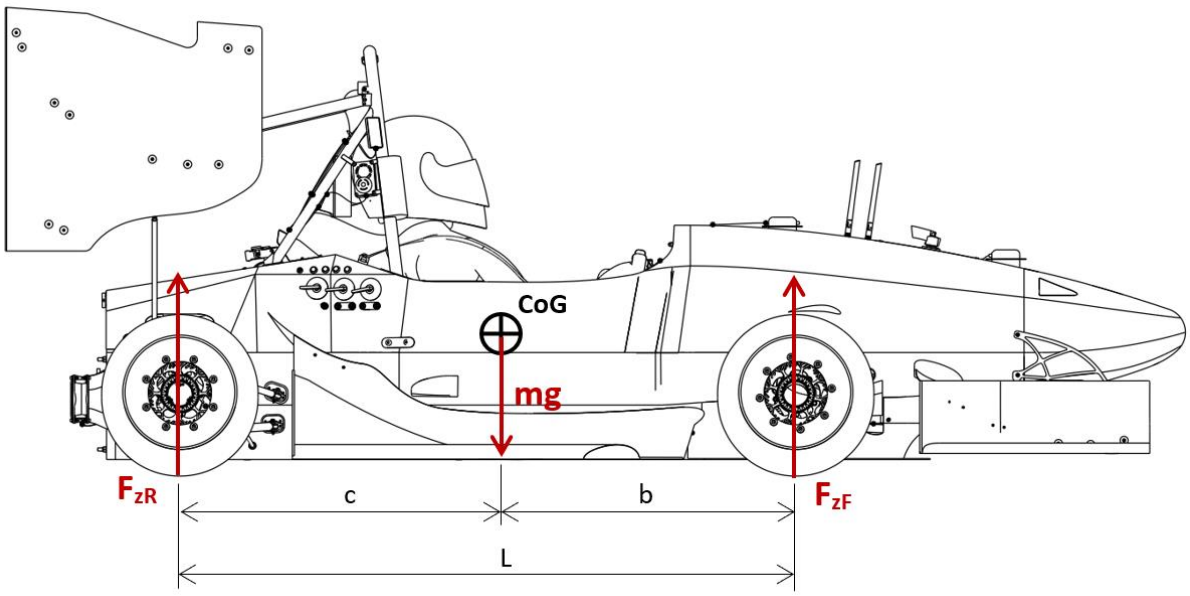

Figure 9 - Vertical equilibrium

Momentum equilibrium for the pitching motion around the vehicle's front contact patch [10]:

$$F_{zR} \cdot L = m \cdot g \cdot b \tag{15}$$

$$\rightarrow \frac{F_{zR}}{g} = \frac{m \cdot b}{L} \tag{16}$$

Where F_{zR} is the rear vertical force and g the gravitational acceleration. For the front axle:

$$\rightarrow \frac{F_{zF}}{g} = \frac{m \cdot c}{L} \tag{17}$$

Where F_{zF} is the front vertical load. Combining lateral equilibrium equations (9-10) with vertical equilibrium equations (12-13):

$$F_{yR} = \frac{m \cdot V^2}{R} \cdot \frac{b}{L} = \frac{V^2}{R} \cdot \frac{F_{ZR}}{g} \qquad F_{yF} = \frac{m \cdot V^2}{R} \cdot \frac{c}{L} = \frac{V^2}{R} \cdot \frac{F_{zF}}{g} \tag{18}$$

Finally, putting together equations for cornering force (1), the fundamental equation for the Ackermann angle (7) and equations for lateral forces (14)

$$\delta = \frac{L}{R} + \left(\frac{F_{zF}}{C_F} - \frac{F_{zR}}{C_R}\right) \cdot \frac{V^2}{g \cdot R} = \frac{L}{R} + \left(\frac{F_{zF}}{C_F} - \frac{F_{zR}}{C_R}\right) \cdot a_y = \boldsymbol{\frac{L}{R} + K \cdot a_y} \tag{19}$$

The equation 19 is the main description of a vehicle's turning response dynamic, where C_F and C_R are front and rear tire stiffnesses, a_y the lateral acceleration, and K the understeer gradient. The equation defines the vehicle's cornering behaviour through the link between the steering angle, turn radius, and either forward velocity or the lateral acceleration, while considering the vehicle's geometry, and tire properties [10].

The parameter K, also known as the understeer gradient, is defined by the ratios of vertical loads on each axle and the tire's cornering stiffnesses. The turning behaviour of the vehicle will change depending on the tire characteristics and how the loads are distributed on each axle [10]. Based on the understeer gradient, there are three scenarios for a vehicle's response to a step steer input.

If the front and rear tire cornering stiffness are the same, and the load on each axle is distributed evenly, the understeer gradient is zero. Such a vehicle is called a neutral steering car. That is a highly desired state for steady state cornering, as the turning radius doesn't change with increasing forward velocity, meaning both front and rear tires will reach their peak at the same time, allowing the vehicle to drive through the turn as fast as possible [10].

In the case of the front axle load being higher than at the rear, the understeer gradient is positive. The front cornering force will have to be of a greater magnitude to maintain force equilibrium and will therefore require a wider steering angle. Such a car is described as Understeering, meaning that for the same corner radius, it will need a higher steering angle. As the front tires are under more load, they will reach their peak quicker, meaning the rear tires are not exploited to their maximum. Such a car is in the racing world usually undesired, as it is "unwilling" to follow the corner path and derails out of the turn with increasing velocity. Understeering is also the result of combining braking and cornering, where the front axle is under more load [10].

The opposite happens, where the load at the rear wheels is more significant, K is negative, and the vehicle is described as oversteering. The tire behaviour is similar as in an understeering car, however, it is the rear tires that are under more force, meaning that to have force equilibrium around a bigger arm at the front, there must be a decrease of force magnitude at the front axle. As a result, to maintain the same corner radius, the steering angle must decrease, otherwise it would lead the vehicle onto a path with a smaller radius. A sightly oversteering vehicle is often beneficial in motorsport, as it is more "agile" while turning into a corner and allows the driver to have more feedback than in a neutral steering car [10].

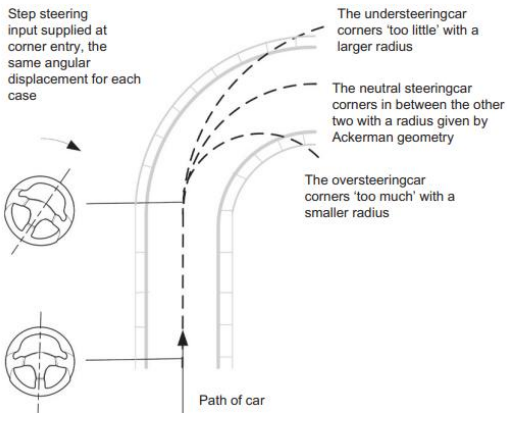

Figure 10 - *Cornering path of an under-, neutral-, and oversteering car [10]*

2.3.2 TRANSIENT STATE TURNING

The steering response of a car in transient state varies from the one in steady state. It has been made clear that a neutral steering car is the best option for driving in a steady state, as it allows to exploit the maximum out of all tires and follows the desired turn radius at the maximum forward velocity. However, it is the transient state that precedes this, and its turning behaviour that dictates, how soon the vehicle achieves steady state, after receiving a steering input [10].

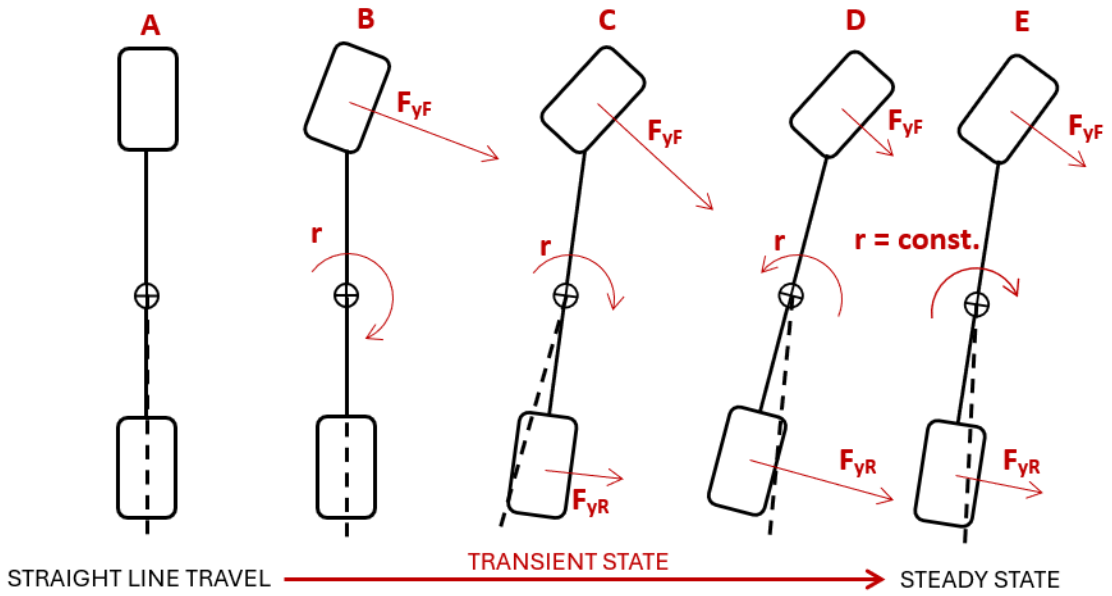

Figure 11 - The phases of a vehicle during a transient turn-in state

Figure 11 illustrates the phases of a transient turn entry. The position A describes the vehicle travelling in a straight line before turning in. Shortly after introducing a steering input in position B, the front wheels develop a small slip angle, and start generating a cornering force at the front. At position C, the whole car has yawed due to the front lateral force, and therefore has generated a slip angle and a side force at the rear. The vehicle is still travelling at a large corner radius, meaning that the lateral force needed to keep the vehicle on the circular path, is smaller than the tire generated forces, resulting in the vehicle moving to the right of the diagram. As time moves further, the yaw velocity catches up and overshoots the equilibrium value, forcing the driver to reduce front cornering force to return to the equilibrium by creating a yaw rate in the other direction. Finally, at position E the steady state is reached, where the yaw moment is zero and yaw rate constant, making the vehicle drive on the intended circular path. [10].

From the figure above, several conclusions can be made. A vehicle that can reach its steady state sooner than another, will be driving at the peak of its cornering ability for a longer time, making it overall faster through the corner, and providing the driver with a faster response. At the same time, preventing the “overswing” illustrated in figure 11 – Phase D further simplifies the process of getting to the limit and doesn’t require any corrective counter-steering [10].

It is therefore desirable for the vehicle to have a steering response as fast as possible, without overshooting the steady, state to achieve maximum cornering performance [10].

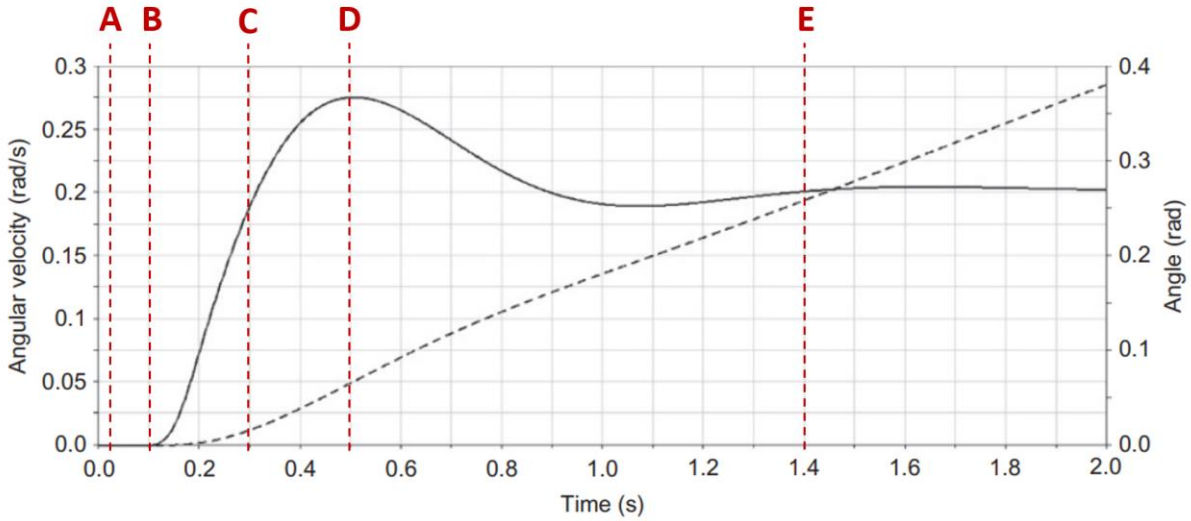

Figure 12 - Yaw rate and yaw angle response to step steer [10]

Figure 12 displays the behaviour of yaw angle (dashed-line curve) and yaw rate (full-line curve) of the vehicle illustrated in Figure 11. By having an overswing, the time in which the vehicle reaches equilibrium is significantly higher. At the same time, by improving the vehicle's reaction to a steering input, the slope of the yaw rate curve at the start will be much steeper, reaching the steady state even faster. Said ideal vehicle behaviour is portrayed in figure 13 by the line "B".

Complex second-order differential equations that consider the motion of a system with a single-degree-of-freedom mass, spring and damper lead to a characteristic that defines the response of yaw velocity to a step-steering input. Defining those equations is not the goal of this thesis, however the end-result can provide a good explanation on how to influence the yaw velocity to improve the vehicle's cornering ability [10].

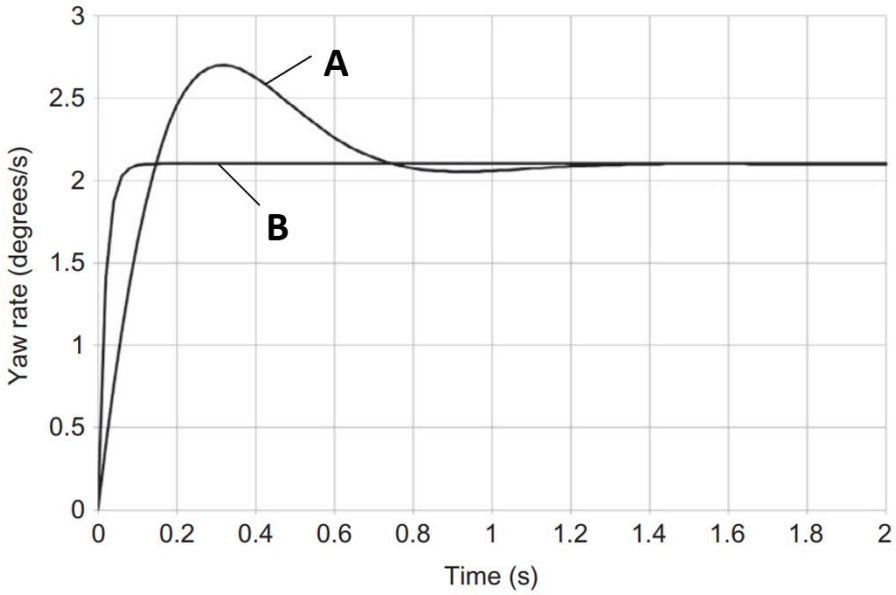

Figure 13 - Steering response for two vehicles [10]

The figure 13 is the comparison of a steering response of two different vehicles. Vehicle A is the original car, which behaviour is portrayed in Figure 11, and vehicle B is an idealised vehicle, which responds to a steering input exactly as it would be desired. The conclusion, which can be drawn from figure 13 is, that to improve vehicle A's cornering performance, it is desirable to increase the speed, at which the turning velocity can build up and ensure, that there is no further increase after reaching the steady state yaw rate values. In such a case, the equilibrium state will be achieved at a faster pace, allowing the vehicle to drive at the limits of cornering for a bigger portion of the corner.

To understand how a torque vectoring system can give the car the possibility of reaching a higher cornering potential explained in this chapter, its functionality must be first described.

3 TORQUE VECTORING

Electromobility has been the centre of development of the automotive industry for the last decade. There are several reasons which forced automobile manufactures to invest in research and development of hybrid or electric cars at the beginning of the 21st century, although the most influential one was the concern for the environment [5]. As a result, the development of electric-powered vehicles has brought to light new technologies for improving vehicle performance, comfort, and safety through control systems - one of them being the active yaw moment control, also known as torque vectoring [6].

3.1 BASIC UNDERSTANDING

In the case of fully electric powered vehicles with the powertrain configuration of two to four motors, the torque vectoring system can be implemented to enhance the drivability, safety, and dynamic performance, both on and off the road [6].

The basic function of the system consists in distributing the motor-delivered torque between the left and right driven wheels (potentially between the front and rear axle as well) in such a way, that a desired control over a vehicle in a cornering state is achieved. The torque difference between the right and left side creates an additional turning moment around the car's Z axis (view Figure 4), which – depending on the objective – either works with, or against the already present yaw moment, induced by the front steering, and as a result influences the cornering response and stability of the vehicle [6].

The system can be used to actively control its oversteering characteristics, providing a safety measure for road vehicles and a potential performance improvement in the case of race cars [6].

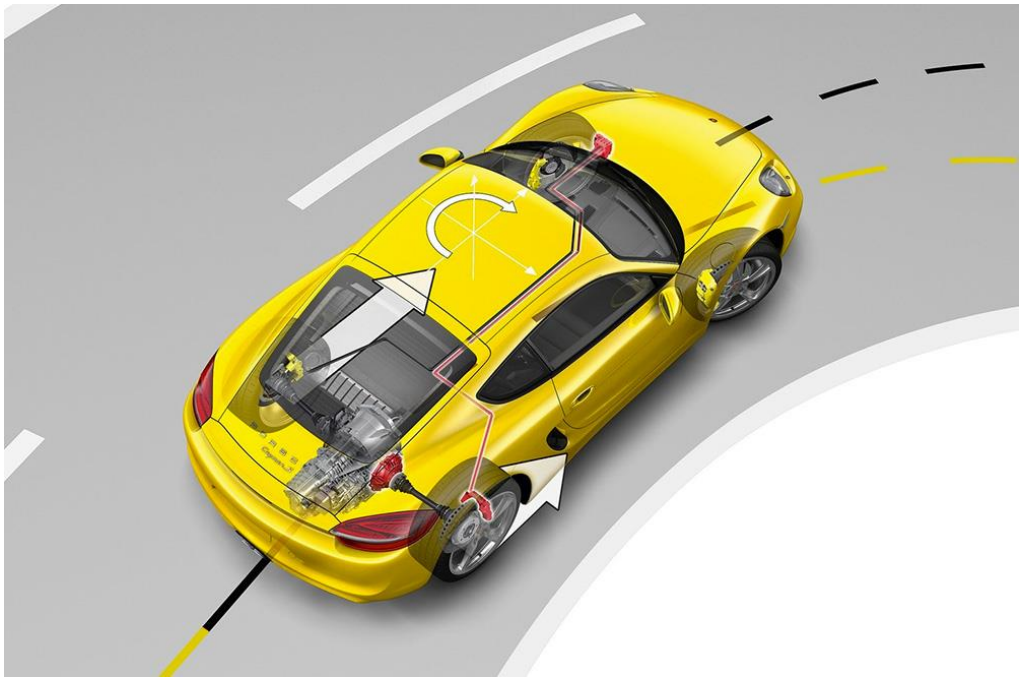

Figure 14 - Basic Torque Vectoring function illustration [7]

3.2 CORNERING UNDER TORQUE VECTORING

The forward driving force can be described as a function of axle torque. In this case, the axle torque equals the wheel torque, and is described by the following equation [25]:

$$T_w = F_x \cdot r_w + I_w \cdot \alpha_w \rightarrow \boldsymbol{F_x = \frac{T_w - I_w \cdot \alpha_w}{r_w}} \tag{20}$$

Where T_w is the wheel torque, r_w the wheel radius, F_x the forward driving force, I_w the wheel angular inertia and α_w wheel angular acceleration. The equation (20) is illustrated in Figure 15:

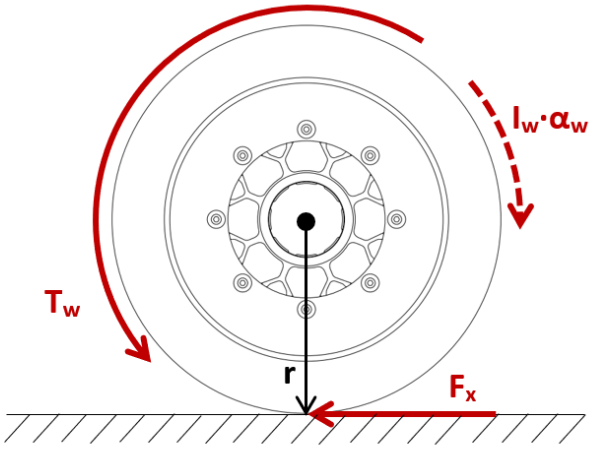

Figure 15 - Dynamics of a driven wheel

It is evident that, by having different torques on each wheel, the forward driving forces will be proportionally of different magnitudes (see equation 20). As a result, such a difference creates an additional yawing moment around the vehicle's centre of gravity, as it is acting at a distance defined by the car's rear axle track dimensions. This moment is represented by the variable M_{TV} in figure 16.

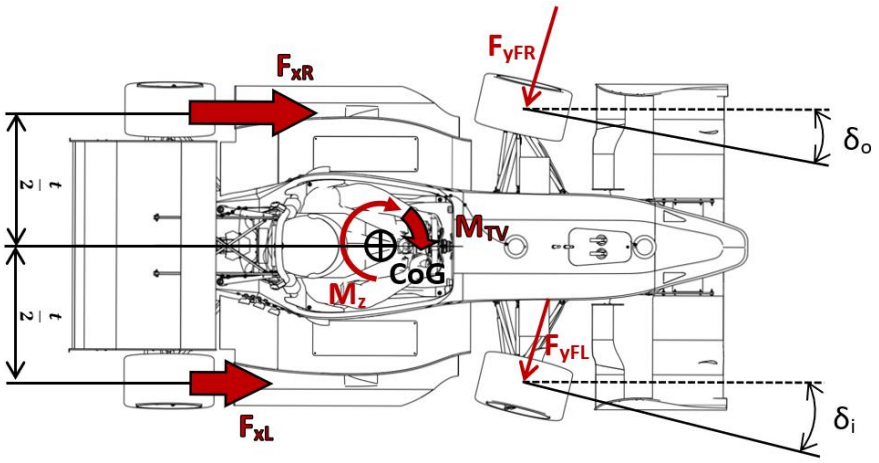

Figure 16 - Yaw moment induced by rear axle torque difference

The effect that yaw moment and velocity have on a cornering vehicle has been analysed in the second chapter of this thesis. By having a torque vectoring system, it is possible to introduce and actively control an additional yaw characteristic which has the potential of increasing the driving performance through the different states of cornering.

3.2.1 INFLUENCE ON STEADY STATE

As established in chapter 2, a vehicle's turning response during a steady state is defined by the understeer gradient, which determines if the vehicle will be following the right circular path or will have an under or over-steering characteristic.

The condition for a neutral steering car:

$$K = 0;\ \delta = \frac{L}{R} \tag{21}$$

By knowing the steering angle introduced by the driver, the radius of the corner is defined. Said radius can then be used to calculate the needed yaw rate [19]:

$$r = \frac{V}{R} \tag{22}$$

Where V is the vehicle velocity. Such yaw rate value is the one that describes a neutral steering car. It is also easily seen from the equation above that an increase in forward velocity will demand a higher yaw rate, to be able to drive at the same turn radius. A solution to this is to increase the steering angle, but if the steering doesn't allow a further increase, the result of a higher forward speed would be an understeering vehicle (as explained in chapter 2). Another solution is to introduce a torque vectoring system, which will measure the current and ideal yaw velocities and by the means of torque distribution correct any error between the two values, to always keep the vehicle at the ideal steering response behaviour.

As a conclusion, a torque vectoring system that would monitor the yawing velocity of a vehicle and then compare it to a calculated value from the two equations above, can assign the needed wheel torques in such a way, that makes the vehicle rotate at the ideal yaw velocity possible, allowing it to travel at a faster speed through the corner.

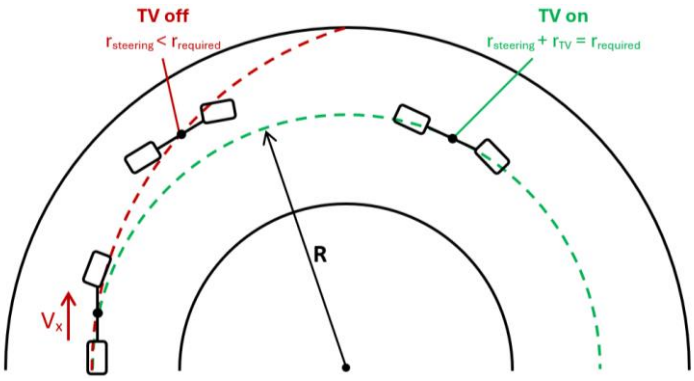

Figure 17 - Steady state cornering with and without Torque Vectoring

If the driving conditions and the current vehicle setup are such, that the car is understeering during a steady state turn, an additional yaw moment from the torque vectoring system would increase the yawing velocity making the vehicle neutral, or over-steering in the process.

3.2.2 INFLUENCE ON TRANSIENT STATE

The individual phases of a transient state turn entry have been described in chapter 2. When putting torque vectoring into the equation, the total yaw moment that acts on the vehicle during corner entry increases in magnitude [6]. Such yaw moment will be described as:

$$M_Z = \dot{r} \cdot I_{zz} + M_{TV} \tag{23}$$

By looking back at Figure 13, the higher the yaw acceleration, the faster the buildup of yaw rate will the vehicle achieve. It is therefore possible to conclude, that by having an active torque vectoring system, the vehicle can achieve a steady state quicker. At the same time, when yaw rate reaches its steady state values, the algorithm can make sure there is no overswing, by monitoring and keeping the yaw velocity at its ideal magnitude for steady state. This is the benefit of torque vectoring in such a case. As a result, by having an active torque vectoring system, it is possible to push the vehicle towards a better steering response and make it behave more like the idealised vehicle B, demonstrated previously in Figure 13.

Furthermore, if the algorithm distributes the driving torque as a reaction to a driver's steering input, it could be possible to shorten the transient state not only by having more yaw acceleration, but by eliminating one phase of the transient state turn-in development. The different phases have been seen in Figure 11, where phase B happens shortly after turning the front wheel, where the yaw moment is introduced, but the vehicle has not had any time to turn yet. By having different torques at each rear wheel when a steering input is introduced, it is arguably possible to jump from phase A to phase C, where the front of the car is yawed by the steering input and the rear by the moment of different torques at each wheel, skipping phase B and therefore achieving a more instantaneous buildup of yaw velocity.

3.3 CONCLUSION

Up until now, the cornering behaviour of a bicycle model car in different driving states has been described and analysed, to figure out the cornering dynamics. After understanding how a vehicle reacts to a steering input in various cases, and how an ideal process of getting through a turn should look like, several conclusions have been made, as to how to increase the cornering performance.

During the transient turn entry, the car needs to reach the ideal equilibrium state as quickly as possible and without overshooting it. Said state is defined by the ideal yaw velocity for a given turn radius. It is therefore desired to have as much yaw acceleration as possible during corner entry, to be able to get the vehicle into steady state cornering the fastest.

Once the vehicle has reached its steady state, it should not overshoot it, so that the driver does not need to make any corrections in the steering. It is desirable for the vehicle to be neutral

steering, so it can go through the turn at maximum possible velocity without influencing the turn radius, while getting the most out of all tires.

Finally, at the end of the corner, the car should start exiting the turn as late into the turn as possible. This will allow the car to travel at steady state for a longer period, making it overall faster through the corner. Similarly, as in corner entry, the highest the yawing acceleration out of the corner, the later into the turn the car can start the exit.

After summarising the influence of torque vectoring in chapter 3, such system could be beneficial in term of increasing the cornering effectivity of the car. The wheel torque difference at corner entry creates an additional yawing moment, increasing the car's yawing acceleration, making the entry into the corner faster. By having the system track the current and ideal yaw rates, and from those decide on the torque distribution, it is possible to keep the vehicle neutral steering during the turn, allowing the driver to go through the corner at a faster pace. At the same time, by having active control over the car's yawing characteristics, it's possible to make sure that no overshoot from the ideal value is made, creating an easier cornering process.

To summarise, a torque vectoring system, which introduces an additional yaw moment during corner entry and exit by creating a torque difference between the right and left driven wheels is a good way to increase cornering performance. By having the system track the current and ideal yaw rates and decide on the torque distribution from these it is possible to keep the vehicle neutral steering while travelling at the optimal yaw rate during steady state, without overshooting the target value at the start. It can make up for any suboptimal driving conditions and actively correct any errors in yaw velocity to provide the driver with an optimal and fast responding vehicle.

Taking into account the potential benefits indicated in this chapter, it is clearly worthwhile to develop a torque vectoring algorithm aiming to improve the cornering performance and the car's handling.

4 DEFINING EQUATIONS

After establishing that the algorithm will be comparing the ideal and actual yaw rate of the vehicle in order to figure out the torque distribution for an optimal cornering behaviour, it is necessary to define what equations will be describing both the dynamics of the turning vehicle, and the torque-allocating controller.

4.1 CORNERING EQUATIONS

Most of these have been explained and defined in chapter 2 and are brought together here. Going back to equation (22), the yaw velocity of a turning car is defined as:

$$r = \frac{V}{R} \tag{24}$$

This equation alone is not enough, as the turn radius is not directly measurable. For this reason, equation (19) must be used as well:

$$\delta = \frac{L}{R} + K \cdot a_y \tag{25}$$

The understeer gradient is defined as zero, to define the vehicle as neutral steering. These two equations above are enough to calculate the ideal yaw velocity the vehicle can achieve, and when combined, give the following result:

$$r = \frac{V \cdot \delta}{L} \tag{26}$$

This simple equation will be used to calculate the ideal yaw rate the vehicle is able to achieve, based on a neutral steering car.

4.2 CONTROLLER EQUATIONS

The heart of the algorithm will be a PI controller, which will take in the difference between the (ideal) calculated and (actual) measured yaw rate, and, based on their difference, will allocate different torques to the right and left driven wheel. To define the controller's Proportional and Integral components, linear model equations of motion are needed to define the relationship between the wheel torques, yawing moment and yaw velocity. Those can be defined from the lateral force and yaw moment dynamics [10].

As defined earlier in equation 5, the moment equilibrium around the vehicle's Z axis is defined as:

$$\Sigma M_z = F_{yF} \cdot b - F_{yR} \cdot c \tag{27}$$

Where M_z as the yawing moment, which can also be defined as [9]:

$$\Sigma M_z = I_{zz} \cdot \dot{r} \tag{28}$$

When combining the equations (27) and (28) with equation (1) for cornering force:

$$I_{zz} \cdot \dot{r} = C_{\alpha F} \cdot \alpha_F \cdot b - C_{\alpha R} \cdot \alpha_R \cdot c \tag{29}$$

Further expanded by the equation (2) for slip angles:

$$I_{zz} \cdot \dot{r} = C_{\alpha F} \cdot \left(\beta + \frac{b \cdot r}{V} - \delta\right) \cdot b - C_{\alpha R} \cdot \left(\beta - \frac{c \cdot r}{V}\right) \cdot c \tag{30}$$

After getting rid of parenthesis and rearranging the segments:

$$I_{zz} \cdot \dot{r} = C_{\alpha F} \cdot \beta \cdot b + C_{\alpha F} \cdot \frac{b^2 \cdot r}{V} - C_{\alpha F} \cdot \delta \cdot b - C_{\alpha R} \cdot \beta \cdot c + C_{\alpha R} \cdot \frac{c^2 \cdot r}{V} \tag{31}$$

$$I_{zz} \cdot \dot{r} = C_{\alpha F} \cdot \beta \cdot b - C_{\alpha R} \cdot \beta \cdot c + C_{\alpha F} \cdot \frac{b^2 \cdot r}{V} + C_{\alpha R} \cdot \frac{c^2 \cdot r}{V} - C_{\alpha F} \cdot \delta \cdot b \tag{32}$$

Next to separate the variables, where the chassis slip angle β is defined as the division of lateral and longitudinal velocities. As a result, the formula for the yawing motion is created. Since the velocity V in the direction x is approximately the forward velocity v_x [10]:

$$\dot{r} = v_y \cdot \left(\frac{C_{\alpha F} \cdot b - C_{\alpha R} \cdot c}{I_{zz} \cdot v_x}\right) + r \cdot \left(\frac{C_{\alpha F} \cdot b^2 + C_{\alpha R} \cdot c^2}{I_{zz} \cdot v_x}\right) - \delta \cdot \left(\frac{C_{\alpha F} \cdot b}{I_{zz}}\right)$$

The dynamics of lateral forces were defined previously in equation (4) as:

$$\Sigma F_y = F_{yF} + F_{yR} \tag{33}$$

By using the same formulas of cornering force and slip angles as previously for the substitution, the detailed version of lateral forces equations reads as:

$$\Sigma F_y = v_y \cdot \left(\frac{C_{\alpha F} + C_{\alpha R}}{v_x}\right) + r \cdot \left(\frac{C_{\alpha F} \cdot b - C_{\alpha R} \cdot c}{v_x}\right) - \delta \cdot C_{\alpha F} \tag{34}$$

The overall lateral force is expressed below based on Newton's Second Law. The lateral acceleration is made of two parts – the centrifugal acceleration and the direct lateral acceleration created by the vehicle's chassis slip angle [9].

$$\Sigma F_y = m \cdot \left(a_y + v_x \cdot r\right) \tag{35}$$

When equations (34) and (35) are combined [10]:

$$m \cdot \left(a_y + v_x \cdot r\right) = v_y \cdot \left(\frac{C_{\alpha F} + C_{\alpha R}}{v_x}\right) + r \cdot \left(\frac{C_{\alpha F} \cdot b - C_{\alpha R} \cdot c}{v_x}\right) - \delta \cdot C_{\alpha F} \tag{36}$$

Lastly, to define the lateral acceleration [10]:

$$a_y = v_y \cdot \left(\frac{C_{\alpha F} + C_{\alpha R}}{v_x \cdot m}\right) + r \cdot \left(\frac{C_{\alpha F} \cdot b - C_{\alpha R} \cdot c}{v_x \cdot m} - v_x\right) - \delta \cdot \frac{C_{\alpha F}}{m} \tag{37}$$

Bringing together the lateral and yaw dynamics equations, it is possible to create a state-space model, where the vehicle's state is described by the calculated yaw rate and lateral velocity. As the goal is to design a torque vectoring system that will increase the vehicle's yawing ability, a corrective yaw moment is added to the yaw moment component of the state-space model.

$$M_{TV} = \dot{r}_{TV} \cdot I_{zz} \tag{38}$$

The final mathematical representation of the bicycle model state is the following:

$$a_y = v_y \cdot \left(\frac{C_{\alpha F} + C_{\alpha R}}{v_x \cdot m}\right) + r \cdot \left(\frac{C_{\alpha F} \cdot b - C_{\alpha R} \cdot c}{v_x \cdot m} - v_x\right) - \delta \cdot \frac{C_{\alpha F}}{m} \tag{39}$$

$$\dot{r} = v_y \cdot \left(\frac{C_{\alpha F} \cdot b - C_{\alpha R} \cdot c}{I_{zz} \cdot v_x}\right) + r \cdot \left(\frac{C_{\alpha F} \cdot b^2 + C_{\alpha R} \cdot c^2}{I_{zz} \cdot v_x}\right) - \delta \cdot \left(\frac{C_{\alpha F} \cdot b}{I_{zz}}\right) + \frac{M_{TV}}{I_{zz}} \tag{40}$$

Written in matrix form:

$$\begin{bmatrix} a_y \\ \dot{r} \end{bmatrix} = \begin{bmatrix} \frac{C_{\alpha F} + C_{\alpha R}}{v_x \cdot m} & \frac{C_{\alpha F} \cdot b - C_{\alpha R} \cdot c}{v_x \cdot m} - v_x \\ \frac{C_{\alpha F} \cdot b - C_{\alpha R} \cdot c}{I_{zz} \cdot v_x} & \frac{C_{\alpha F} \cdot b^2 + C_{\alpha R} \cdot c^2}{I_{zz} \cdot v_x} \end{bmatrix} \begin{bmatrix} v_y \\ r \end{bmatrix} + \begin{bmatrix} \frac{C_{\alpha F}}{m} & 0 \\ \frac{C_{\alpha F} \cdot b}{I_{zz}} & \frac{1}{I_{zz}} \end{bmatrix} \begin{bmatrix} \delta \\ M_{TV} \end{bmatrix} \tag{41}$$

4.3 INPUT CONSTANTS AND VARIABLES

After successfully defining the equations that will drive the algorithm, it is important to set the input parameters, which will be fed into it, and make sure that the assigned values align with reality, to create the most accurate model possible.

4.3.1 MOMENT OF INERTIA

The Moment of Inertia I_{zz} is defined by the vehicle's mass and geometry and represents its "willingness" to change directions. It is only the inertia around the vehicle's Z axis that is relevant.

A rig that can oscillate around a vertical axis and is designed to withstand a vehicle's weight, was used for the measurement. The car, together with a sitting driver, was positioned on the rig and fixed by wheel rims in such way, that the centre of gravity (CoG) of the car was directly above the axis of rotation. The driver's head was secured in a single position to avoid interference with the oscillations.

Figure 18 - Vehicle setup for Inertia measurement around Z axis

To get rid of any measurement interference caused by the suspension springing and damping, rigid dummy dampers were installed at the front and rear axles. Both front and rear ride heights, together with weight distribution, were set to usual racing conditions.

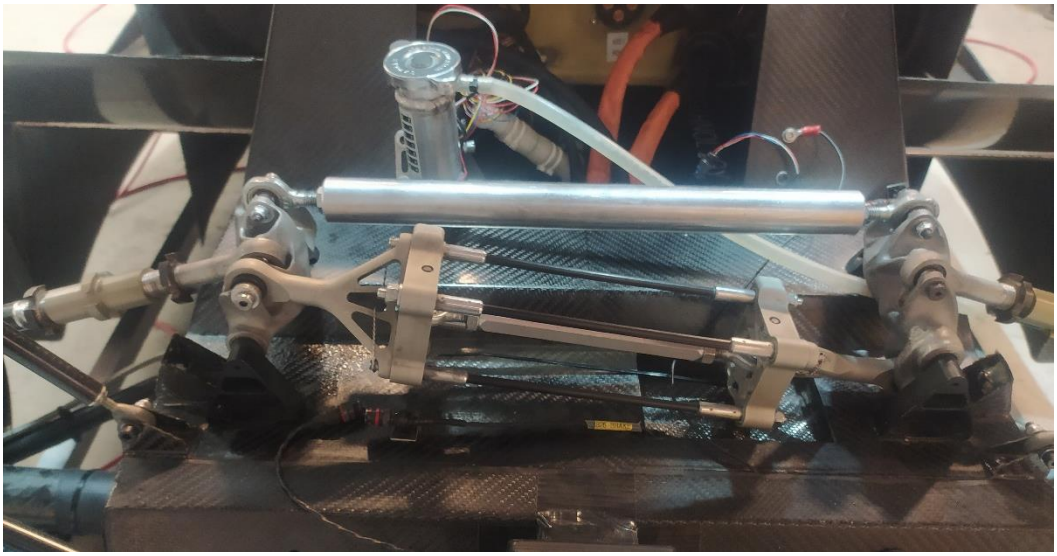

Figure 19 - Rear axle rigid dummy dampers

After 10 measurement cycles of the rig with, and without the vehicle, the moment of inertia of the vehicle alone around its Z axis was calculated. The deviation of the calculated value from the value in the CAD model was 1,2%, meaning well within tolerance.

Table 1 - Data from moment of inertia measurement

Izz					
test rig			test rig + vehicle		
n.	t [s]	Izz [Kg.m^2]	n.	t [s]	Izz [Kg.m^2]
1	0,456443	315,26	1	0,528567	422,76
2	0,456934	315,94	2	0,528434	422,55
3	0,455423	313,85	3	0,529014	423,48
4	0,456643	315,54	4	0,528313	422,36
5	0,455681	314,21	5	0,528672	422,93
6	0,455348	313,75	6	0,528572	422,77
7	0,455242	313,60	7	0,528795	423,13
8	0,455239	313,60	8	0,529261	423,87
9	0,455232	313,59	9	0,529708	424,59
10	0,455507	313,97	10	0,529279	423,90
mean	314,332		mean	423,235	
Izz			**108,9**	**Kg.m^2**	

4.3.2 WHEELBASE AND CoG POSITION

The Wheelbase is the distance between the front and rear axle, and is designed to be 1 528 mm. The position of the centre of gravity (projected on the XZ plane of the vehicle's coordinate system) dictates the dimensions "b" and "c", which define the distance between the wheel centres and the CoG. The usual weight distribution goal during suspension setup of the single seater was 50/50 based on vehicle behaviour, so that all tires are exploited to the maximum. This distribution that was considered during the vehicle design as well. When measuring the CoG position in the CAD model, its value is at 49.94% to the front, where the deviation from 50% is within the measuring tolerance of the scales that are used for suspension setup. It is therefore safe to assume an even weight distribution at both axles.

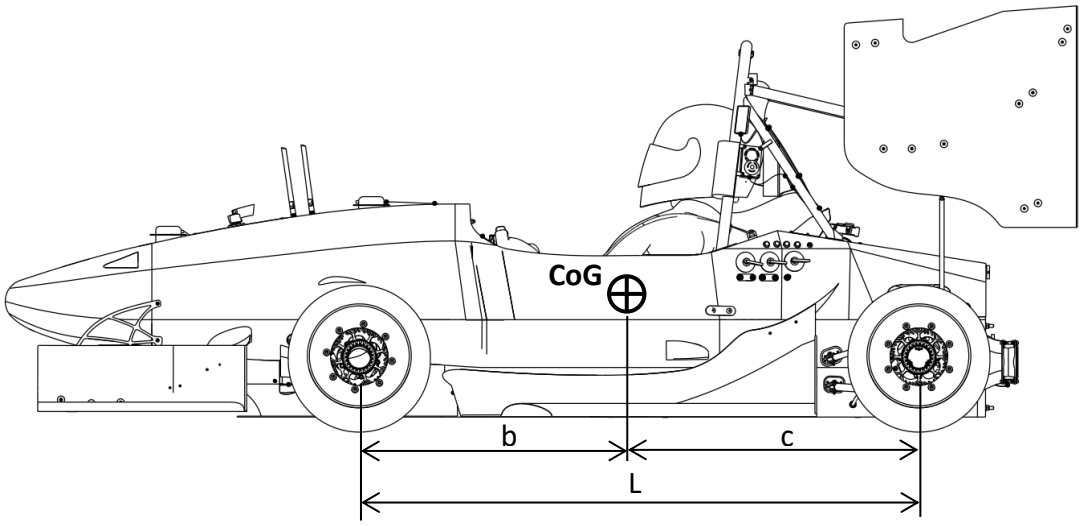

Figure 20 - Wheelbase and CoG location

Table 2 - CoG dimensions based on weight distribution

CAD model	L – Wheelbase	[mm]		1528
	Weight distribution	Front	[Kg]	123,85
		Rear	[Kg]	124,15
	Weight difference	[Kg]	0,3	
Error factor	Scales tolerance	[Kg]	±0,5	
Measured and rounded	L - Wheelbase	[mm]	1 528,3	1528
	Weight distribution	Front	[Kg]	123,85
		Rear	[Kg]	124,15
	b - distance to front axle	[mm]	**764**	
	c - distance to front rear	[mm]	**764**	

4.3.3 TIRE CORNERING STIFFNESS

The cornering stiffness (together with weight distribution), defines the understeer gradient (as seen in equation 13) and is a part of defining the state-space bicycle model of the car, as seen in equation 41. It is characterised as the slope of the cornering force at low slip angles. The current tires, that are being used on the latest single-seater Dragon e3, are the 10” tires Hoosier 16.0-7.5-10 R20, which are widely used in Formula Student.

To define the cornering stiffness, the tire’s lateral characteristics are needed. The Formula SAE Tire Test Consortium (FSAE TTC), together with the Calspan Tire Research Facility (TIRF) provide high quality tire data for the whole Formula Student community and will therefore be used to define the cornering stiffness of the mentioned tires. The data is provided in raw form, some post-processing and graph creation was necessary [14].

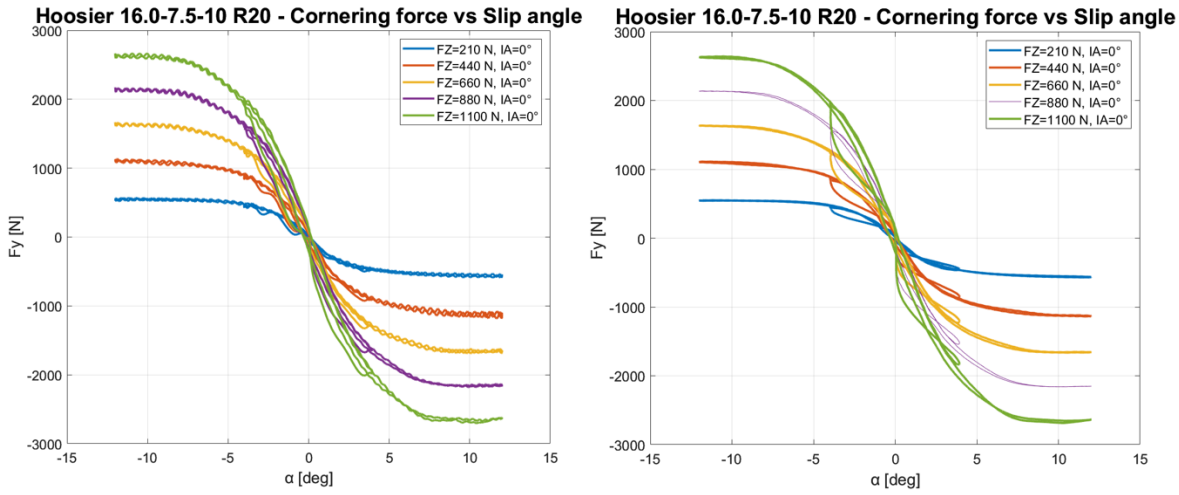

Figure 21 - Unfiltered and filtered Hoosier 16.0-7.5-10 R tire data for cornering force [14]

Out of all the measurements, the setup with a tire pressure of 83kPa and an inclination angle of 0° was most suitable and closest to representing the real tire setup at the rear wheels. After filtering and graphically presenting the selected measurement, the characteristic of lateral force on slip angle for all vertical loads was obtained. The cornering stiffness was defined from the measured data for smaller slip angles, where the characteristic is linear, and was compared for the vertical loads.

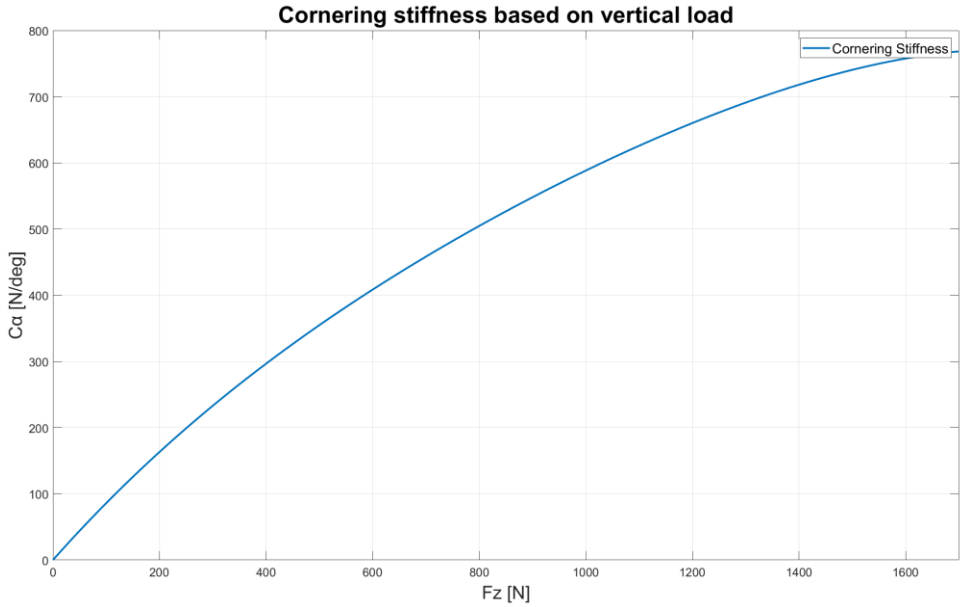

Figure 22 - Cornering stiffness based on vertical load

As weight transfer is neglected, the vertical load is defined by the static weight distribution, which was defined earlier as being equal on both axles, and it is therefore possible to define the tire cornering stiffness for the front and rear tires from figure 22:

Table 3 - Definition of Cornering force based on wheel load

Vehicle weight		Driver weight	
[Kg]	[N]	[Kg]	[N]
174	1707	74	726
Front axle		Rear axle	
[Kg]	[N]	[Kg]	[N]
124	1216	124	1216
Single wheel load [N]		608	
Tire cornering stiffness [N/deg]		**412**	

4.3.4 STEERING WHEEL ANGLE

The steering wheel angle (SWA) value is easily obtained from a rotary magnetic encoder that is mounted on the floor of the chassis and connected via a belt to the steering wheel pinion that transforms the rotational motion of the steering to the translational motion of the steering rack shaft.

Table 4 - sensor specifications [26]

Sensor	Contelec Vert-X 22E	
Specifications	Range	360°
	Sample rate	500Hz

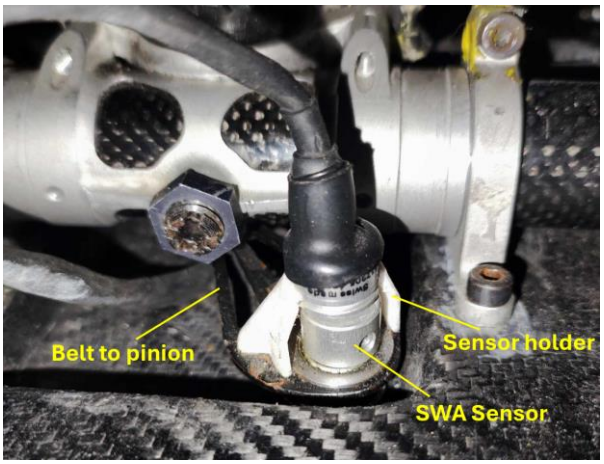

Figure 23 - SWA sensor mounting

The steering angle of the front wheel, which is needed to calculate the ideal yaw rate, is directly tied to the steering kinematics and to the angle of the steering wheel and can be calculated once the SWA value is logged.

4.3.5 VELOCITY

There are multiple sources from which it is possible to obtain the vehicle's forward velocity. A wheel speed sensor is mounted at the front non-driven wheels, from which it is possible to directly calculate the car's velocity. A limiting factor is lower accuracy at low speeds and the risk of losing data when locking the front wheels. The primary car's speed data will be obtained from the inertia unit, which can measure speeds in all three axes [16]. The wheel speed sensors will be used as a fail-safe option in case the inertia navigation module malfunctions.

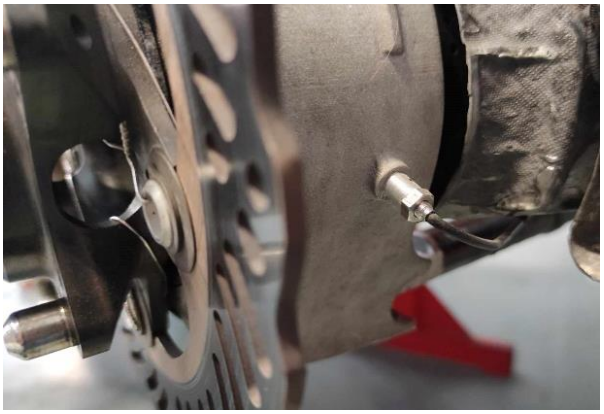

Figure 24 - Front wheel speed sensor

4.3.6 YAW RATE

The car's yaw velocity around its axis is calculated by the inertia navigation module Vectornav vn300 which measures the vehicle's angular position. Two antennas are used to figure out the vehicle's GPS location and the NavState subsystem generates outputs of the position state and its delta values at a default rate of 400Hz [16].

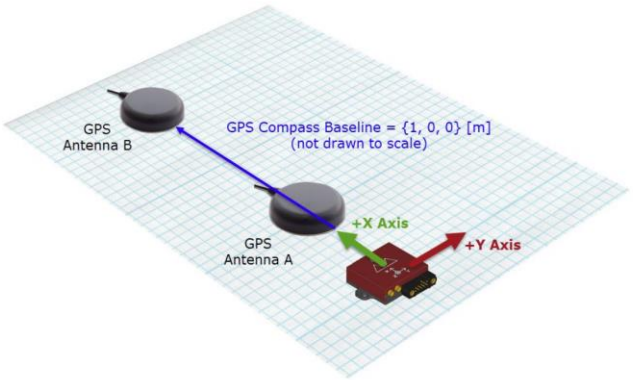

Figure 25 - GPS Compass baseline of the INS [16]

4.3.7 THROTTLE POSITION SIGNAL

The throttle position signal (TPS) will be defining the amount of torque demanded by the driver. Said value will then go through the torque vectoring system. For an accurate read of the throttle pedal position, two ELPM linear position sensors are mounted between the bottom of the chassis and the pedal to cancel any undesired movement to other directions, than the pedal travel, and are calibrated to send the value between 0 (no acceleration demanded) and 1 (full throttle signal), after manually setting the end pedal position based on the driver's preference.

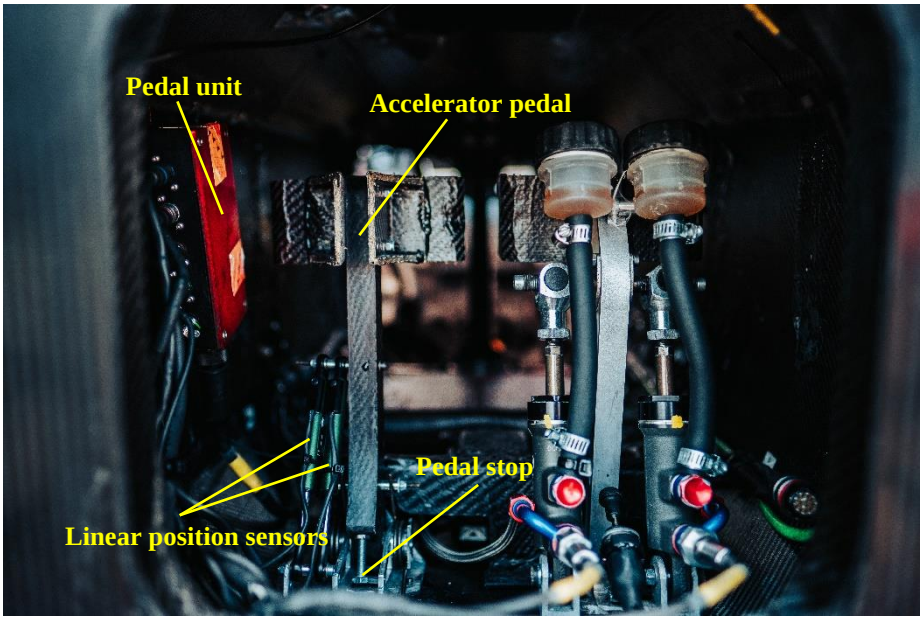

Figure 26 - Pedal assembly of Dragon e3 [15]

5 ALGORITHM DESIGN

After defining the equations, as well as the input parameters, it is possible to start building the system algorithm. The torque vectoring system will be uploaded on the Vehicle Central Unit (VCU) where the relevant data is collected. After calculating the ideal torque distribution, the command will be sent to the inverter, which then distributes torques to both rear wheel motors. The single-seater is driven by two electric motors Fisher TI085-052-070 with a custom-designed cooling jacket, and after connecting it to a gearbox of the team's design, it can deliver a torque of up to 348 Nm on the driven wheel.

Figure 27 - Dragon e3 Gearbox and motor models [17]

Before deciding that a regulator will be distributing the wheel torque based on a yaw rate difference, a purely mathematical model was considered as a less demanding option, as theoretically, it could generate the most accurate values based on measured and calculated data from the equations defined earlier in chapter 3. This however proved unattainable, as detailed information about road surface friction, tire properties and in-time load transfer data needed to be available, to complete the calculations, and neither the time nor resources were available for such a model. Therefore, a more practical approach with a PI regulator was chosen.

The algorithm design is done in MATLAB Simulink and transformed into C-code before uploading it to the VCU. Its block scheme is the following in figure 28:

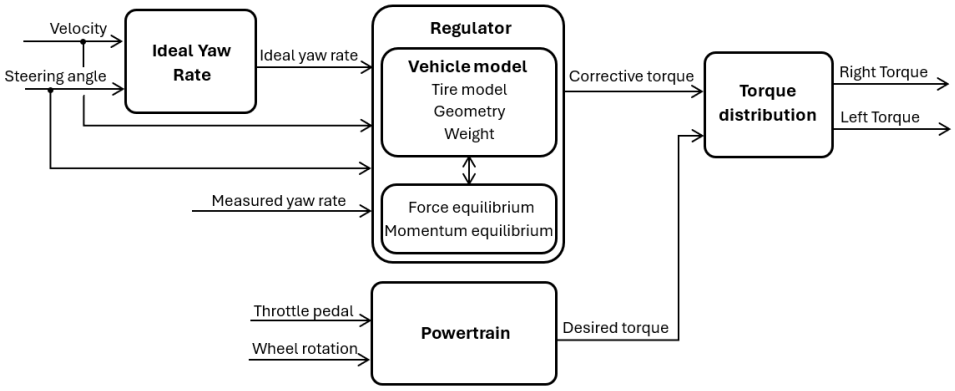

Figure 28 - Block scheme of the Torque Vectoring algorithm with a PI regulator

5.1 IDEAL YAW RATE

The ideal yaw rate, in reference to the vehicle velocity and applied steering angle, is calculated from the equation (24). It is possible to do an in-between step and calculate the turn radius from equation (25), however it is unnecessary, and division by yaw rate creates a further complication of risking dividing by zero, when driving on a straight line.

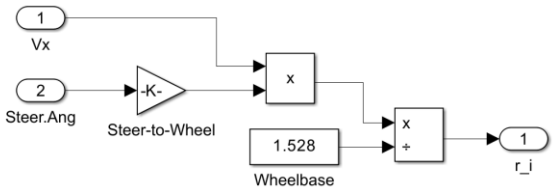

Figure 29 - Ideal yaw rate calculation block

5.2 POWERTRAIN MODEL

The vehicle's central unit processes the throttle pedal signal and sends it off to the inverter in the form of electrical current, which is then converted to the desired torque value and sent into the motors. To be able to analyse and change the assigned torques in the torque vectoring algorithm, their value needs to be defined earlier.

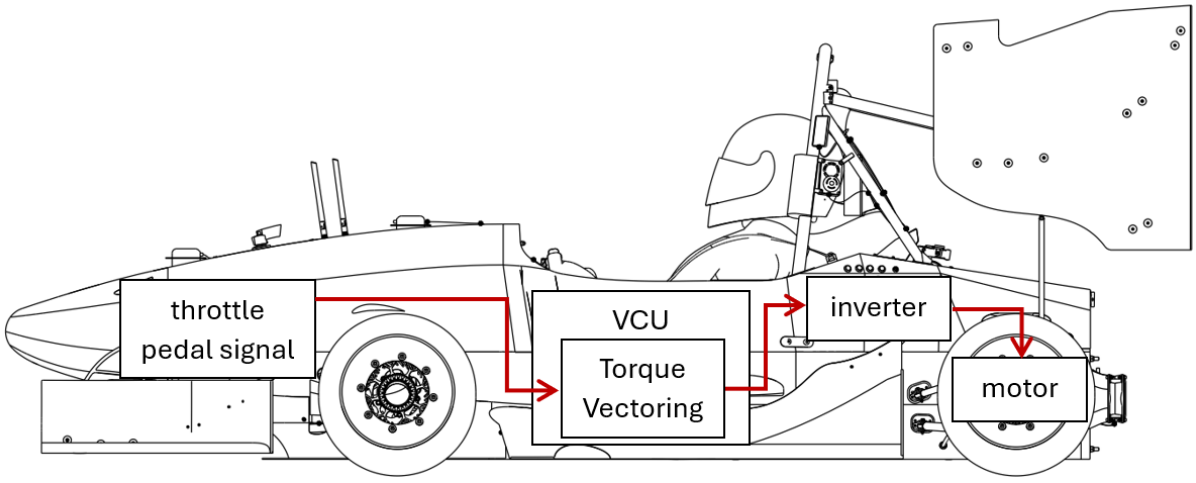

Figure 30 - Throttle pedal signal path

A Simulink model of the powertrain system was created, which converts throttle pedal signal and wheel rotational velocities to motor torque, based on tabular data from the motor characteristics. Said model is seen in figure 31. As a result, the algorithm defines the desired torques and assigns them new values based on the circumstances after analysing the vehicle behaviour. Finally, the distributed torques are converted back into an electrical current signal, which is sent to the inverter, to be allocated to the right and left wheels.

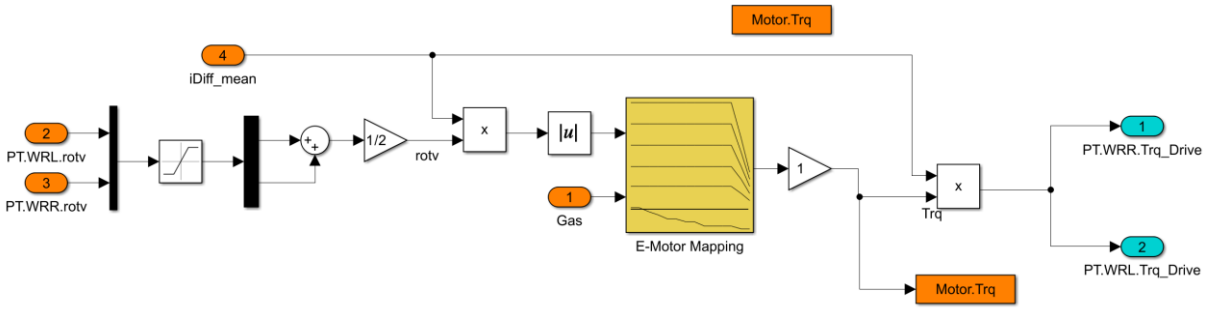

Figure 31 - Powertrain Simulink model of Dragon e4

5.3 REGULATOR

A regulator – seen in figure 32 – was designed, to decide on the torque distribution, based on difference between the ideal and measured yaw rates. It is characterised by its fundamental proportional and integral values. The regulator is further expanded by the integral time constant T_i as a function of the car's longitudinal velocity, a steering compensator block and an anti-windup control [18].

The regulator's further detailed design, simulation and testing process is the subject of another thesis. It will therefore not be further described in this paper.

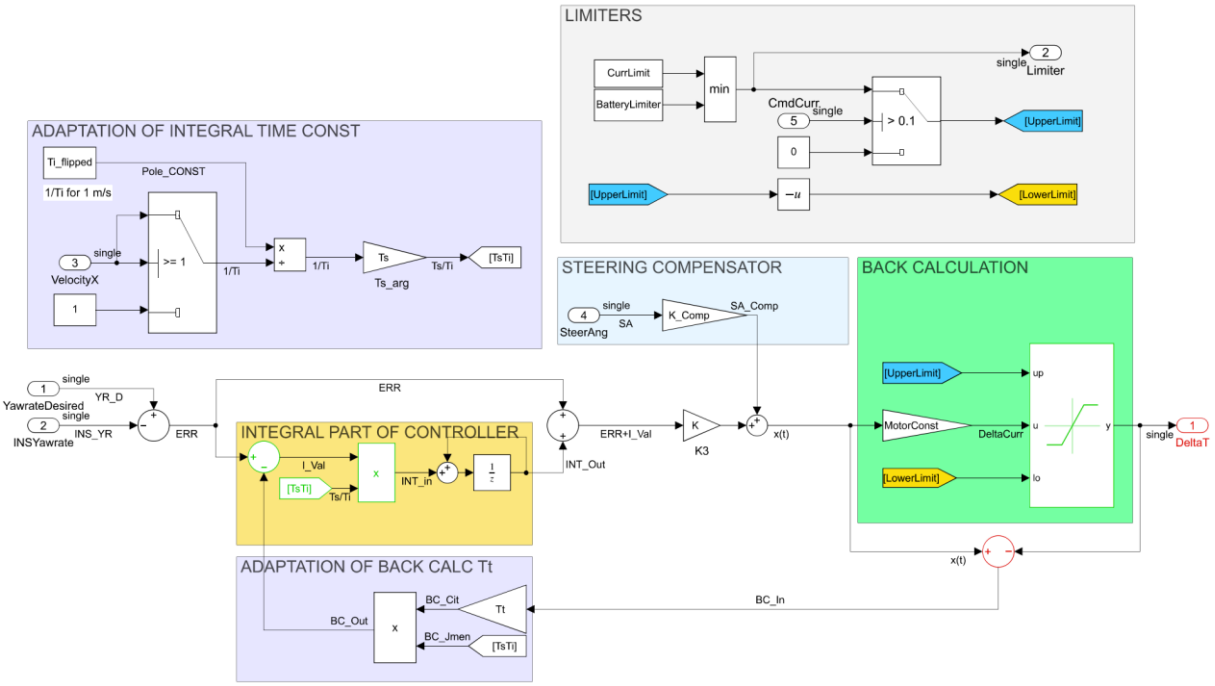

Figure 32 - Simulink scheme of the PI regulator [18]

5.4 TORQUE DISTRIBUTION

When deciding how the torques should be allocated, three possibilities were considered. When driving through a corner, the corrective torque output from the torque vectoring system can either be added to the outer wheel, subtracted from the inner wheel, or evenly distributed between both by adding half to the outer, and subtracting half from the inner.

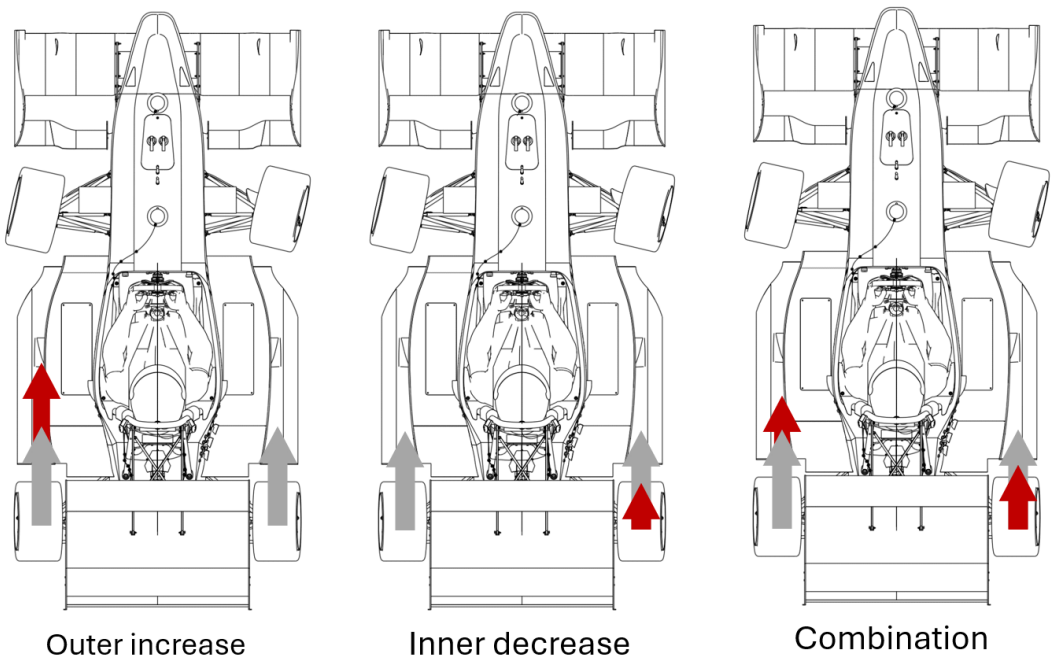

Figure 33 - Torque distribution options

Combining both wheels is the best way to provide the widest range of yaw moment available. The motors can deliver a maximum torque of 348 Nm to a driven wheel. If the torque vectoring system requests more torque than it can provide, it will be cut off at an upper limit defined in the VCU. Similarly, if the needed decrease of torque on the inner wheel goes down to zero, it is possible to use it for recuperation or it can be simply cut off at a minimum defined value.

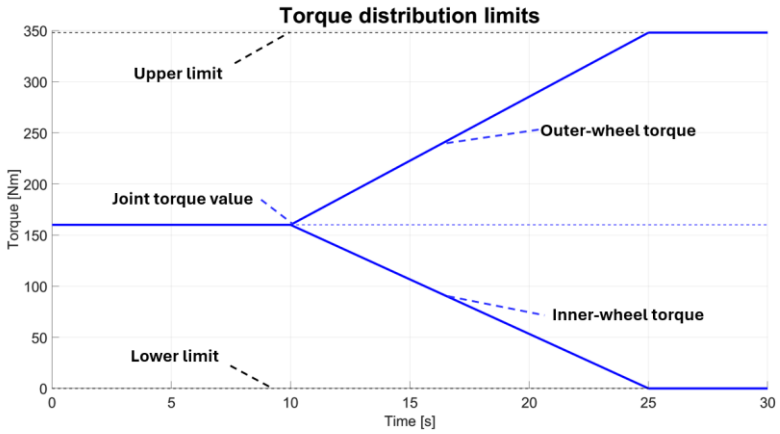

Figure 34 - Torque limiter function

The resulting designed torque vectoring algorithm containing all the described subsystems is the following in figure 35:

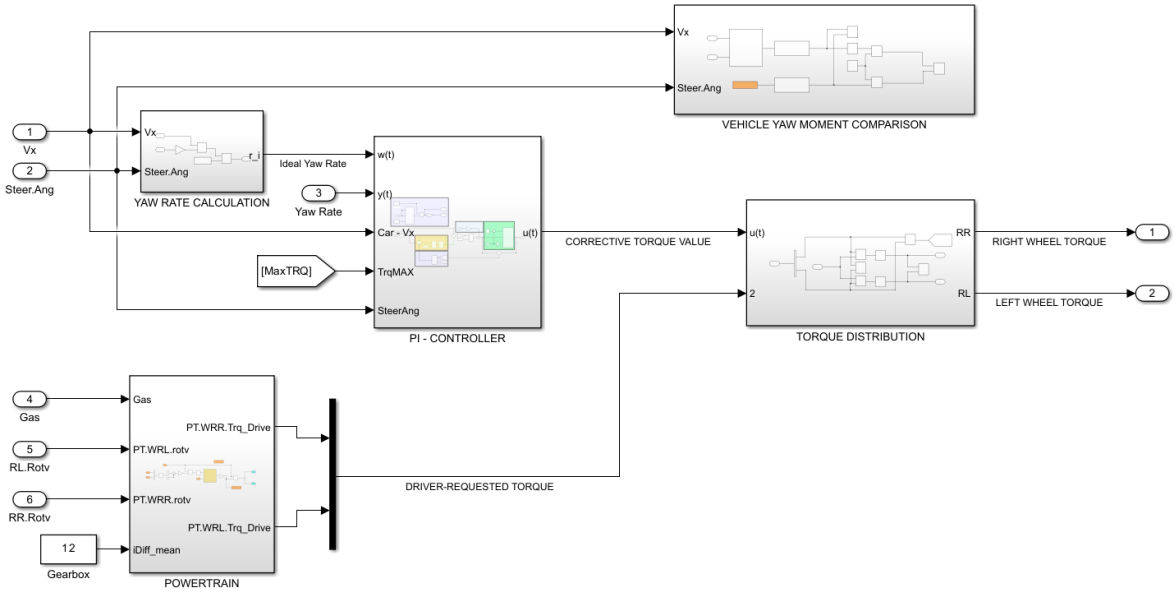

Figure 35 - Torque vectoring algorithm design

Although the yaw moment calculation block in figure 35 is not necessary for the proper functionality of the system, it is a good way to pinpoint areas of corner entry and exit, where the vehicle is lacking in performance.

It is important to note, that the algorithm is driven by the difference in yaw velocity, which is derived from the assumption, that the vehicle is in a steady state, however it is the transient state that dictates corner entry and exit. As described in chapter 2, it is desirable to enter the turn as fast as possible, meaning that the reference of maximum yaw acceleration is more appropriate during corner entry and exit, however such model would be too complex for a first generation of this system. As a result, the torque vectoring takes as reference the steady state yaw rate value at all parts of a corner. This means that, at corner entry and exit, the vehicle might still not be reaching its full potential. When entering a corner, the algorithm doesn't assume, that it's desired to increase the yaw acceleration to the maximum, it assumes that the car wants to drive in a steady state at the given steering angle.

Yaw moment and acceleration would be another contributing variable for an improved torque vectoring system in the future, where it would possibly determine a more accurate torque distribution for the transient part of cornering.

6 SIMULATION

Before implementing the torque vectoring system into the vehicle, a simulation and analysis of the whole algorithm and its key segments is necessary, to ensure that it functions properly and processes the data as intended.

6.1 MEASURED TRACK DATA

Previously measured track data were put into the algorithm as a first test. This does not test the efficiency of the regulator but allows to check if all blocks are written correctly and how each calculated variable compares to real time measurements.

Track data from the last testing session were used. Figure 36 shows the GPS tracking of the car during the drive and outlines the overall shape of the test track. For a better analysis, only the fastest lap was used out of the whole driving session.

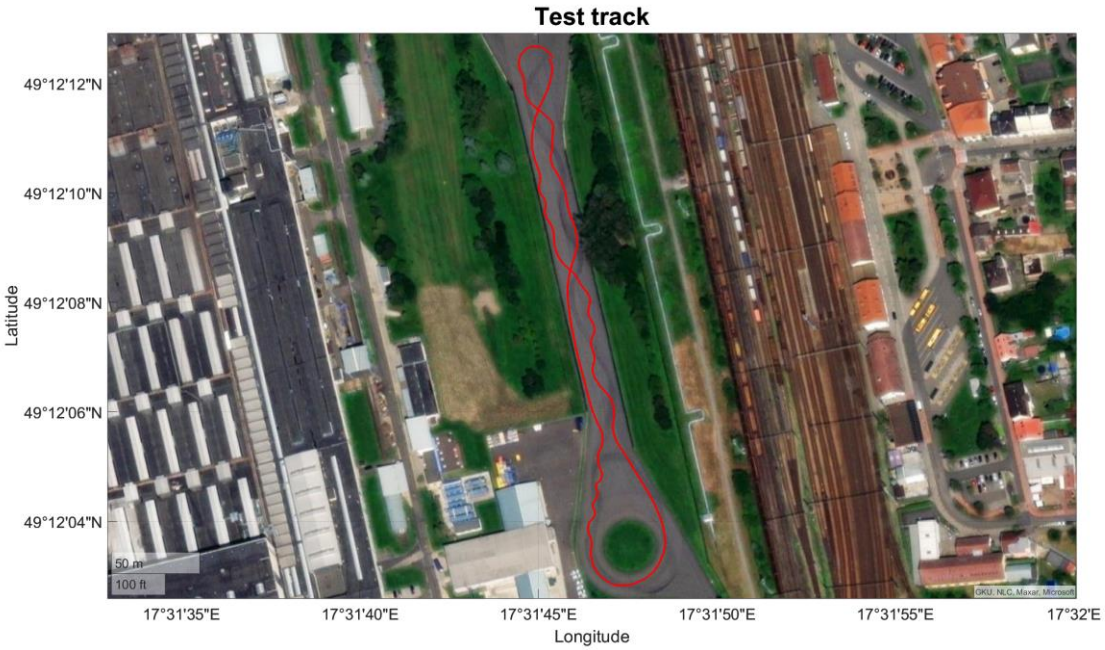

Figure 36 - Test Track outline

The input variables are throttle pedal position, wheel angular velocity, car velocity, steering wheel angle and yaw rate. The data were expressed in time domain for one lap.

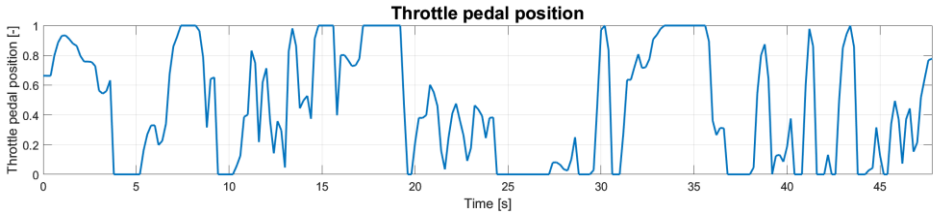

Figure 37 - Throttle pedal position input into the powertrain model

All signals were filtered to erase noise and sent as inputs into the Simulink model.

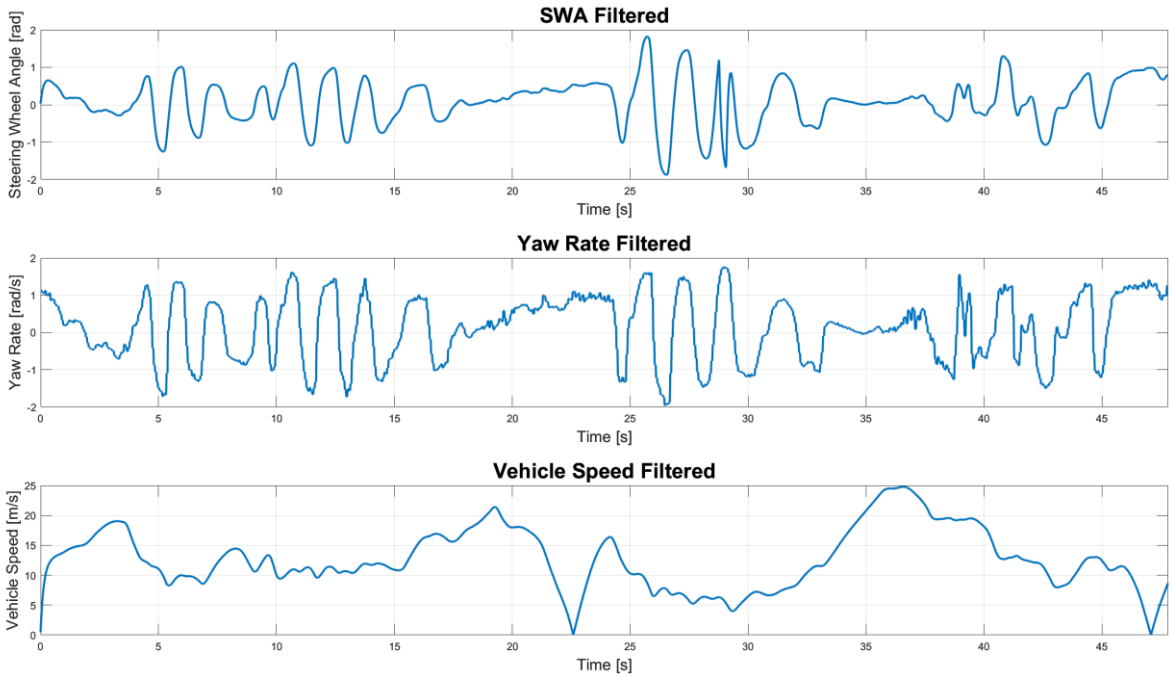

Figure 38 - Input data for one lap

Throttle pedal signal and wheel angular velocity are inputs to the powertrain model seen in figure 31, where the output is the calculated driver-desired torque. Compared together with the measured torque values in figure 39, the alignment is sufficient to declare the Simulink powertrain model to be considered accurate. The only deviation of the calculated value from the actual one is during sudden and short-lasting peaks seen in the figure 39. Such peaks are the result of uncouth driving and will not be considered for the torque vectoring algorithm, as it would make the vehicle too unstable.

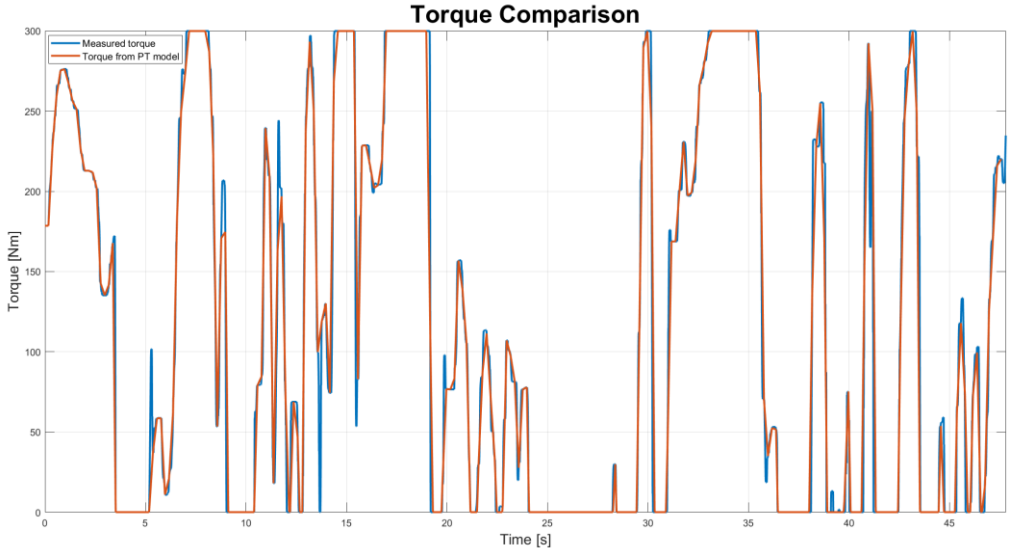

Figure 39 - Measured and calculated torque output comparison

Similarly, the calculated yaw velocity data was compared with the measured yaw rate for the driven lap. It is possible to observe in figure 40, that the calculated value does align with the

real measurements, however it is bigger in magnitude for almost every corner, confirming the theory that there is room for improvement in cornering performance, as the maximum potential of the car is not reached.

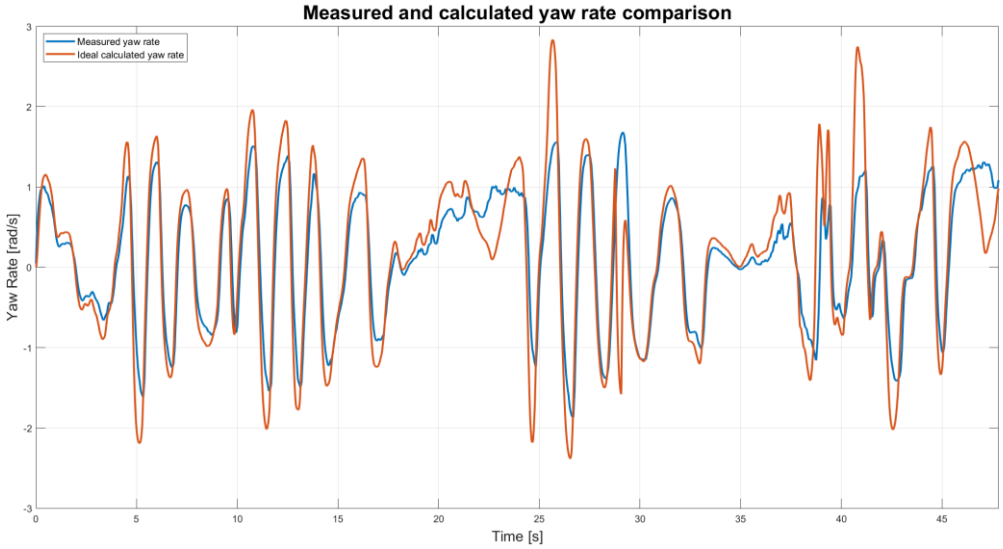

Figure 40 - Yaw rate comparison

Even though it is yaw rate that serves as reference of the current vehicle state and drives the PI regulator, it is also beneficial to analyse the progress of yaw moment. It allows to illustrate how much performance is to be gained at corner entry and exit, as yaw acceleration defines the slope of the yaw rate curve in figure 40, and defines, how soon the car will reach steady state.

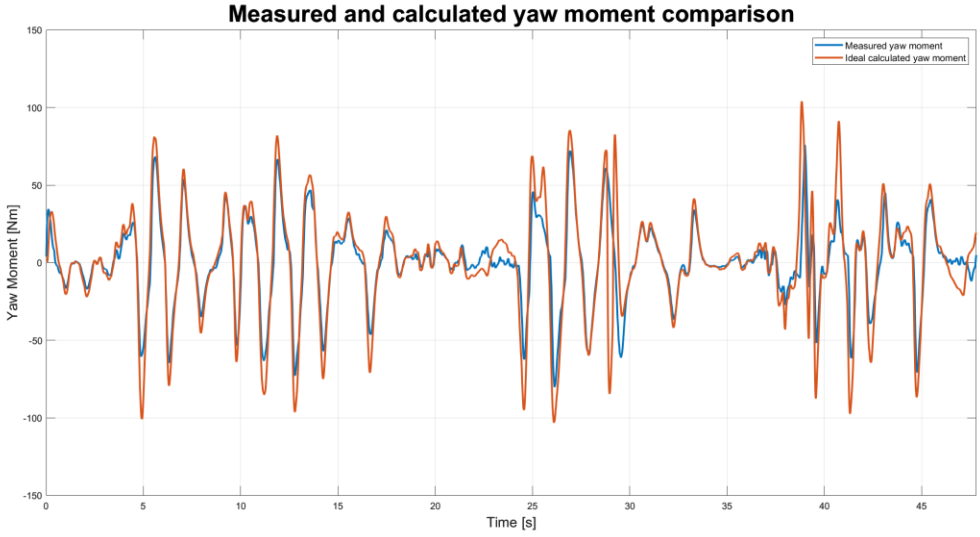

Figure 41 - Yaw moment comparison

It is possible to observe from figure 41 that in most cases, the ideal yaw moment was not reached, meaning that during the drive, the car was understeering. This is particularly notable at high-speed corners which require a quick and sudden change in yaw acceleration where the vehicle's inertia is working against the driver.

6.2 VIRTUAL TESTING ENVIRONMENT

To test the algorithm and its regulator together, a virtual simulation with a vehicle model needed to be created. IPG Carmaker is a simulation software for virtual test driving with the option to connect with Simulink, for easier testing of control systems. It allows detailed driver, track, and virtual vehicle creation, and was therefore suitable to simulate the control algorithm [20].

6.2.1 VIRTUAL VEHICLE CREATION

The first step is to define the virtual vehicle to correspond as much as possible to the real car. Values that affect the torque vectoring algorithm the most are centre of gravity (CoG) position, moment of inertia, overall vehicle geometry and tire properties. However, to obtain reliable simulation results, the definition of the whole vehicle needs to be as accurate as possible.

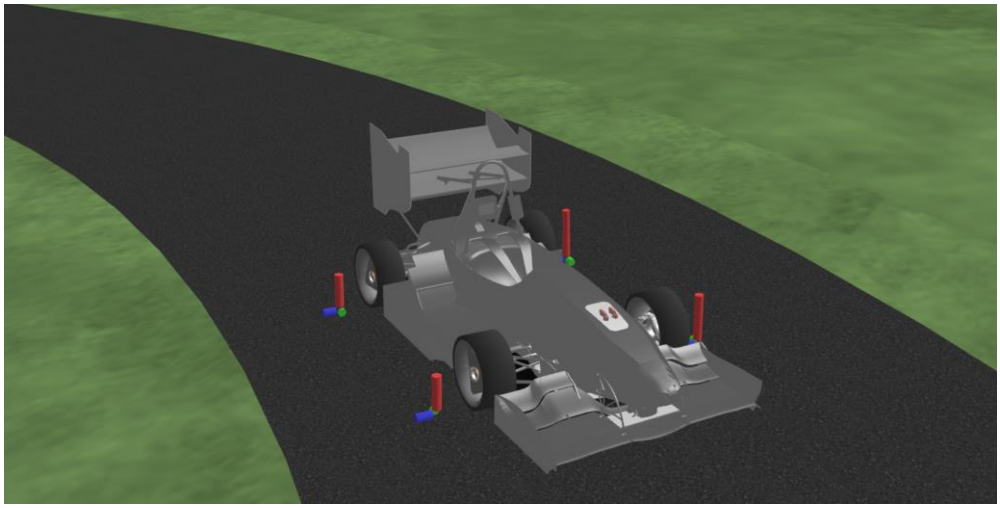

Figure 42 - Dragon e4 virtual vehicle model

The virtual car's geometry, kinematics and individual pickup points were taken from the last vehicle design. As the Dragon e4 has a decoupled roll-heave suspension, it needed to be transfigured into a symmetric suspension model, while keeping the wheel rates, motion ratios, together with spring and damper properties identical, to make sure the virtual model has the same load transfer properties as the physical car during rolling motion.

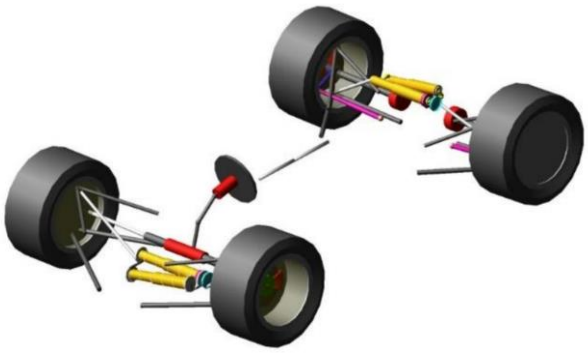

Figure 43 - Dragon kinematics ADAMS model [22]

The kinematics model in IPG Kinematics needs to be validated by a simulation, before being implemented into the car. The limit values for spring compression and the with movement of the steering rack were set as control parameters for the simulation. The input data contained the CoG position, Wheelbase, braking ratio, and mass of the vehicle, together with tire rate and wheel geometry positions, which served as simulation inputs for the kinematic model.

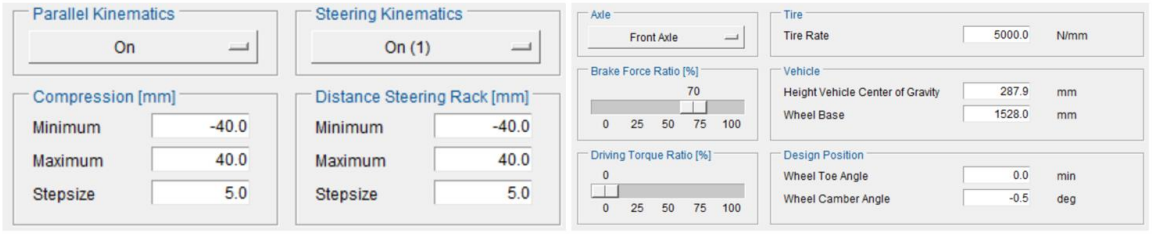

Figure 44 - example of the front axle's kinematic validation settings

To have an accurate overall mass and moment of inertia, each of the vehicle components were assigned mass and inertia properties, including the driver.

Springs and dampers were set based on the most common setup, that the car usually drives on, and the conversion of steering wheel angle to the front wheel angle was taken from the steering kinematics of the usual Ackermann setting.

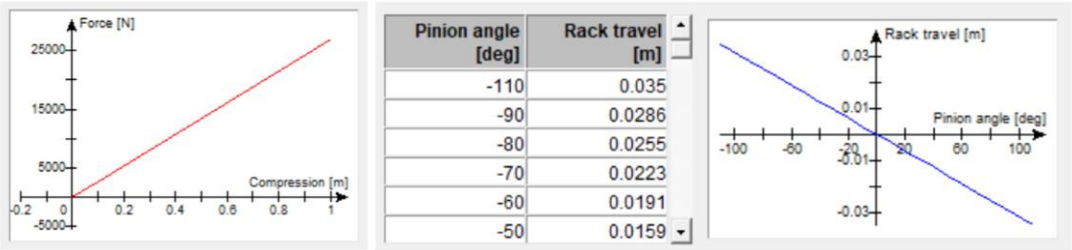

Figure 45 - Springs (left) and steering (right) definition

Individual bushing stiffness based on previous measurements were defined for the suspension components, to include the effect of elastokinematics (view figure 46).

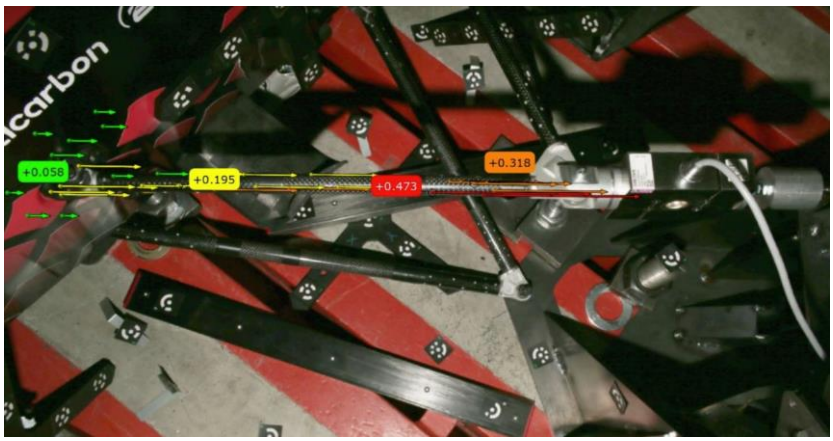

Figure 46 - Front axle elastokinematics measurement [23]

The chassis was assigned the torsional stiffness obtained from last year's measurement results. The composite chassis is placed on a rig with a swing arm, on which a torsion force is applied. A photogrammetry camera is used to measure the deformation of each individual point, that is placed on the chassis (seen in figure 47), from which it is possible to obtain the overall torsional stiffness of the car [21].

Figure 47 - Validation of the chassis torsional stiffness via a photogrammetry method [21]

Aerodynamic properties were taken from the last aeromaps, defined for the last season's Dragon single-seater.

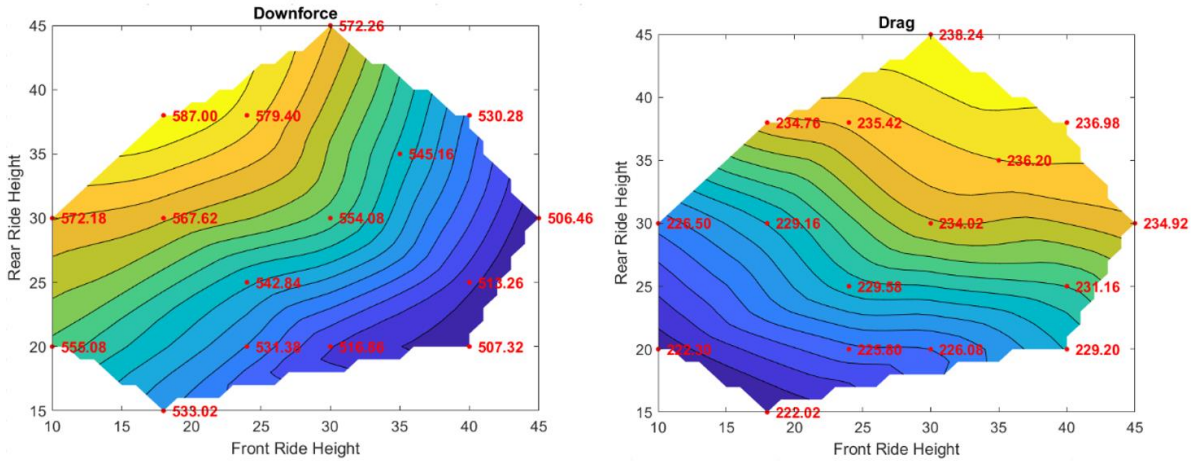

Figure 48 - Downforce and drag values for ride heights combinations [24]

The powertrain model was disregarded, as it was fully implemented already in Simulink (view figure 31), and the 10" formula student tire model was already pre-defined in the simulation program.

IPG Carmaker allows to define virtual sensor mountings, which provide simulated data acquisition, and gives a first estimate of how the data will be measured and processed. The virtual INS unit was placed in the vehicle's centre of gravity and its output connected to the Simulink model.

After the virtual vehicle, the driver and track settings needed to be updated as well.

6.2.2 TEST TRACK

Formula Student tracks are more akin to karting tracks than to those of Formula 1. These tracks are indicated by cones, they range roughly 3 meters in width, and are made mostly out of corners. The layout of the endurance track from the 2023 competition held in Hungary can be seen in figure 49. The figure illustrates, how the track compares in size to the Hungaroring racetrack itself, on which it is built.

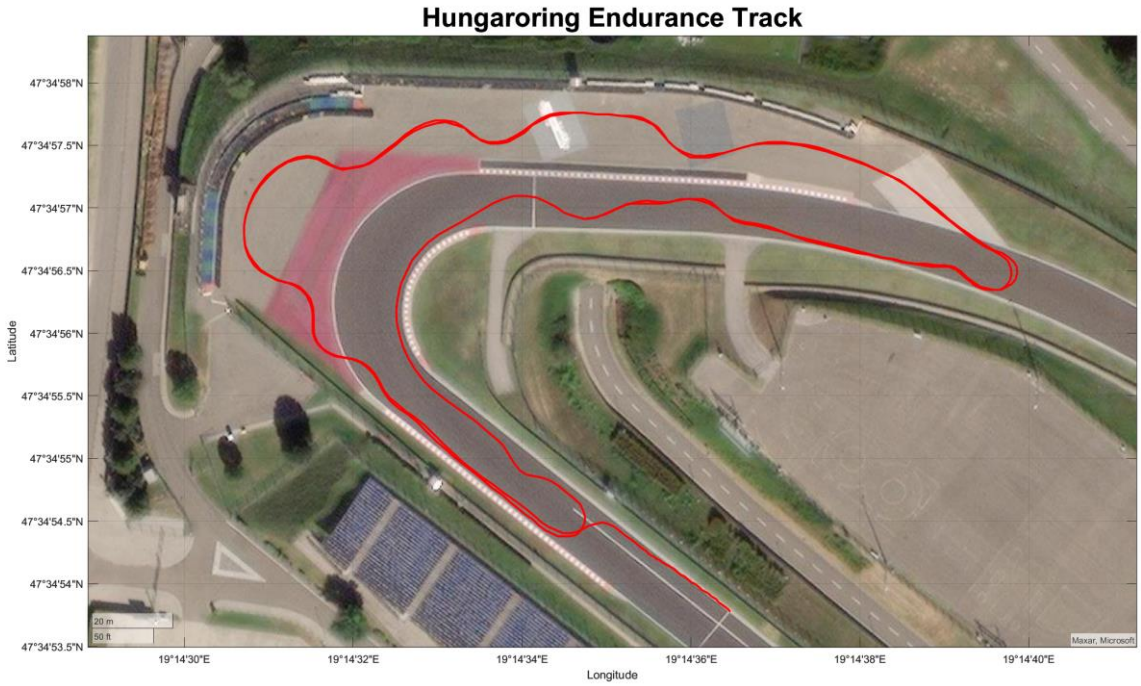

Figure 49 - Endurance track layout at Hungaroring

A layout model of the FSG track from previous years was already available in the Carmaker library but showed itself to be too complex for the first testing and tuning of the algorithm. For this reason, a simpler track (seen in figure 50), made from corners most common for a formula student track, was designed. It consists of a single and double lane change segment, low and high-speed corners, a U-turn after a long straight line and a full circle, which tests the steady state cornering.

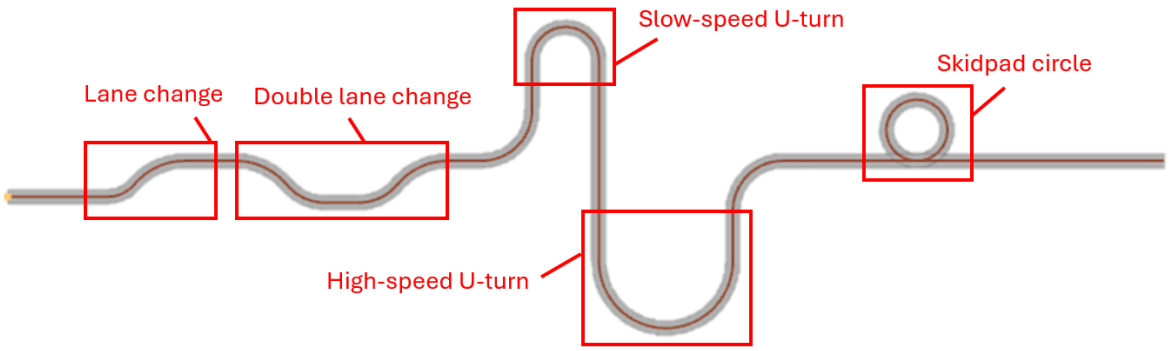

Figure 50 - Torque vectoring virtual test track

6.2.3 DRIVER SETTING

The driver has a major influence on where the vehicle will be in term of performance during the drive. It is thus crucial to define him correctly, to be able to benefit from the torque vectoring system. The virtual driver is defined through maximum lateral and longitudinal accelerations he is allowed to reach. A preset of an "aggressive" driver was chosen as he should represent a racing driver, and his maximum longitudinal and lateral accelerations were taken from previously measured track data to represent the driving style of the team's driver (figure 51).

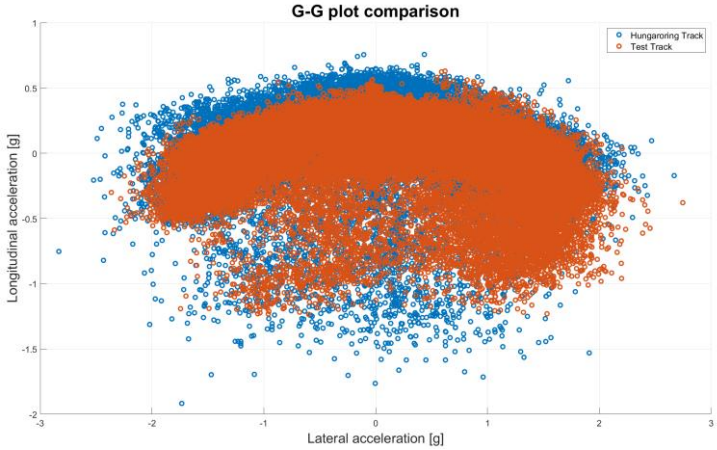

Figure 51 - G-G plot of two different track drives

However, after running the simulation, the thought of creating a custom driver to simulate the team's driver style proved to be a false approach. As the torque vectoring system is supposed to create more available cornering speed, its increase is connected to a higher lateral acceleration (as seen in equation 9) which is then blocked by the driver settings. As a result, when driving with torque vectoring, the driver is not allowed to cross his defining acceleration, making him compensate for the added yaw moment by reducing the steering wheel angle while maintaining the same speed (view figure 52).

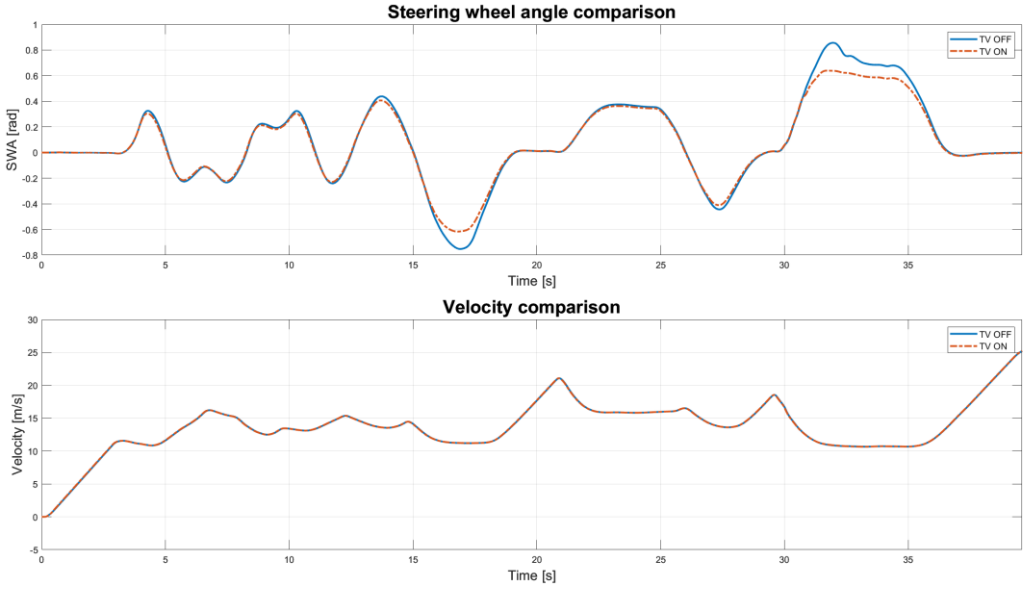

Figure 52 - Steering angle and velocity data from a drive with the custom driver

To solve this issue a racing driver setup, where a series of manoeuvres define the vehicle's driving limits, proved to be a better option. Those are saved into the driver's settings, making him always drive at the limit of handling, presumably resulting in the fastest lap time. Said driver was defined separately for the vehicle with, and without the torque vectoring system, to observe the difference between the two car's limits. Even though this setting does not show, how the system could benefit a non-professional driver, it allows to observe how the torque vectoring system increases the vehicle's performance barrier, which is the main goal of its implementation.

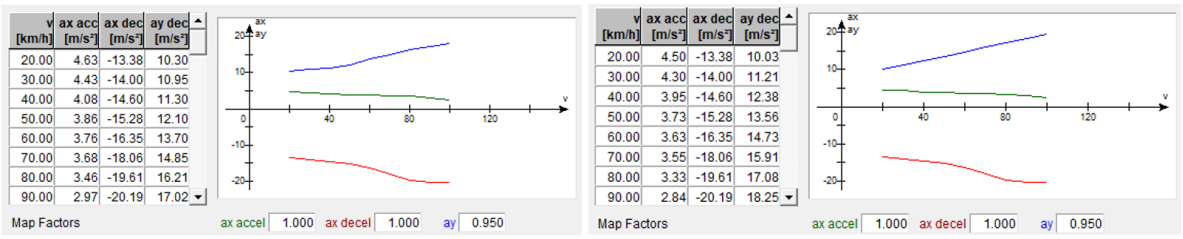

Figure 53 - Race driver definition for a vehicle with (right) and without (left) torque vectoring

By comparing both drivers, while the longitudinal acceleration experienced minor changes, and the deceleration remains almost identical (view figure 53), the lateral acceleration (indicated by the blue line in figure 53) is the main differentiating factor between the two settings. The driver adapted for the vehicle without torque vectoring has a lower threshold of lateral acceleration, which at the same time increases at a slower rate, than the driver trained in the vehicle with the system activated. This already proves, that the vehicle with the implemented torque vectoring algorithm has an increased cornering potential, as it provides the driver with more lateral acceleration, giving him the possibility of driving through the turn at a higher velocity, as the two variables are directly related (equation 9).

Table 5 - lateral acceleration limits of both drivers with increasing velocities

Velocity [km/h]	Lateral Acceleration [m/s^2]	
	Without TV	With TV
20	10.30	10.03
30	10.95	11.21
40	11.30	12.38
50	12.10	13.56
60	13.70	14.73
70	14.85	15.91
80	16.21	17.08
90	17.02	18.25
100	18.11	19.43

6.2.4 ALGORITHM IMPLEMENTATION

After having fully defined the virtual environment, the necessity of making some adjustments in the torque vectoring algorithm appeared, so that it may be implemented it in the simulation. IPG offers the option to fully integrate the Carmaker functionality into the Simulink environment. Combining both software results in the possibility of altering simulation signals and implementing custom system blocks through Simulink into the Carmaker simulation [20].

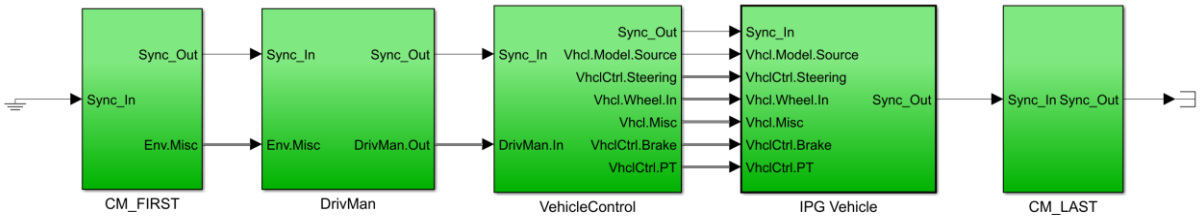

Figure 54 - Carmaker execution block in Simulink [20]

The torque vectoring block was implemented in the IPG Vehicle block, where it alters the torque values that are sent from the motors to the wheels. The input parameters were defined through specific Carmaker-for-Simulink call functions, and yaw rate was read directly from the inertia sensor in the vehicle. The driver-requested torque was defined in the powertrain model block by reading the throttle pedal signal and wheel rotational velocities. The signal was combined with the PI regulator output, which defines the corrective torque value that needs to be assigned to the wheels. A block with limiting factors was added at the end, where the torque vectoring is switched off if the throttle pedal signal is zero, or if the steering wheel angle is within a small angle range, so that there is no additional torque being distributed when coasting or travelling in a straight line. The resulting algorithm scheme is seen in figure 55.

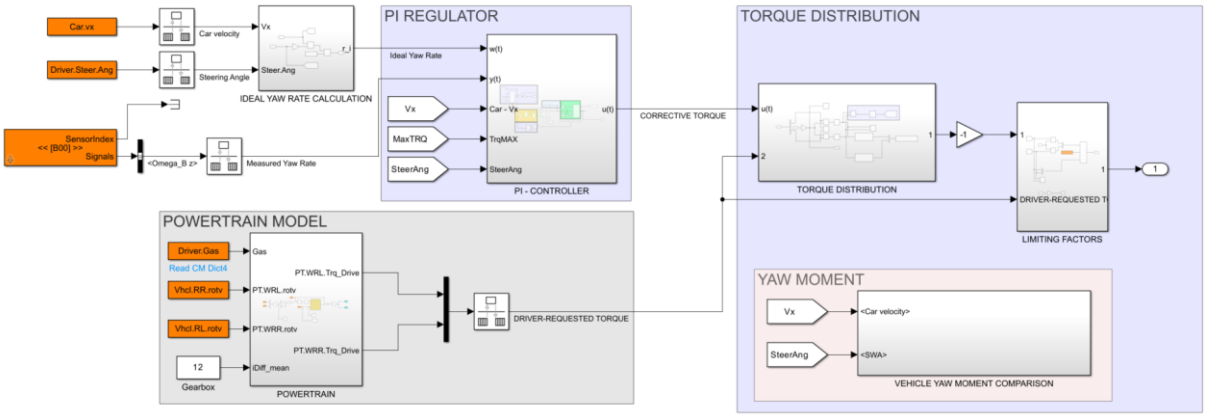

Figure 55 - Torque Vectoring control system block

6.3 SIMULATION WITHOUT TORQUE VECTORING

As a first test of the whole virtual environment, a successful drive through the track without the TV system was computed. The simulation results allowed for a first comparison of measured and calculated variables and a first analysis of the PI controller output. Table 6 shows peak data values from the track drive. Values at the end of entry and exit straight lines of the track are excluded, to compare the driver behaviour at corners, which is the main objective.

Table 6 - Peak simulation values without TV at corners

Drive without torque vectoring	
Maximum values at corners	
Lap time [s]	40.541
Velocity [m/s]	19.391
Steering wheel angle [rad]	0.702
Yaw Rate [rad/s]	1.246
Throttle pedal position [-]	0.648
Lateral acceleration [g]	1.350

6.3.1 DRIVER INPUTS

The vehicle completed the lap in just over 40.54 seconds without exceeding any track limits. The driver inputs are shown in figure 56, where the progress of throttle pedal and steering wheel angle positions are displayed, allowing for a first analysis. There is no major twitching motion of neither the steering wheel nor the throttle position, indicating a clean drive through the track.

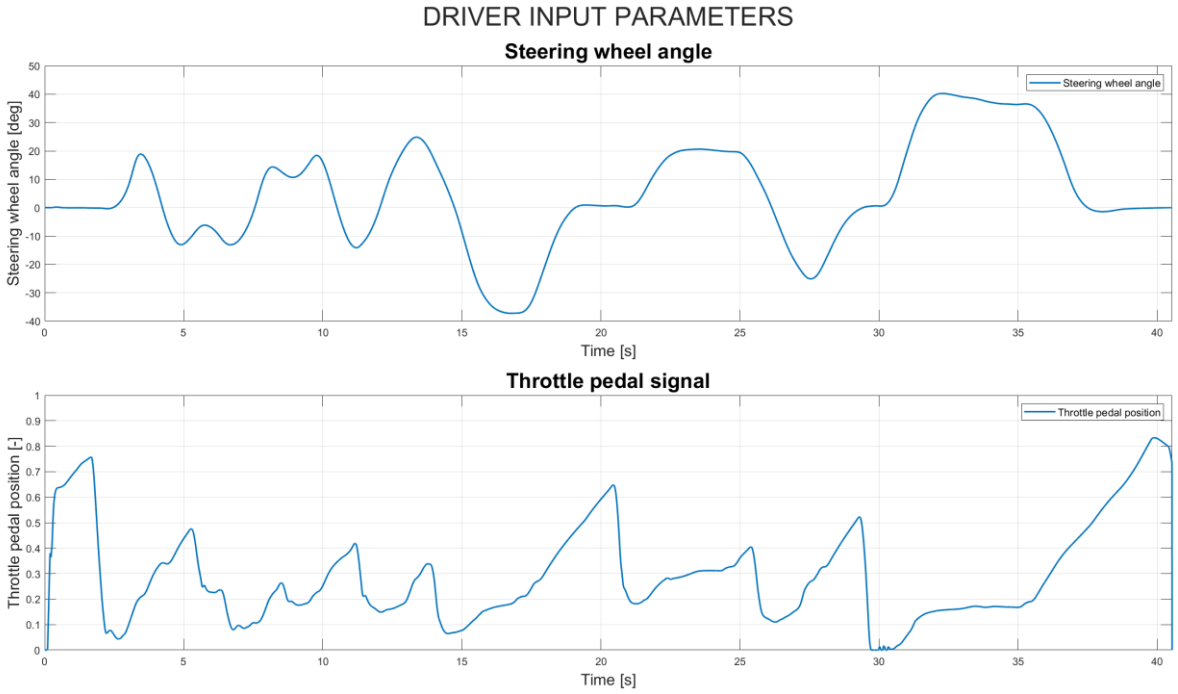

Figure 56 - Driver request signals from simulation without TV

6.3.2 YAW RATE

An analysis of the ideal vs measured yaw rate comparison was made and indicates the potential gap in cornering performance. As defined earlier, the ideal yaw rate is calculated from steering wheel and vehicle velocity data. As the simulation is done in an ideal virtual environment with a perfect racing driver, the difference between the ideal and measured yaw rate is not in all cases as large as the one calculated from previous track data shown in figure 40. Nonetheless, the virtual vehicle does not reach its potential yaw velocity in every corner.

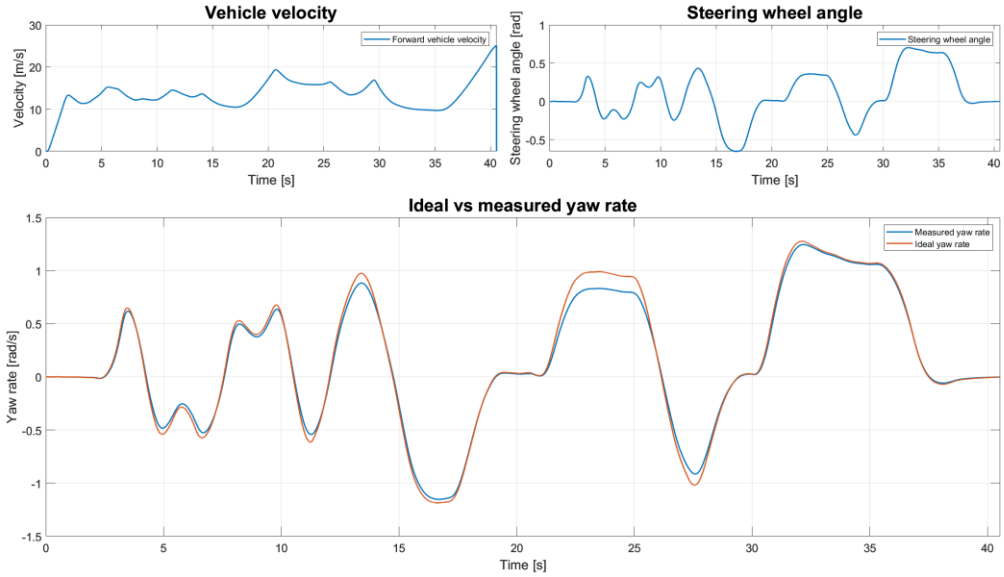

Figure 57 - Ideal and measured yaw rate simulation results (no TV)

Despite the smaller difference in figure 57, there is still performance to be gained from implementing the torque vectoring system. The ideal yaw rate reaches higher values for every corner, even if its difference varies throughout the track. The closest that the vehicle gets to the ideal value is during the drive through the steady state circle (view figure 58). On the contrary, the highest potential for improvement is at the high-speed U-turn corner. Otherwise, there is small amount of yaw velocity difference at every corner section of the track.

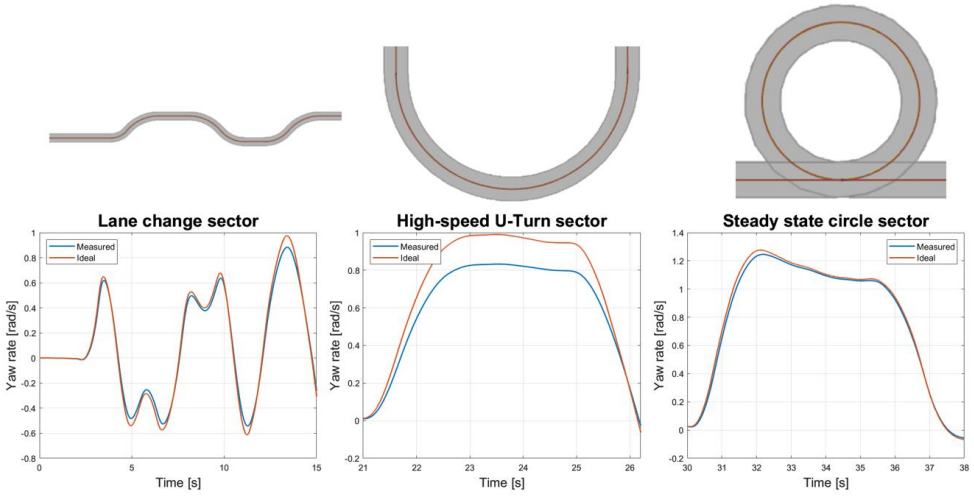

Figure 58 - Yaw rate comparison for track sectors

6.3.3 REGULATOR OUTPUT

The yaw rate difference enters the PI regulator as an acting variable, where the output is wheel torque value, which is subtracted and added to the corresponding driven wheels. The original regulator output is portrayed in figure 59 in the upper graph, which shows it is in need of some refining for the virtual simulation. When comparing yaw rate data from figure 57 with the regulator output, the steady state circle needs very little torque difference, as the measured yaw rate is very close to the ideal one. On the other hand, much larger torque difference should be allocated during the high-speed U-turn. However, when looking at the untuned regulator output, the opposite is true, where much more torque difference is being sent to the wheels when it is not needed.

This was caused by the steering compensator value inside the PI regulator which needed to be reduced, as it overly emphasised the steering wheel angle. The PI values were further tuned, for the regulator to give most reasonable simulation results. Its resulting output is portrayed in the bottom graph of figure 59. Its value is now much more realistic when compared to the yaw rate error in figure 57. More refining will be done during practical testing, as the virtual and real environment are not alike, and it is crucial to make the system work correctly on track.

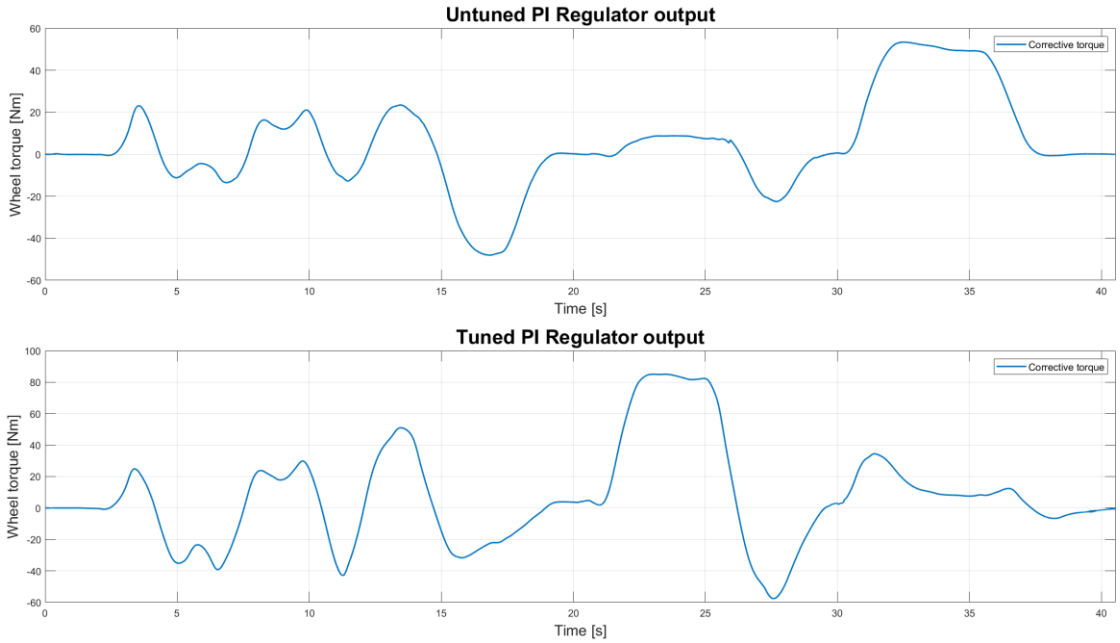

Figure 59 - PI regulator output signal

6.3.4 YAW MOMENT

Although the single-seater Dragon is not equipped to properly measure yaw acceleration and therefore yaw moment, their comparison can be done by correctly processing the measured yaw rate data. Yaw moment is not an acting variable in the torque vectoring system but enables the observation of the ideal and actual values of yaw acceleration during the corner entry and exit, to further understand the vehicle's behaviour. Yaw moment peak values are a useful indicator of the vehicle's responsiveness at turn in and out of the corner, where the higher the yaw acceleration, the faster the vehicle can reach its steady state, making yaw moment a good indicator of the car's agility (discussed in chapter 3).

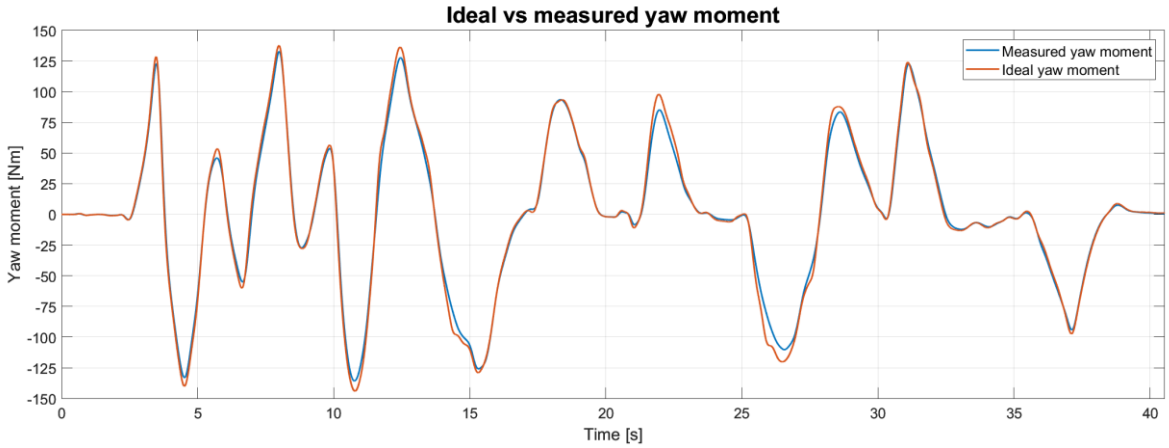

Figure 60 - Yaw moment comparison (no TV)

It is no surprise that the yaw moment behaviour in figure 60 follows yaw rate behaviour, where the biggest improvement in corner entry and exit can be at the high-speed U-turn. Compared to yaw rate, it is not possible to observe the car behaviour in a steady state due to yaw acceleration being zero. Figure 60 shows that turn entry and exit can be improved for most of the track's corners, and it could even be desirable to exceed the ideal yaw moment value, as it would make the vehicle oversteer, thus making yaw velocity rise at a faster rate, reaching steady state earlier.

6.3.5 WHEEL TORQUE

Lastly, it is possible to observe in figure 61 the torque allocation that would have happened if the system was active during the drive. The wheel torques values are being altered smoothly and according to the regulator output from figure 59. However, they are bottoming slightly at certain points, creating the possibility of not always reaching the ideal yaw rate. A more detailed analysis of torque allocation will be done, after running the simulation.

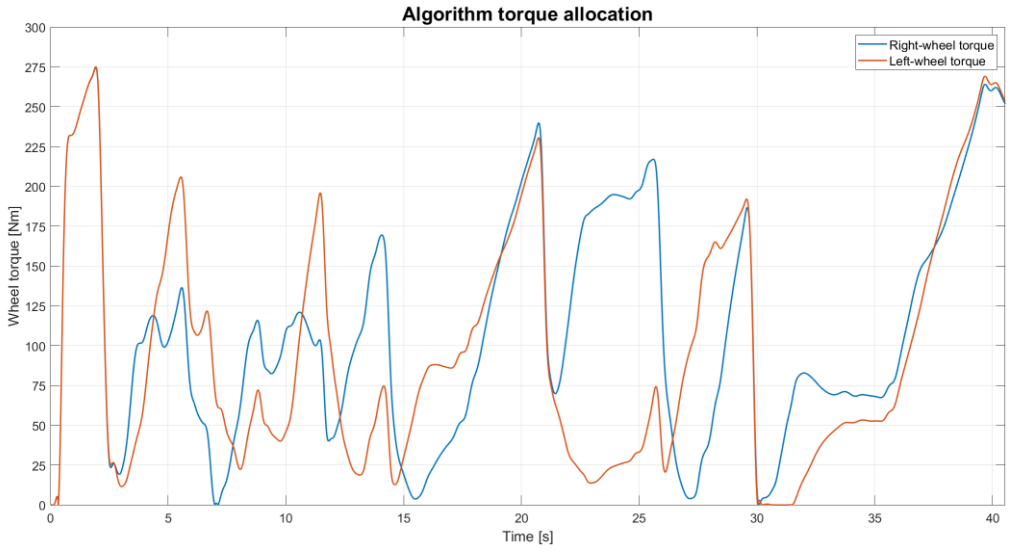

Figure 61 - Theoretical wheel-torque distribution

6.4 SIMULATION WITH TORQUE VECTORING

From the vehicle behaviour analysis in the previous chapter, the vehicle with torque vectoring seems to be better at reaching its potential at low-speed corners but lacks in performance in high-speed corners, as well as quick-turns, which require a quicker response to steering inputs. The simulation was run again, this time with an activated torque vectoring system and with a racing driver adapted to it.

Table 7 - Peak simulation values with TV at corners

Drive with torque vectoring	
Maximum values at corners	
Lap time [s]	38.589
Velocity [m/s]	19.540
Steering wheel angle [rad]	0.688
Yaw Rate [rad/s]	1.304
Throttle pedal position [-]	0.657
Lateral acceleration [g]	1.511

The peak values expressed in Table 7 are listed for indicative reasons, and a deeper data analysis is necessary to establish the influence of torque vectoring. However, the track time was reduced by 1.942s, which represents a significant improvement. Further, the peak yaw rate value increased, although not by as much as expected, followed by an increased maximum velocity. An unexpected change has been recorded in steering angle peak, which is lower than in table 6. The vehicle goes through the same turn with a smaller SWA.

To appropriately compare all inputs and variables between the two drives, the driven track distance is set as the graph's x-axis, to have the data align properly. If the comparison was to be done in time domain, there would be an offset between the data with and without TV, as both lap times are different.

6.4.1 DRIVER INPUTS

The throttle pedal position in figure 62 shows the second driver putting in a higher throttle request at corners.

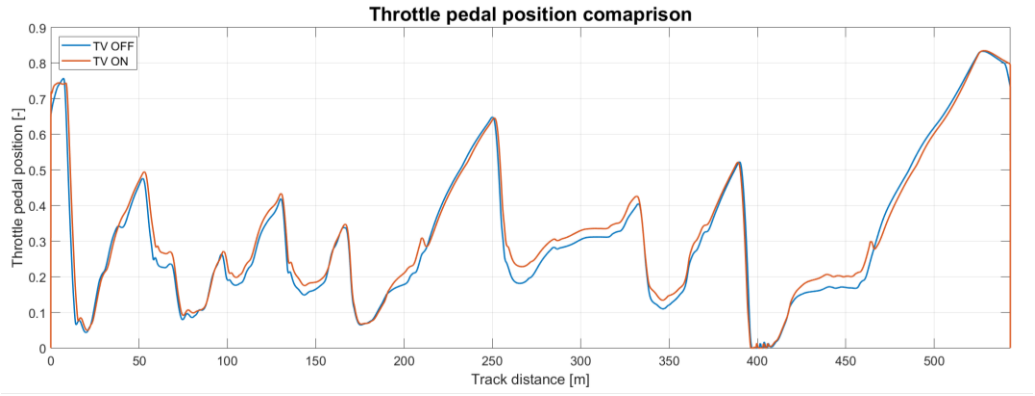

Figure 62 - Throttle pedal position comparison

Figure 62 also shows that the driving style does not vary significantly, the throttle pedal signal progress throughout the track is similar for both drives. On a straight line, both drivers have similar signal inputs, meaning that the straight-line driving is not affected by torque vectoring. However, there are two sudden step-decreases in throttle pedal position, both at an exit out of a corner onto a longer straight line. This might indicate a potential downside of having a torque vectoring system at corner exit and is analysed further in this thesis with other variables.

When comparing the steering wheel angle, its value is slightly lower for every corner, as seen in figure 63. The same driver behaviour was undesired when dealing with a custom driver (view figure 52), however the difference is much smaller.

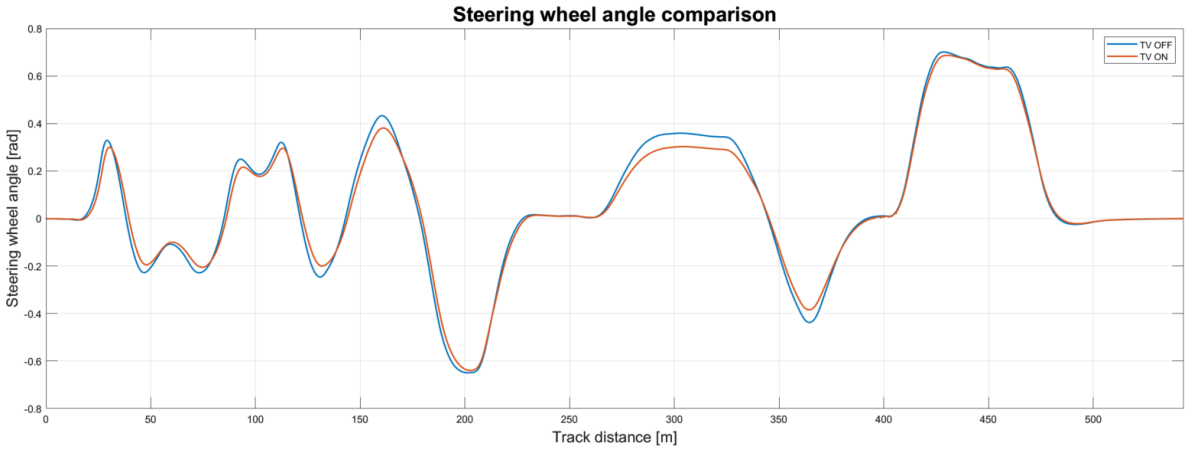

Figure 63 - Steering wheel angle comparison

As the driver's limits were not defined manually, but through driving manoeuvres in the simulation, the suspected reason for still not reaching the original steering wheel angle entirely are tire limits. The tire can withstand a certain combination of longitudinal and lateral force, where the magnitude of one is affecting the other [9]. With torque vectoring applying a higher torque on the outside wheel comes the consequence of reducing the maximum possible lateral force said tire is capable of generating. If the driver would try to reach the original steering wheel angle, there is a possibility of loss of grip due to exceeding the maximum lateral force, that the tire is capable of holding. On top of that, with the torque vectoring system active, an increase in steering wheel angle increases the ideal and measured yaw rate difference, adding more torque to the outside wheel and further reducing the maximum lateral force.

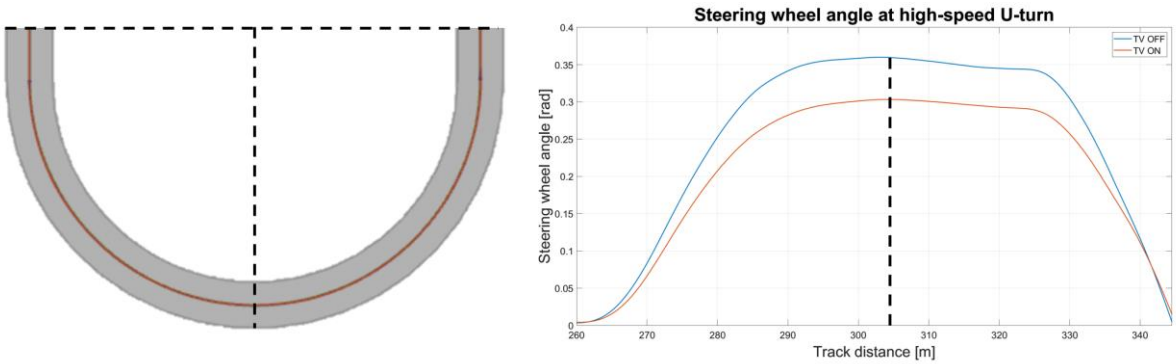

Figure 64 - SWA comparison at the high-speed U-turn sector

This reasoning was confirmed when observing the high-speed U-turn segment of the track seen in figure 64, where the difference between the steering wheel angles is the most significant. When looking at the tire model, it is possible to analyse the available combination of maximum longitudinal and lateral forces that it can withstand. To establish where the vehicle is situated on the friction ellipse, the following values at the middle of the turn for the rear outside tire were taken, as it is the one under the highest vertical load.

Table 8 - Dynamic values for the rear outside tire

Variables	Symbol	Unit	TV OFF	TV ON
Vertical wheel load	F_z	[N]	1481	1614
Longitudinal force	F_x	[N]	388	934
Tire slip angle	α	[deg]	-1.321	-1.865
Latera force	F_y	[N]	902	1284

With the information above it is possible to pinpoint where the two cars put the rear outside tire on a friction ellipse.

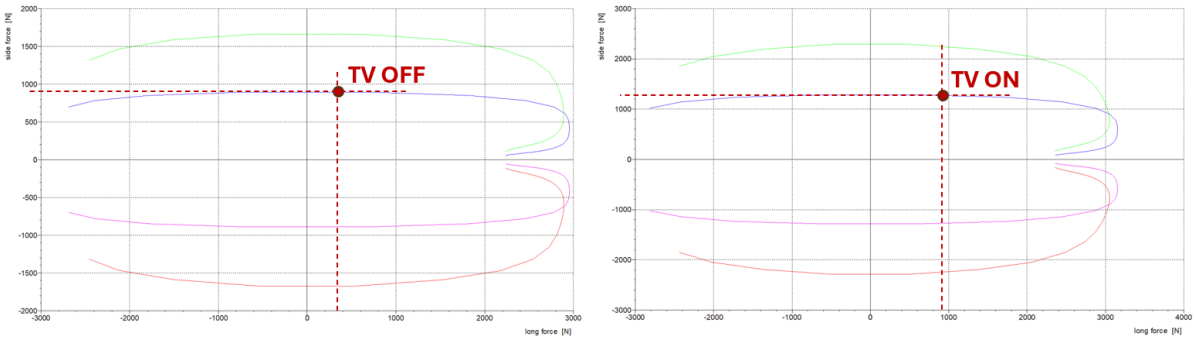

Figure 65 - Comparison of the rear outside tire properties

Figure 65 shows that the car with torque vectoring puts the rear outside tire more towards the right side of the plot by having almost three times more longitudinal force (see table 8). Consequently, the maximum side force, that the tire can generate is reduced. However, the reason why the tire can still generate more overall side force than the one without TV is that, by having more velocity, meaning a higher lateral force, the outside wheel is under a higher vertical force (view table 8) due to load transfer, increasing the maximum tire limits as a result.

The conclusion that can be drawn from this is that, compared to figure 52 where the limits were defined by the driver's capabilities, it is now the physical tire properties that are preventing the car from reaching the ideal yaw rate that was assumed during the drive without torque vectoring. If the driver attempted to match the steering angle of the previous drive, an increase in the longitudinal force would create a decrease in lateral force. Since the driver is already driving at the tire's limit, the current side force would be too high for the tire, resulting in a loss of grip.

In conclusion, the assumption of the vehicle reaching the original ideal yaw rate after implementing the system was partially incorrect, as introducing more torque to the outside

wheel reduced the side force potential. As a result, it is a combination of the reduction of the ideal yaw rate and an increase of the actual one that makes both values meet.

Such a change in behaviour should not negatively affect the cornering ability of the car, since the torque vectoring system is designed to correct any yawing error, and it is only the physical limits of the car that prevent it from reaching the assumed ideal value which was calculated from the drive without the system. From further analysis conducted in this chapter, torque vectoring can clearly increase the vehicle performance limits. However, it might take some time for the drivers to get used to the car's new behaviour and to adapt their driving style. Special care when tuning the regulator during testing will be necessary to ensure a good balance between performance and handling, as it is not possible to directly measure the wheel forces as it is in the simulation.

Despite the steering angle difference, the driver is performing equally as smoothly as in the car without the control system, the exception being the breaking point before entering the steady state circle. Looking closer at the data in figure 56, the driver is already turning in, therefore it is suspected that the torque vectoring system is delivering torque to the outside wheel despite the driver pressing the brake pedal. This is reaffirmed in figure 66 on the left side, where the right-wheel torque never reaches a zero-value during deceleration and starts to increase in magnitude instantly whereas the inner wheel remains at zero-value for a longer time. Although this should not cause any complications during driving as the highest oscillation has a peak-to-peak value of 0.01 rad (0.573°), which is within the free play range of the steering wheel, it was resolved by implementing a condition block that stops all torque distribution if the brake pedal value became non-zero and the car showed no further issues (view figure 66 – right side).

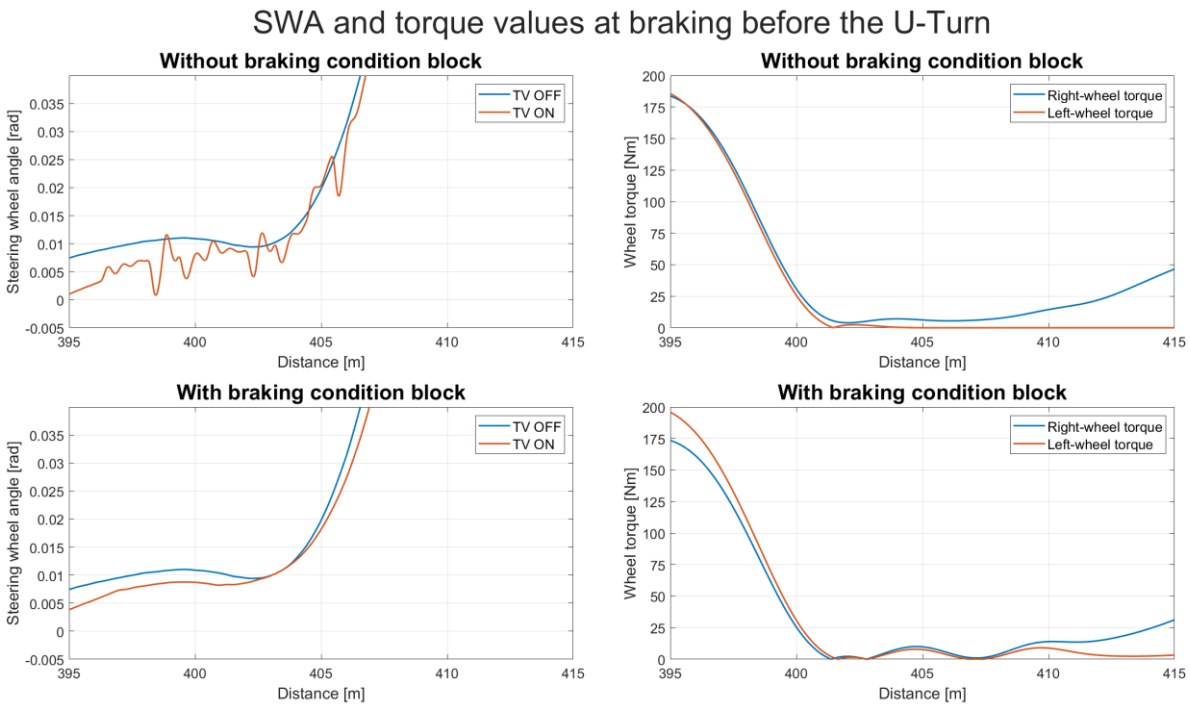

Figure 66 - Resolving the unstable steering behaviour due to torque distribution at braking

6.4.2 VELOCITY AND YAW RATE

The positive impact of torque vectoring can be already seen from the faster lap time. Another indicator, which will be subject to further analysis, is an increase in velocity during cornering.

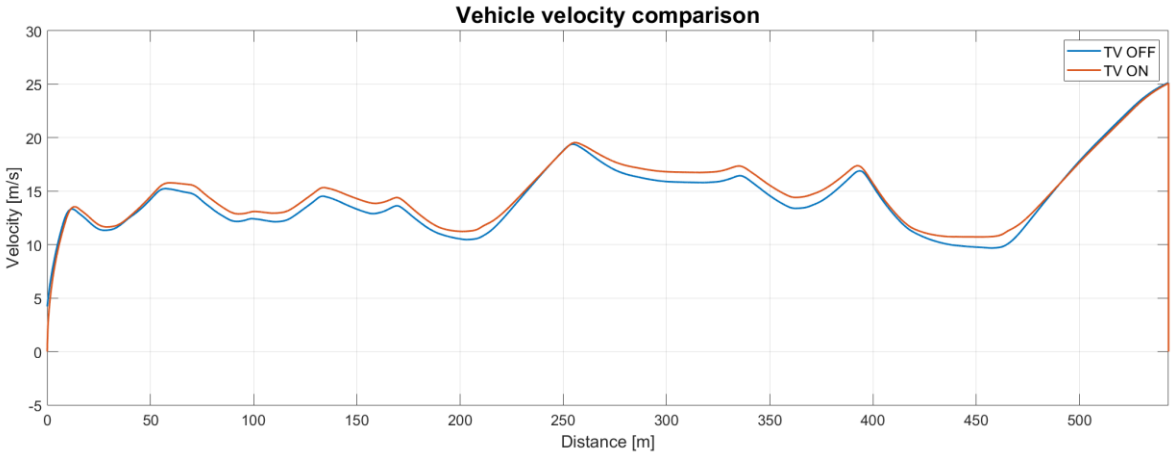

Figure 67 - Vehicle velocity comparison

As figure 67 clearly shows, higher cornering speeds were achieved by implementing the TV system, as well as a more consistent speed profile at steady states (view figure 68). As already observed in throttle pedal signal in figure 62, the figure above shows the longitudinal velocity experiencing a decrease in slope when rising in value, resulting in a smaller acceleration out of a corner. Nonetheless, the car with torque vectoring is accelerating from higher cornering speeds, therefore staying ahead most of the time. A conclusion as to why the driver doesn't exit the turn faster will be made after analysing all data outputs from the session.

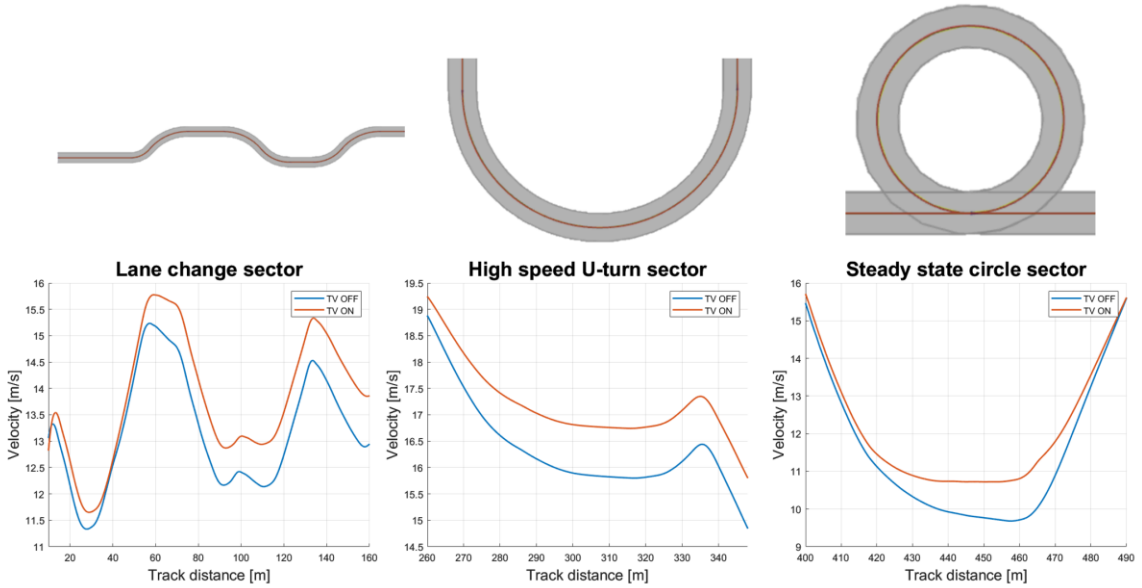

Figure 68 - Track segment comparison for velocity

The original gap between the ideal and measured yaw rate previously shown in figure 57 should be compensated by the torque vectoring system. As it was observed from driver inputs, the original supposition of the measured yaw rate catching up to the ideal one was not entirely

correct, as the ideal value also changed from the original one, due to a change in steering angle. At the same time, torque vectoring enabled an increase in velocity during cornering (shown in figure 67 and 68 in details) and impacts both yaw rate values as well. The resulting change in both ideal and measured yaw rate values is shown in figure 69.

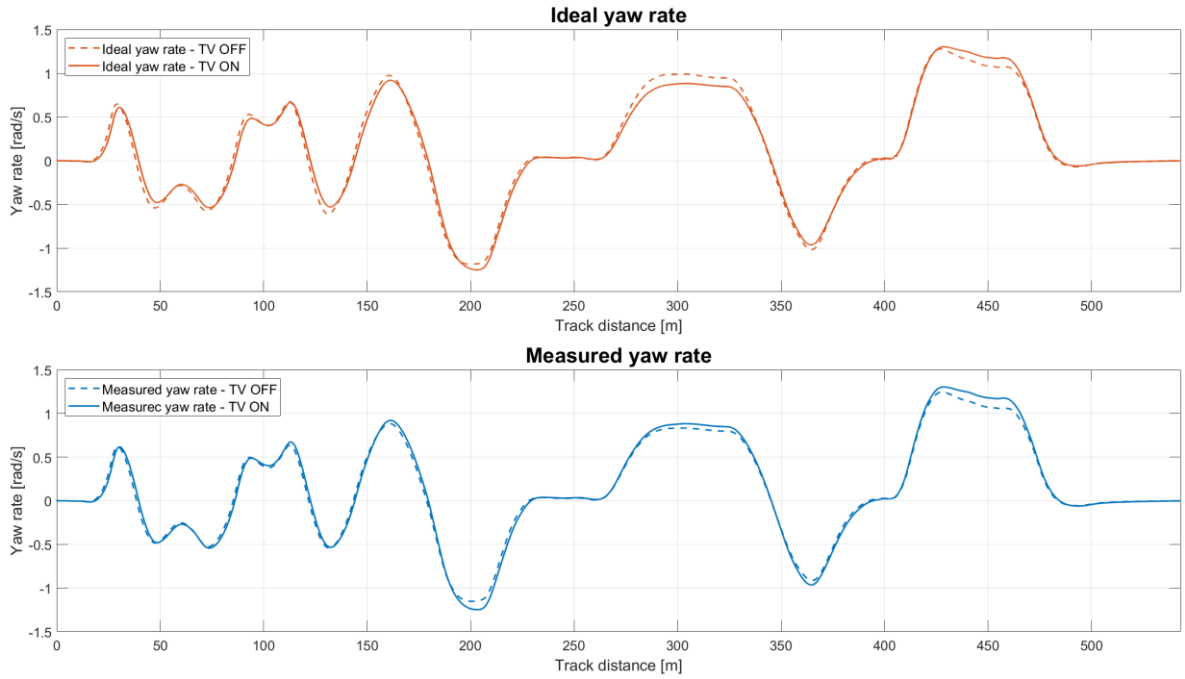

Figure 69 - Change in ideal and measured yaw rate

Going back to equation 26, both steering angle and velocity have the same impact on yaw rate values. However, the change in one unit of velocity affects the result differently than the change in a unit of steering angle. That is why the ideal yaw rate value is lower than the original one, even if there is an increase in velocity, as the decrease of steering angle makes proportionately more difference. An exception to this is the steady state circle at the end, where the difference in said angle is very small (view figure 63) and the difference in velocity surpasses it.

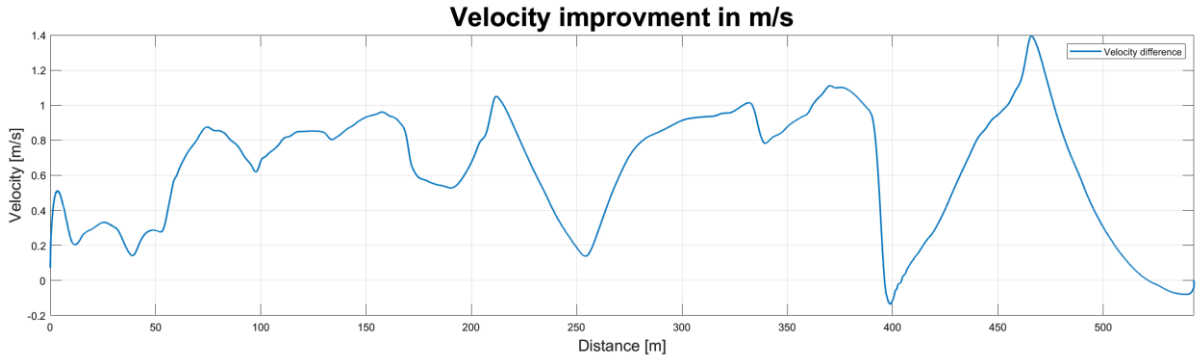

Figure 70 - Velocity improvement during the drive with TV

The steering wheel angle ranges into both positive and negative values. Figure 71 shows the difference between steering angle of both drives in both positive and negative range.

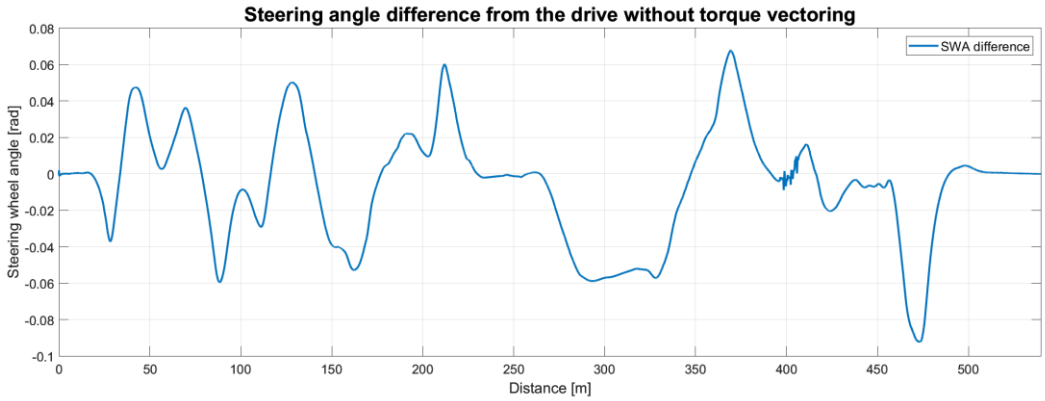

Figure 71 - Steering angle deterioration during the drive with TV

The final values of ideal and measured yaw rate after implementing the torque vectoring system can be taken from figure 69 and are shown overlapping in the figure below.

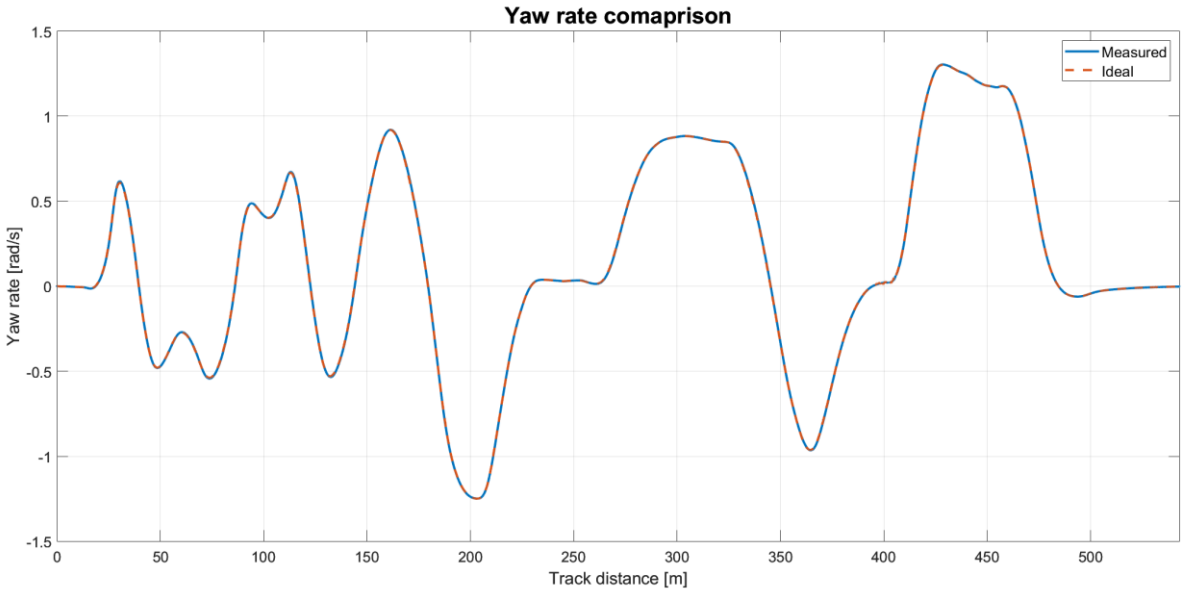

Figure 72 - Ideal and measured yaw rate simulation results (TV ON)

The torque vectoring system together with its PI regulator are defined well enough for the driver to be able to reach the ideal yaw rate. The illustrated behaviour in figure 72 is the ideal scenario, in which the vehicle behaves exactly as it should. It reaches the ideal yaw rate that is defined from a neutral-steering vehicle, allowing the driver to drive through the corner at higher speeds (seen in figure 67). The torque vectoring system manages to exploit the vehicle's potential at all segments of the track resulting in a lap time that is 1.942s shorter. It should be noted that this is a simulation of an ideal driver in an ideal environment, therefore bearing ideal results when everything is defined correctly. The results of this simulation show, that the torque vectoring algorithm is well designed, and its PI regulator well-tuned. Nonetheless, an extended practical testing session is expected to be able to benefit from the system on a real track with imperfect data acquisition and an unprofessional driver.

6.4.3 YAW MOMENT

The ideal and measured yaw moments are compared in figure 73 to illustrate corner entry and exit behaviour. With the torque vectoring system active this time, the measured yaw moment exceeds the ideal one at every corner, meaning that the car is oversteering at both corner entry and exit. Although this was not the objective, it is a desired behaviour, as the car reaches its steady state sooner. The yaw moment comparison is mostly indicative, expanding the understanding of the vehicle's behaviour, but does not take part in the torque vectoring system.

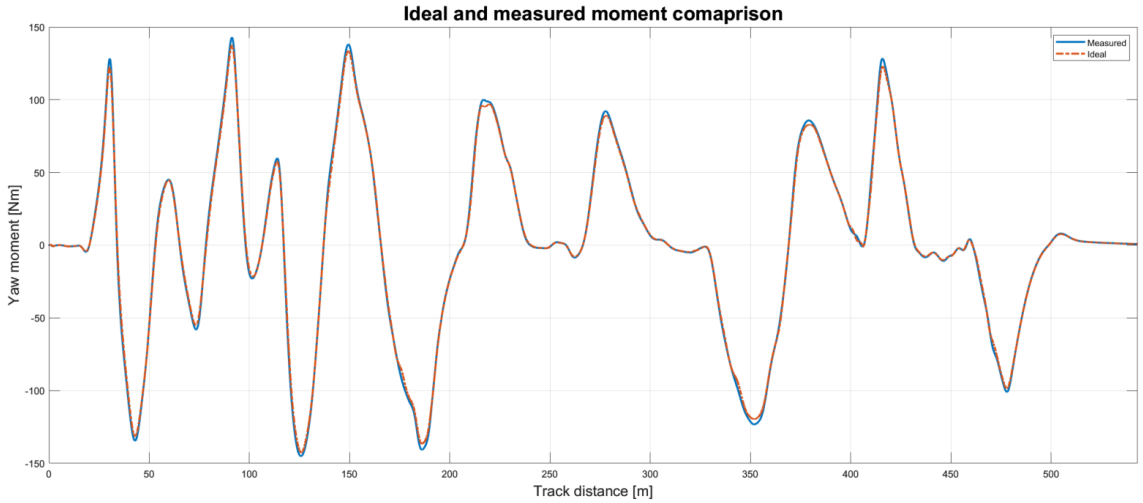

Figure 73 - Yaw moment comparison (with TV)

Yaw acceleration (and therefore yaw moment) could be a future expansion of the algorithm. So far, it is only steady state car behaviour which serves as an ideal car reference. Making yaw acceleration an active part of the system could distribute the torques at corner entry and exit in such a way that the steady state is reached as fast, as the vehicle limits would allow, potentially increasing the vehicle performance even more. Such an expansion would require a two-track vehicle model and advanced information about load transfer and tire properties and is therefore too advanced to be implemented in the first generation of the torque vectoring system. However, it is a possible future improvement once this algorithm is refined enough. Lastly, figure 74 shows the yaw moment difference between both simulation sessions.

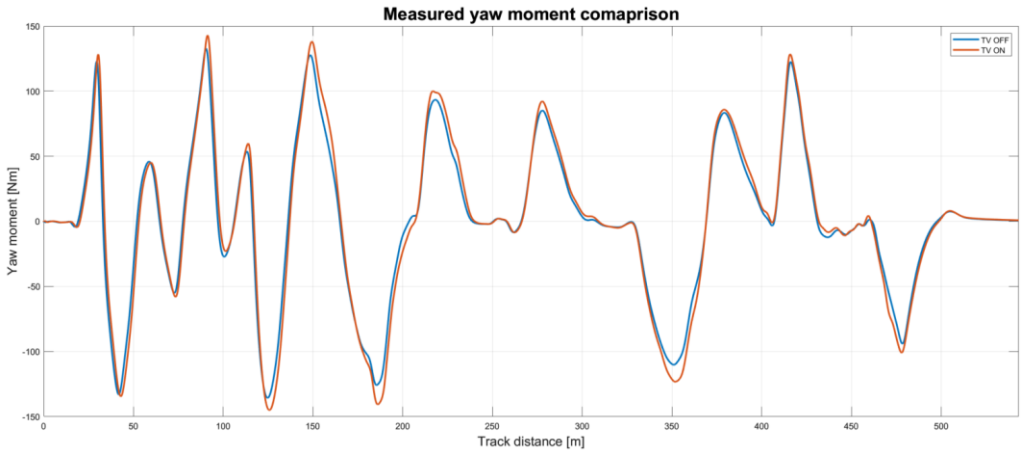

Figure 74 - Measured yaw moment comparison between both drives

6.4.4 WHEEL TORQUE

The resulting wheel torque distribution can be seen in figure 75. The data vary slightly from the ones in figure 61 due to different driver behaviour and therefore different regulator inputs. It is possible to assume that the torque allocation is done correctly due to the overlapping ideal and measured yaw rates in figure 72, which serve as reference. Their values change at a fast enough pace to always deliver the higher torque to the outside wheel during quick turns and there are no oscillations whatsoever. There are still times when the inner wheel reaches a torque value of zero, which was considered as a potential problem in terms of reaching the ideal yaw velocity. However, figure 72 clearly shows it is not the case, so there is no need to address it. If this turns out to be an issue during testing, it will be examined more closely.

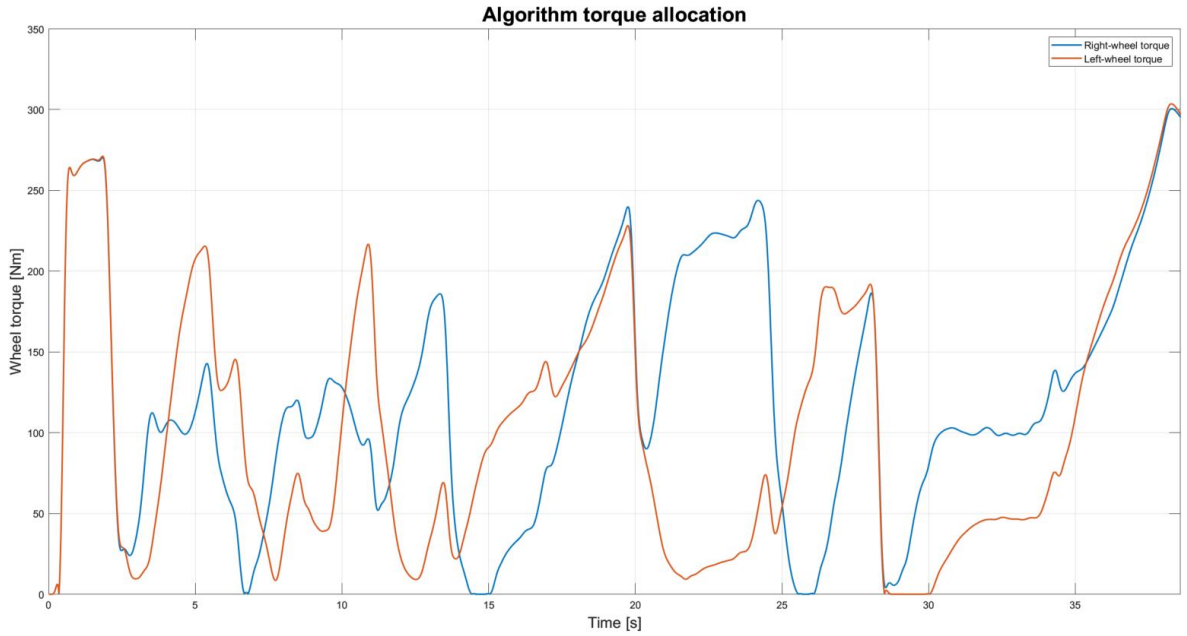

Figure 75 - Final torque distribution of the algorithm

As expected from the yaw rate difference, the highest torque difference is recorded at the high-speed U-turn, where the left-wheel torque comes close to zero values. Both the left and right wheel have equal torque values when driving on a straight line and at heavy braking points. The two different cases are pictured in figure 76.

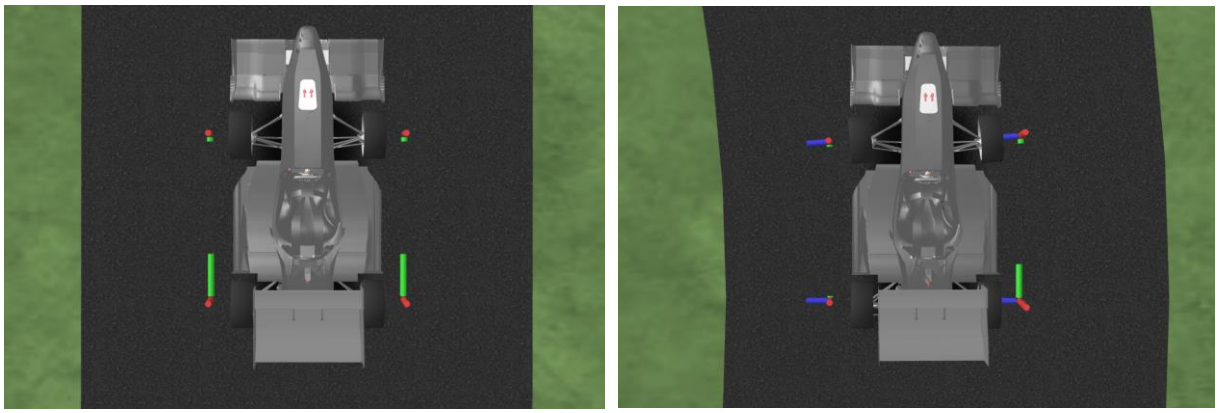

Figure 76 - Torque distribution on a straight line (left) and the high-speed U-turn (right)

6.5 VEHICLE COMPARISON

From the simulations of the virtual Dragon e4 model, it is possible to summarise the difference that the torque vectoring system makes in terms of control and performance. The simulation track was divided into sectors (view figure 77) for a better visualisation in different corners. For each corner the key variables that were analysed before, are divided into corner entry, middle and exit, for a better understanding of which part of each corner is influenced by torque vectoring the most, and to determine if there are similarities between the sectors.

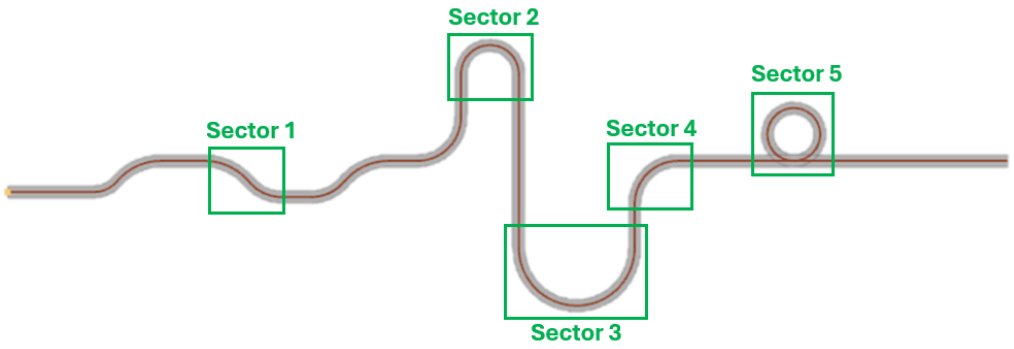

Figure 77 - Track division into sectors made from different types of corners

6.5.1 VELOCITY

By having the system active, the driver was able to achieve higher velocities and lateral accelerations. The overall improvement from the original speed throughout the whole track drive is expressed in both m/s and percentage and displayed in the figure 78.

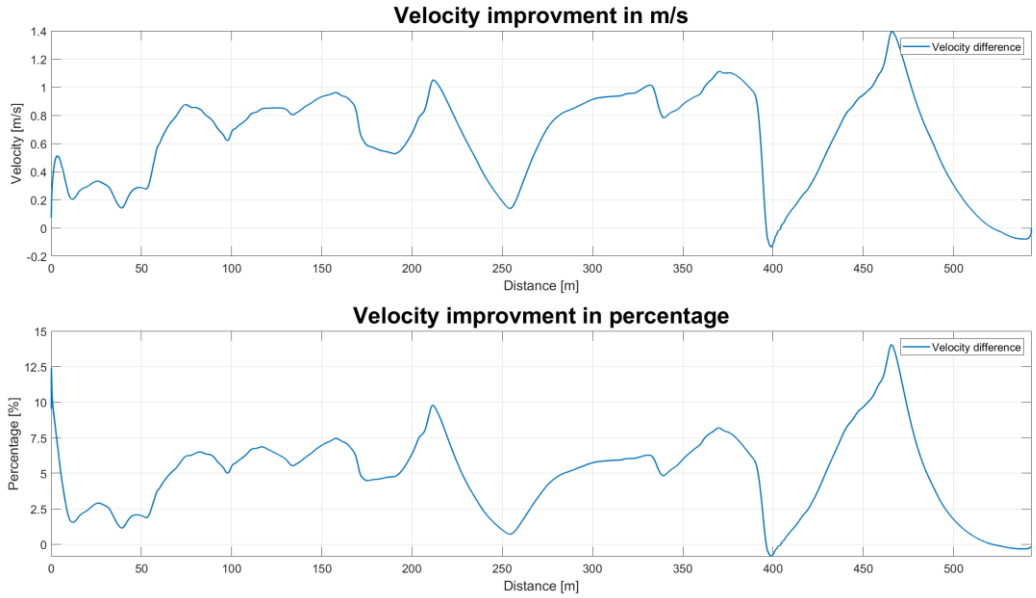

Figure 78 - Increase in velocity after activating the TV system

Figure 78 shows the progress of the velocity difference throughout the track and table 9 lists individual values at defined sector entries, middles and exits.

Table 9 - Velocity improvement at track segments

Vehicle velocity improvement						
Track sector	Corner segment					
	Entry		Middle		Exit	
	[m/s]	%	[m/s]	%	[m/s]	%
1	0.409	2.67	0.379	2.57	-0.391	-2.812
2	0.571	4.776	0.759	7.245	0.28	2.174
3	0.289	1.639	0.86	5.406	0.844	5.211
4	1.008	6.805	0.948	7.023	0.692	4.74
5	0.37	3.028	0.863	8.749	0.783	6.686

Figure 78 shows that the vehicle with the system active is faster through most of the turns, except at the corner entry of the steady state circle, where its velocity is smaller by 1% of the original value. This was caused by the unstable braking and was resolved by implementing the braking condition block. It is possible to observe that the highest velocity difference is mostly in the middle of the corner, that is during steady state cornering. The exception to this is sector 4, where entry speed is higher by 0.059 m/s. Although table 9 represents individual speeds at different parts of a corner, figure 78 enables to see higher increases in velocity situated in-between the defined segments, where the highest is at the end of the circle turn.

6.5.2 YAW RATE

The vehicle reached higher yaw rate values at most corners with the torque vectoring system active, despite the driver turning the steering wheel at a smaller angle. The system maintained the car yawing at the ideal yaw rate, based on which the wheel torques were distributed.

Figure 79 - Measured and ideal yaw rate difference between both drives

The yaw rate data were taken from the comparison of measured yaw rates between both drives seen in the bottom plot of figure 69. Since it ranges into the negative values for right-wheel turns, the absolute values of both yaw rate outputs were used in order to conveniently picture the improvement for all corners (view figure 79).

The sudden drops into negative values of yaw velocity improvement are moments when the yaw rate of the car without TV crosses zero while the car with TV does not. This is another by-product of performance loss at corner exit where, although the yaw acceleration is higher and yaw rate is dropping faster, it reaches its zero value later due to driving at a higher yaw rate during steady state while not dripping to zero fast enough. Further confirmation of this observation is seen in figure 69: at most corner exits, the measured yaw rate of the car with TV reaches zero after the vehicle, that drives with even torque values.

To better visualise the improvement at each track sector absolute values were used to define the difference in positive values and percentage in table 10.

Table 10 - Yaw rate improvement at track segments

Vehicle yaw rate improvement						
Track sector	Corner segment					
	Entry		Middle		Exit	
	[rad/s]	%	[rad/s]	%	[rad/s]	%
1	0.006	1.348	0.005	0.921	0.024	22.857
2	0.043	14.053	0.063	5.063	0.01	3.817
3	0.022	6.897	0.048	5.916	0.001	0.276
4	0.036	19.672	0.041	4.361	0.013	2.702
5	0.048	9.658	0.093	7.648	0.085	19.676

Similarly to velocity, the highest improvement at a corner is during steady state (in basic units, not percentage). As the vehicle reference is its steady state yawing velocity, it is the middle of the corner that should give the most accurate data, making the torque vectoring most effective. The turn entry is improved – although not as much – at all corners, where the highest percentage being 19.672% at the entry to sector 4, and 19.676% at the High-speed U-turn exit. As it has been said, the corner exit is lacking in performance in reference to the original value, and it is possible to see this in both table 10 and figures 67 and 69.

6.5.3 YAW MOMENT

The yaw moment values seen in figure 74 increased in magnitude as well, making the car go from understeering to oversteering behaviour based on the ideal reference value indicating a neutral-steering car. Absolute values were compared again for the same reason, as with yaw rate data.

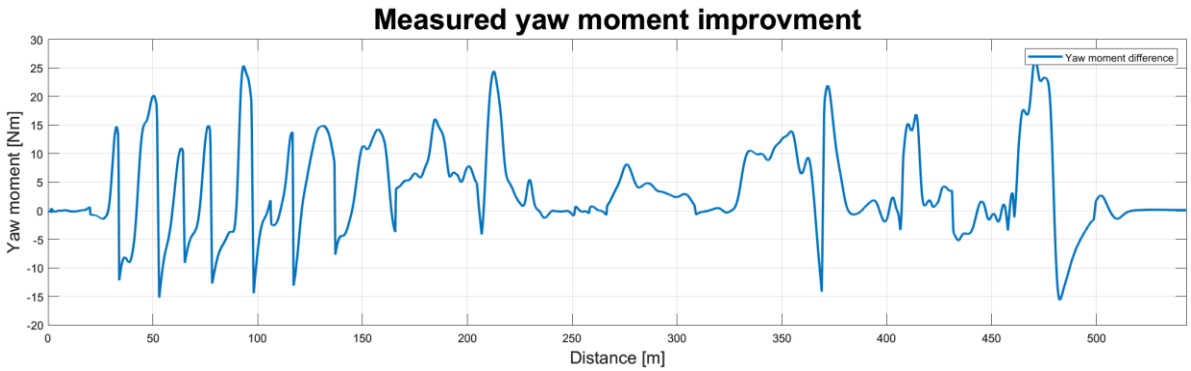

Figure 80 - Yaw moment improvement after activating the TV system

The yaw moment progress shows similar issues as yaw rate, where the car with torque vectoring brings it to zero later, making the improvement drop to negative values. Figure 74 already pictured that the entry and exit yaw moment is higher for every corner, meaning the car oversteers more with torque vectoring. However, seeing both yaw moment curves dropping from their peak at a similar rate in figure 74 confirms the presumption about yaw rate not dropping fast enough.

Table 11 shows improvement in absolute values at the indicated sectors. The middle of each turn was not considered, as yaw moment is near-zero values and doesn't affect the drive, while the improvement in percentage is extremely variable, due to a high sensitivity at smaller values.

Table 11 – Yaw moment improvement at track segments

Vehicle yaw moment						
Track sector	Corner segment					
	Entry		Middle		Exit	
	[Nm]	%	[Nm]	%	[Nm]	%
1	6.098	10.646	-5.959	189.65	-18.949	-16.666
2	13.177	9.468	2.178	74.074	1.742	2.156
3	11.326	12.381	0	0	18.731	18.475
4	8.494	6.964	4.029	41.111	-0.327	-0.405
5	13.721	10.881	3.484	32.99	21.889	21.73

Table 11 indicates an even improvement at corner entry of all track sectors, where the percentage increase varies from 6 – 10%. The percentage reference is the yaw moment at the same track segment that the car without torque vectoring had. The corner exits show a more chaotic behaviour than at the entries, and even a decrease in yaw moment at exits of sectors 1 and 4. On the contrary, the exit of sectors 3 and 5 are characterised by the highest difference in yaw moment, meaning the highest increase in moment, which turns the car outwards of the corner. Clearly, the corner exit is not under full control of the algorithm.

6.5.4 DRIVER ACCELERATION

To summarise the improvements and deteriorations analysed in this chapter, is tantamount to analysing the difference of acceleration limits that both cars provide to the driver. A comparison of lateral and longitudinal accelerations (G-G plot) is represented in figure 81, where both cars, with and without torque vectoring, are compared.

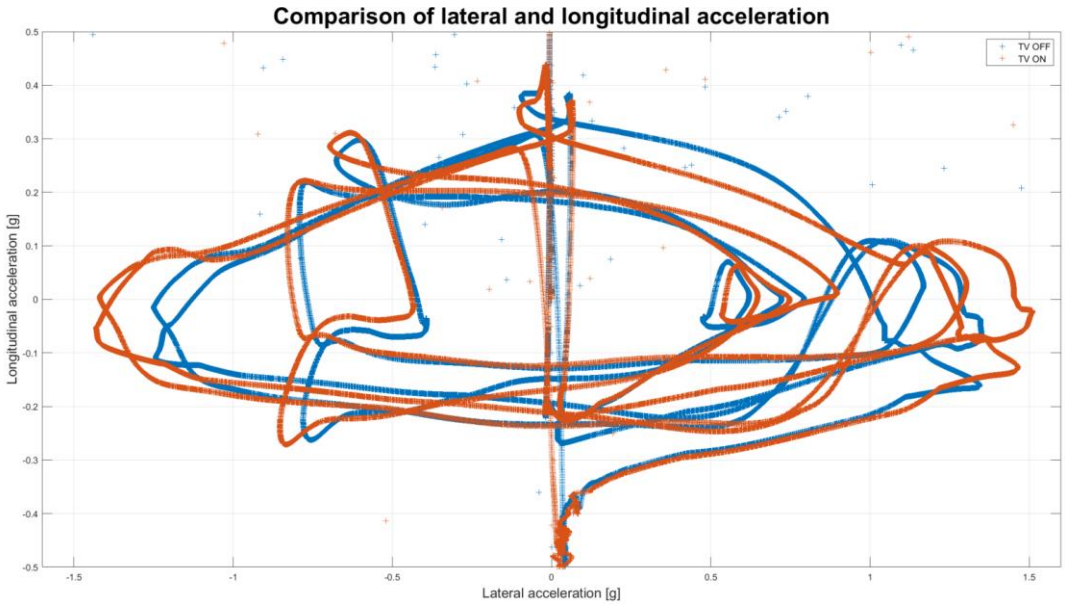

Figure 81 - Comparison of lateral acceleration during both simulations

Figure 81 confirms that a higher lateral acceleration potential is offered to the driver by turning on the torque vectoring. The pure lateral acceleration of the car with the system active is improved to 1.852g, making it an increase of 0.055g. The difference from the tables 6 and 7 are not considered, as they indicate a single maximum point on the figure 81. Within the window of ± 0.1g of longitudinal acceleration the lateral one stays ahead of the car without TV. It becomes apparent that the highest improvement in lateral acceleration has been attained when the longitudinal one is close to zero – which describes the steady state driving.

When starting to brake, (negative longitudinal acceleration), there is no uniform change that could provide any clear conclusion. However, at most levels of deceleration, the car with torque vectoring puts the lateral acceleration slightly more towards the outside of the plot, indicating a slightly better lateral acceleration during turn entry.

Lastly, all corner exit values that indicated a loss of performance are confirmed in the driver's g-g plot in figure 81 above. The pure longitudinal acceleration is not affected, but as soon as some lateral acceleration is introduced, the curves of both drives vary. It is made apparent, that for the car with torque vectoring a lower longitudinal acceleration is available, when being under a side force, resulting in a slower pace when exiting a corner.

6.5.5 LAP TIME

The time it takes for the car to drive through each segment shows the contribution that each turn has to the overall faster lap time when driving with torque vectoring. Table 12 contains the time the car with and without torque vectoring spent in each track sector.

Table 12 - Time comparison

Time spent in each defined track sector			
Track sector	TV OFF	TV ON	Difference
	[s]	[s]	[s]
1	1.09	1.07	-0.02
2	3.54	3.36	-0.18
3	4.1	3.92	-0.18
4	2.12	1.99	-0.13
5	6.04	5.59	-0.45
Overall lap time	**40.541**	**38.589**	**-1.952**

Table 12 shows that the vehicle with the torque vectoring system goes faster through every defined sector of the track. The improvement at sector 1 is the smallest, due to it being a quick high-speed turn. However, the lap time at both U-turns is improved by 0.18s each. The highest improvement of 0.45s was recorded at the steady state circle. The difference in time it takes for the cars to drive through each sector confirms that it is in fact the steady state of driving that is the most beneficial for this type of torque vectoring system. Table 12 shows the overall time gained throughout the whole track as being 1.952s, of which 23.1% is exclusively drive through the circle-turn. The overall track improvement was 1.952, meaning that the car with torque vectoring was faster by 4.815%.

6.5.6 TEST TRACK SIMULATION SUMMARY

In this chapter, a designed torque vectoring algorithm was tested on a virtual track by implementing it in the vehicle and comparing it to another vehicle without the system. The objective was to test if the algorithm was defined correctly and compare both cars' performance.

At corner entry, the vehicle with torque vectoring is entering the turn at a higher yaw acceleration, due to a higher yaw rate demand set by the controller, which then distributes a higher torque to the outside wheel. As a result, the driver can enter the corner at a higher velocity, reaching the steady state sooner, than the car without the system.

During steady state, the algorithm holds the distributed torques, so that a higher ideal yaw velocity is achieved, letting the vehicle travel at a higher speed through the middle of the corner.

Performance at corner exit represents a downside of the way the algorithm is defined. As its primary reference is an ideal yaw rate value defined from the assumption of driving in a steady state, it does not always provide the car with enough yaw moment at the exit to be able to accelerate at the same rate as the car without torque vectoring. The overall performance was raised, however there is still room for improvement at entry and exit of the corners.

To summarise the simulation, the overall lap time was improved by 1.952s (4.845%) from the original time. The car with torque vectoring was travelling at higher velocities between 0.2 – 1.5m/s while needing a smaller steering wheel angle to go through a corner of the same radius, than the car without the TV system. A clear improvement in performance and handling was made, although there is still potential of increasing the effectivity of torque vectoring, by upgrading the systems' effectivity at corner entries and exits.

6.6 SKIDPAD

The track simulation revealed that torque vectoring is working as intended, although without reaching its full potential. It is most effective at steady state cornering, which is why a simulation on a skidpad track could yield the most accurate results aligning the most with reality together with the highest improvement in lap time.

Skidpad is a dynamic discipline that takes place at every Formula Student event. It consists of two concentric circles with the same radius built into a pattern of eight (view figure 82) and is meant to test the vehicle's performance at steady state cornering [27]. During the event, the driver goes through both circles twice before exiting the track, resulting in a scored lap time of all individual circles that were driven through. Both the left and right circle were travelled by the cars with and without torque vectoring to compare the improvement of each. The same car and algorithm settings as for the previous track simulation were used.

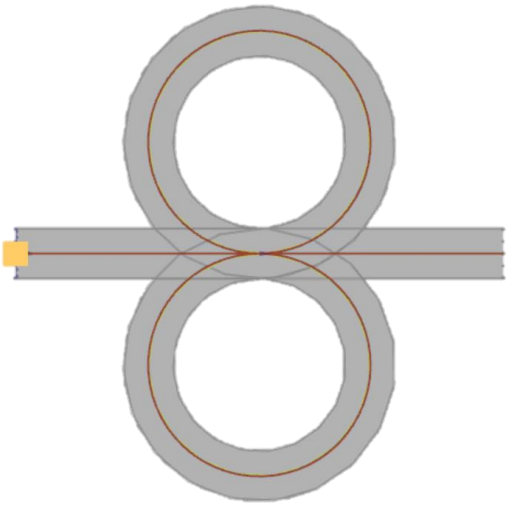

Figure 82 - Virtual skidpad track layout

6.6.1 DRIVER INPUTS

Analogously to the previous simulation, driver behaviour was analysed first. Indeed, the throttle pedal signal in figure 84 is not as uniform as it was in the track simulation. Due to the drivers choosing different paths at the first turn entry, the compared data by distance are slightly offset.

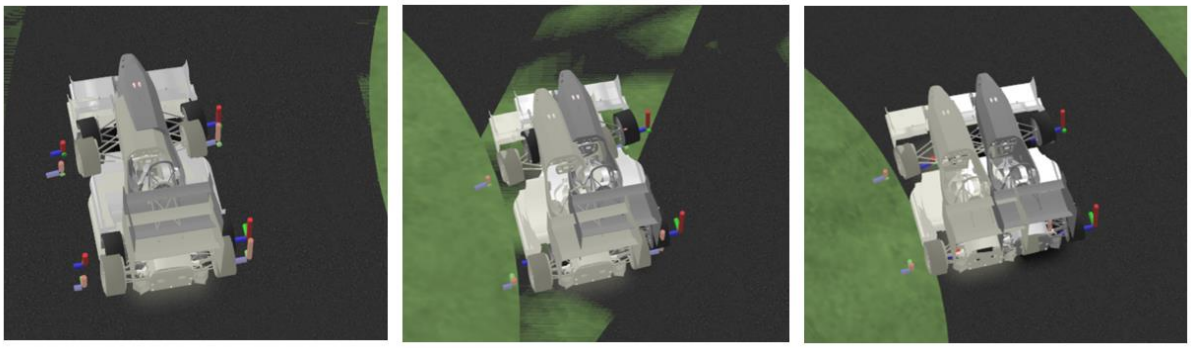

Figure 83 - Corner entry of the car with (coloured) and without (transparent) torque vectoring

Figure 83 shows that the vehicle with torque vectoring goes wider into the first corner, which is the main difference in driving behaviour between both cars. By analysing the figures further in this chapter, it is apparent that the car without TV turns into the corner sooner, resulting in a late buildup of yaw rate (seen in figure 86) for the vehicle with TV. However, the data of yaw rate and steering wheel angle in figures 85 and 86 further show that the car without TV must correct its course soon after entering the corner due to being too aggressive, while the car with TV – although with a later entry – is able to go through the circle smoothly, thus passing the first car mid-corner.

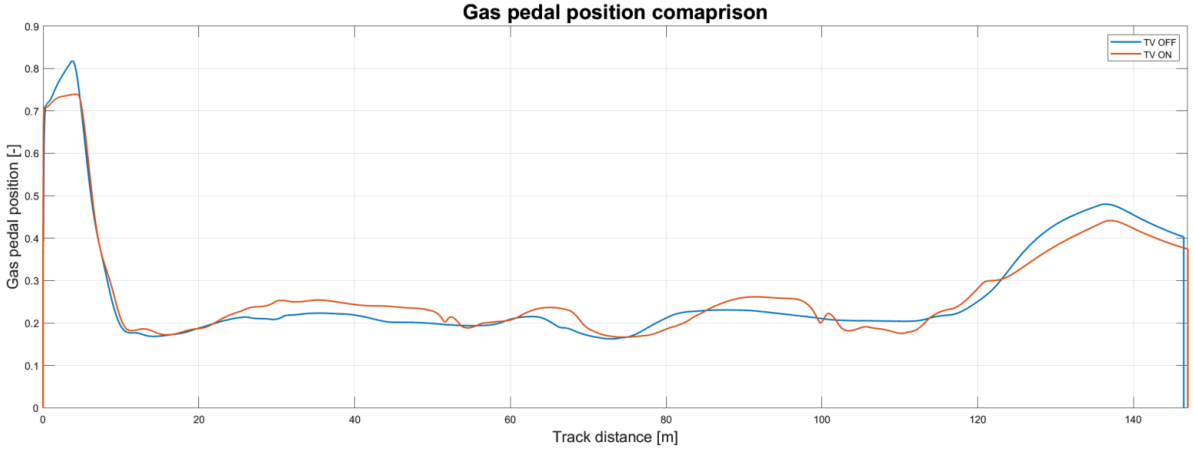

Figure 84 - Throttle pedal position signal through the skidpad drive

The driver with torque vectoring accelerates more carefully at the start. Although he is applying a steady and higher demand at the first steady state turn, he goes through the second one altering the throttle position much more. The steering angle progress in figure 85 indicates that a smaller angle is demanded by the driver when having the TV system activated – in the same way it was during the track drive. It is also possible to see, from the first drive's data, that a correction in steering angle had to be made before the vehicle reached the steady state due to a more aggressive turn entry.

The conclusion that can be drawn is, that the car with torque vectoring provides to the driver the opportunity of entering the turn later, while maintaining a steady drive through it.

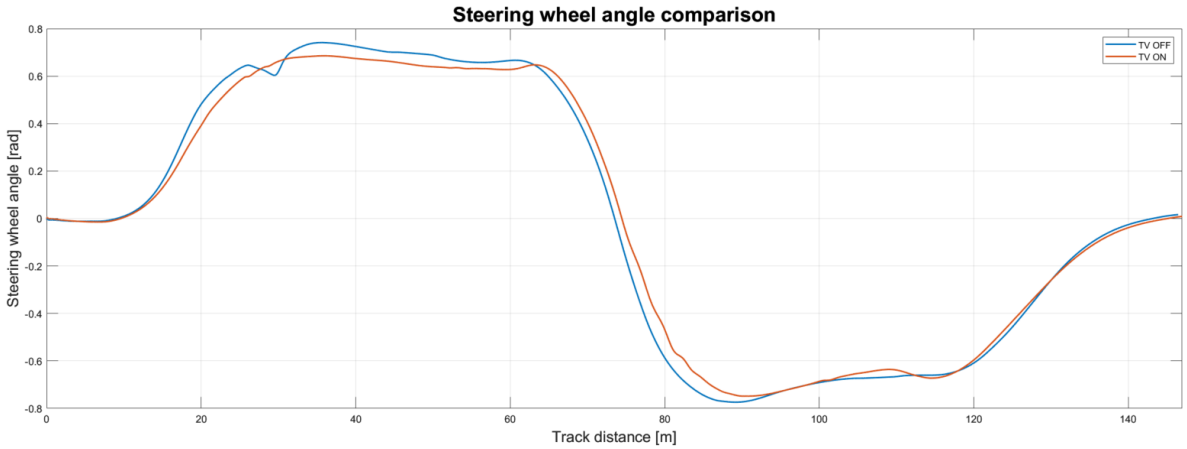

Figure 85 - Steering wheel angle signal through the skidpad drive

6.6.2 VELOCITY AND YAW RATE

As for the virtual track drive, the torque vectoring algorithm provided the car with a higher potential of yaw velocity. The later turn-in, which was explained, is the cause of yaw velocity building up later into the drive. However, the driver with TV does reach a higher value at steady state for both circles but lacks in performance at corner exit due to the reasons summarised in the previous chapter.

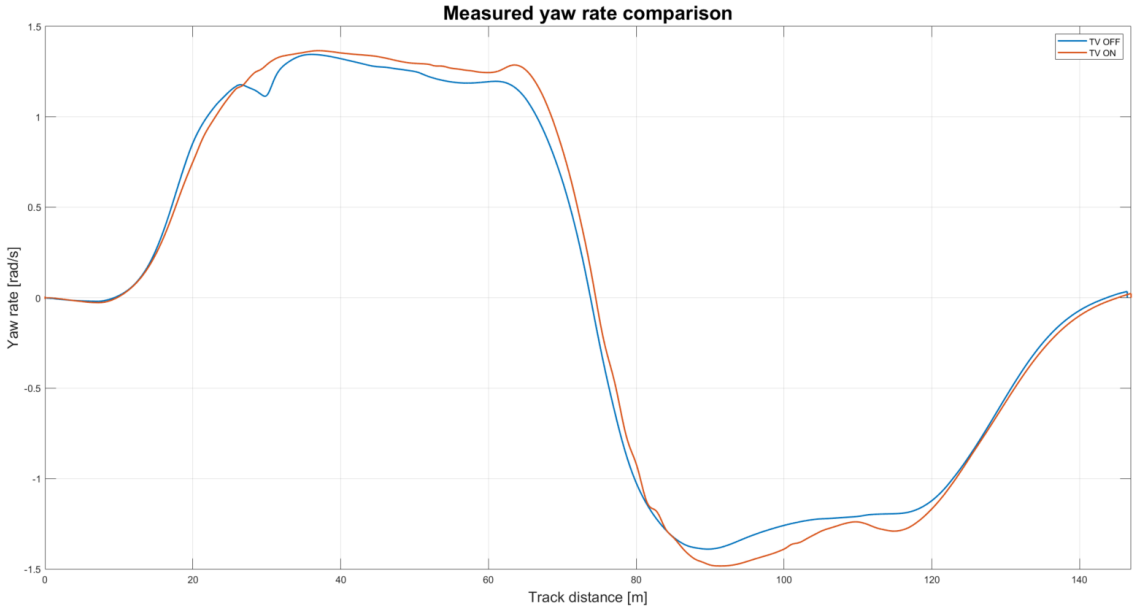

Figure 86 - Yaw rate comparison of both cars for the skidpad track

The result is the difference in velocity: figure 87 again shows a clear increase in cornering speed, together with a less effective exit onto a straight line at the end of the second turn. The exit is however not considered during the skidpad discipline, as only the drive through the turns is later portrayed in points.

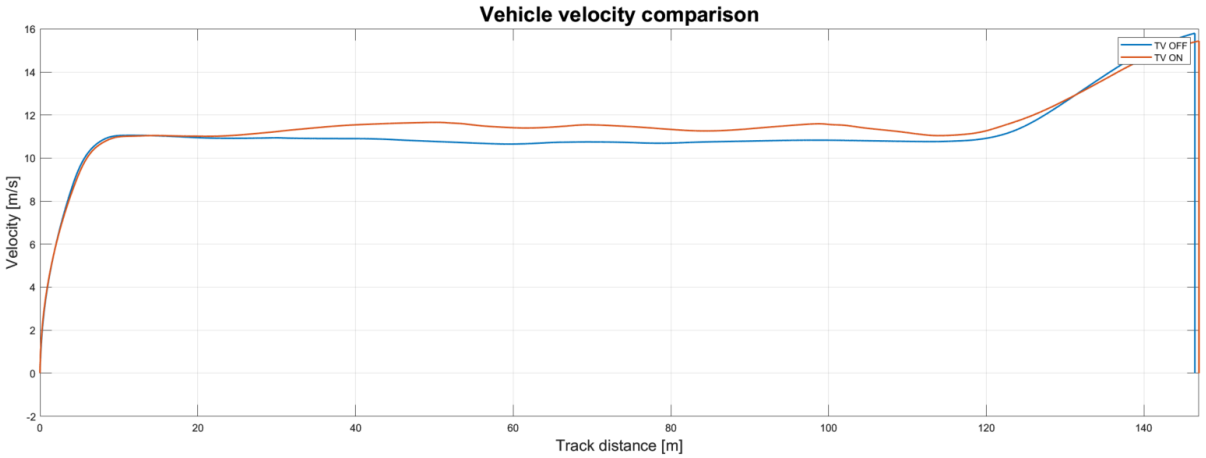

Figure 87 - Velocity comparison of both cars for the skidpad track

The differences in both drives after comparing the simulation outputs are listed in Table 13 below. All values are considered only during both turns, excluding the straight-line entry and exit.

Table 13 - Skidpad key variables comparison

SKIDPAD TRACK DRIVE RESULTS			
Variable	Units	TV OFF	TV ON
Max. gas position	[-]	0.263	0.343
Max. velocity	[m/s]	11.057	12.115
Max. steering angle	[rad]	0.775	0.749
Max. yaw rate	[rad/s]	1.389	1.482
Lap time - Turn 1	[s]	5.3	4.99
Lap time - Turn 2	[s]	5.17	4.69

6.6.3 LAP TIME

The overall time improvement is 0.31s on the first turn and 0.21s on the second. Turn one has a higher time improvement due to the correction at the turn entry, where the car without TV lost time. Table 14 shows the new potential placement at last year's competitions if an improvement of 0.21s in time would have been made in the fastest lap.

Table 14 - Time difference and potential position improvement in previous competition

Potential skidpad position improvement		
Time improvement		
Lap 1	[s]	0.31
Lap 2		0.21
TRACK	Position in 2023	Potential position
FS Czech	4	→ 2
FS Germany	14	→ 7

6.7 SIMULATION AT A FORMULA STUDENT TRACK

After successfully designing, tuning, and testing the algorithm on the test track, the car was sent to a racetrack from the Formula Student Germany competition from 2017, to record an estimate as to how much improvement can be made on a competition track. The track is available in the Carmaker's library for Formula Student, but a few modifications were in order, as some corners were too sharp for any vehicle to drive through.

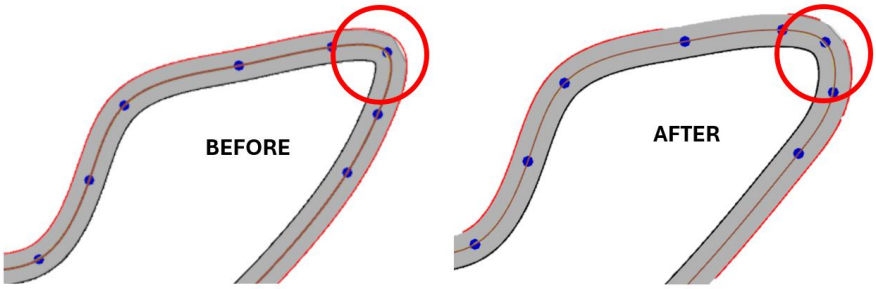

Figure 88 - Track corner modification

Figure 89 shows the whole track model. For a more convenient analysis, the track is divided into different segments to see where the car improves in lap time the most.

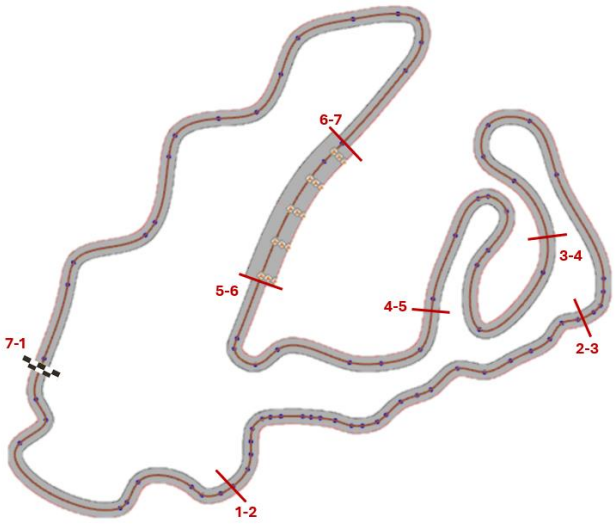

Figure 89 - FSG 2017 racetrack model

After completing a lap with both cars, the following sector times were obtained.

Table 15 - Sector times through the FSG track

FSG track time [s]								
Sector	1	2	3	4	5	6	7	Overall
TV OFF	11.901	9.17	9.25	8.34	11.21	0.76	15.96	66.597
TV ON	11.571	9.01	8.88	8.24	11.08	0.77	15.41	64.928

Table 15 shows that almost every sector was improved by turning on the control system. The exception is sector 6 – the slalom course – where the car was slower by 0.01s. The individual improvements in both seconds and percentage of the original time are displayed in table 16.

Table 16 - FSG track sectors improvement

FSG track time improvement		
Sector	[s]	[%]
1	-0.35	2.773
2	-0.17	1.775
3	-0.38	4
4	-0.13	1.199
5	-0.1	1.16
6	0.01	-1.316
7	-0.55	3.446
Overall	1.669	2.506

The car with torque vectoring improved the overall lap time by 1.669 seconds. Compared with the previous time set by a car without TV, the highest improvements are at sector 7 and 1 of the racetrack. As sector 7 is the longest, the highest improvement in time was expected. However, it is also the part where the highest difference in percentage was recorded.

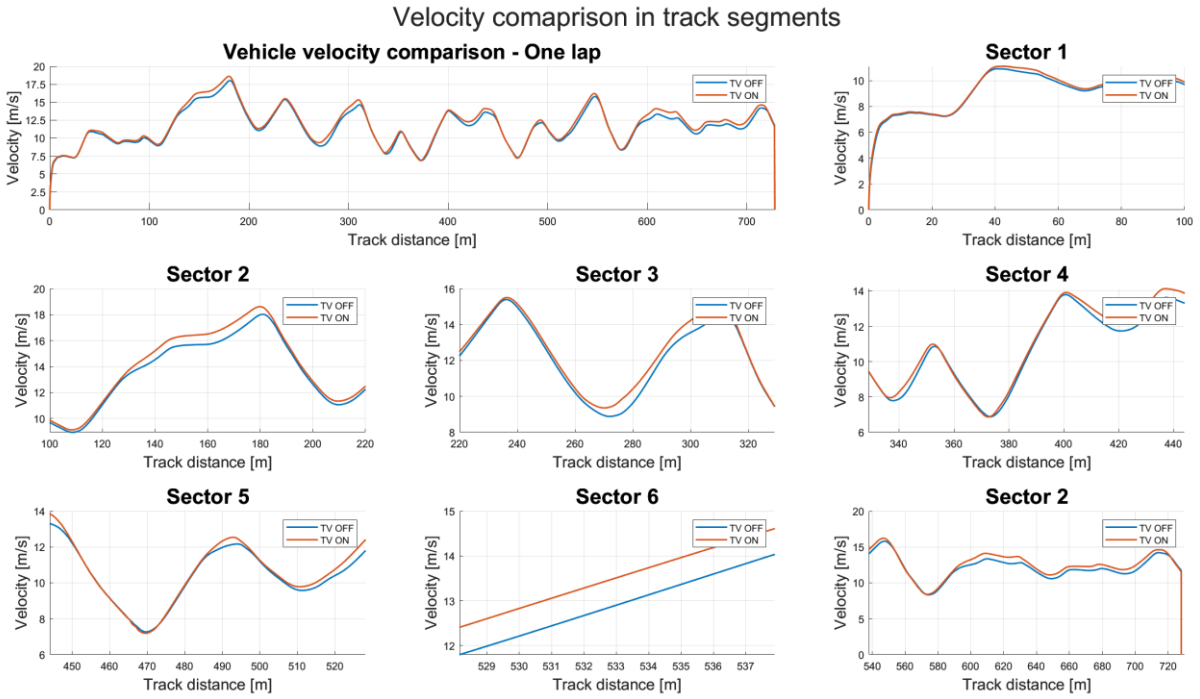

Figure 90 - Velocity analysis in different sectors

Similarly, based on the results obtained from the virtual track, the deceleration of both cars is the same, although the car with torque vectoring has a higher velocity at corners. Both the test track and FSG track are alike, except the overshoot of the ideal yaw rate at both sharp corners of sector 4 of the FSG track. Figure 90 shows velocity of both cars in all sectors.

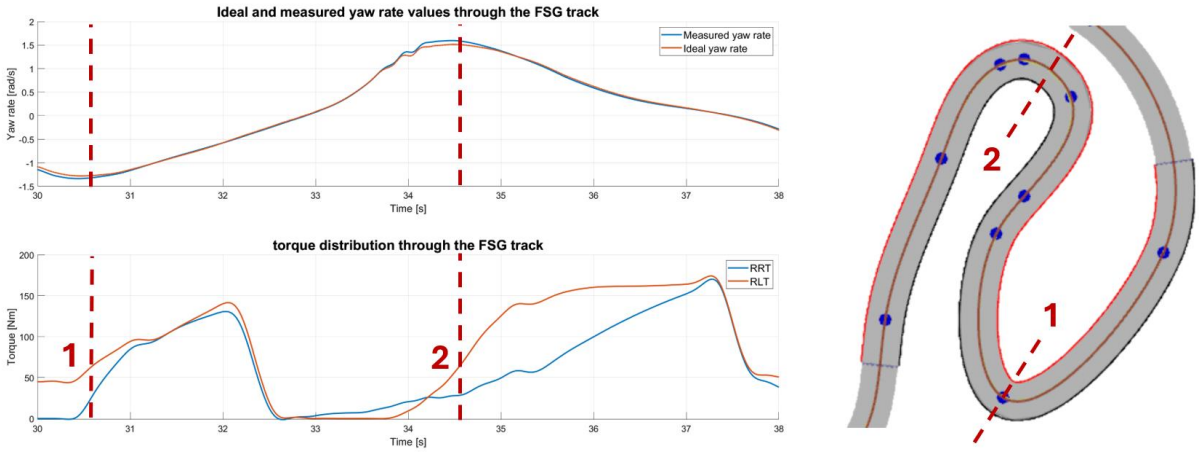

Figure 91 - Overshoot of the ideal yaw rate at sector 4

Data in figure 91 show that, at both apexes of the two corners in sector 4, the car reaches a higher yawing velocity than the regulator sets as a target. As the first corner is at the end of a bigger right-turn, upon reaching the apex, the right-wheel torque rises in a spike but doesn't surpass the torque of the outer wheel. However, the driver goes through the second turn having a much higher torque on the inner wheel, which is then evened out as the driver exits in a straight line.

No wheel spin or loss of grip occurred. This event would be highly undesirable during a race, as it could result in a sudden understeer behaviour or a loss of grip due to a higher torque on a less loaded wheel. The torque data will be analysed during testing, to ensure no sudden changes of higher torque occur mid-turn.

Figure 92 shows an identical superposition of the ideal requested and vehicle measured yaw rates which corresponds to the data from the previous track. It also contains the same exception related to sector 4.

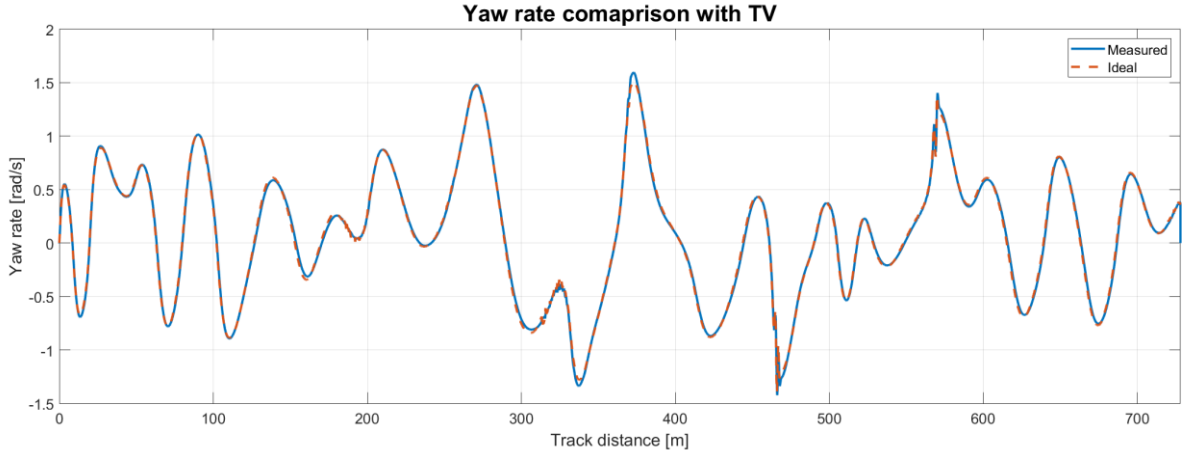

Figure 92 - Ideal and measured yaw rate comparison at the FSG track with torque vectoring

Despite said exception, the car managed to improve its lap time, as seen in table 16. The overall driver and vehicle behaviour remained much the same as at the test track, with a slightly smaller steering wheel input, an increased throttle pedal request and higher velocities through a corner.

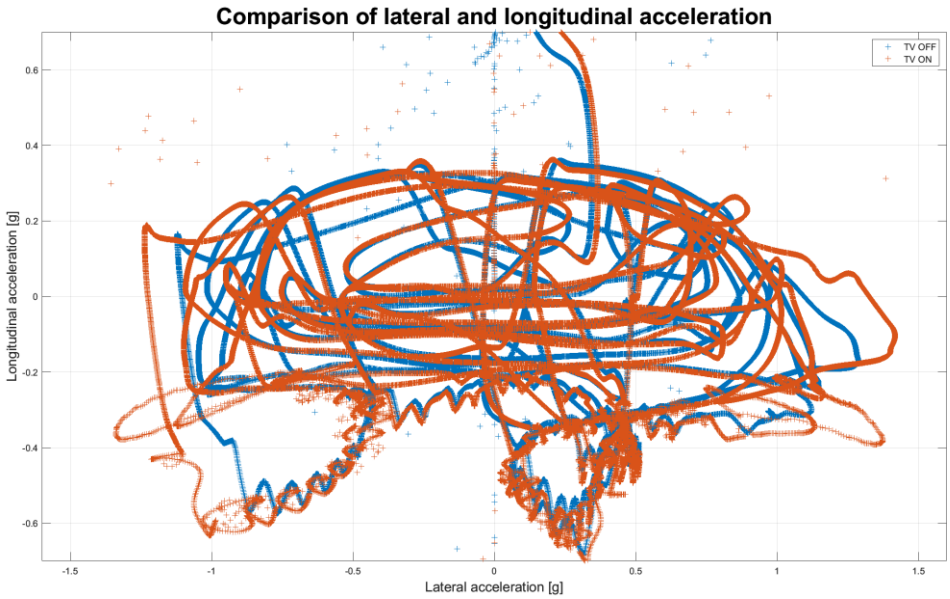

Figure 93 - lateral and longitudinal acceleration for both drives

Same as in figure 93, there is a clear improvement in the maximum lateral acceleration the driver reaches and much less deterioration in the longitudinal acceleration due to a Formula Student track being made mostly out of corners.

7 TESTING

The designed and simulated torque vectoring algorithm needed to be validated on track to see if the simulated results align with real vehicle behaviour and if the added yaw moment and velocities benefit the real driver as much as they did the simulated one.

7.1 VEHICLE AND TRACK PREPARATION

First, the car needed to be setup in the same way it was represented in the simulation, and in the way it is usually prepared before a race. The front and rear axle ride heights were set as usual, where the front is slightly lower for a better angle of attack of the aero packet, and the weight distribution of the car was calibrated to 50%. The wheel toe and camber geometry were modified for the rear wheels to have maximum possible grip and the front wheels based on driver feedback.

Figure 94 - Suspension setup before testing

The test track (figure 95) was built from two high speed U-turns, a few low-speed turns and a straight line, in order to analyse the algorithm's response at steady states, quick turns and to a straight-line exit, to see it reacting to different steering inputs, and compare with the simulation.

Figure 95 - Torque vectoring testing track

7.2 TRACK TESTING

First, the car was setup with the TV system deactivated. The driver was instructed to do a few laps to get used to the track pictured in figure 96, to feel how the car behaves and to warm the tires up. After the warm-up, regulator output and sensor data were analysed to compare the first regulator output and the theoretical torque distribution that would have been sent to the wheels.

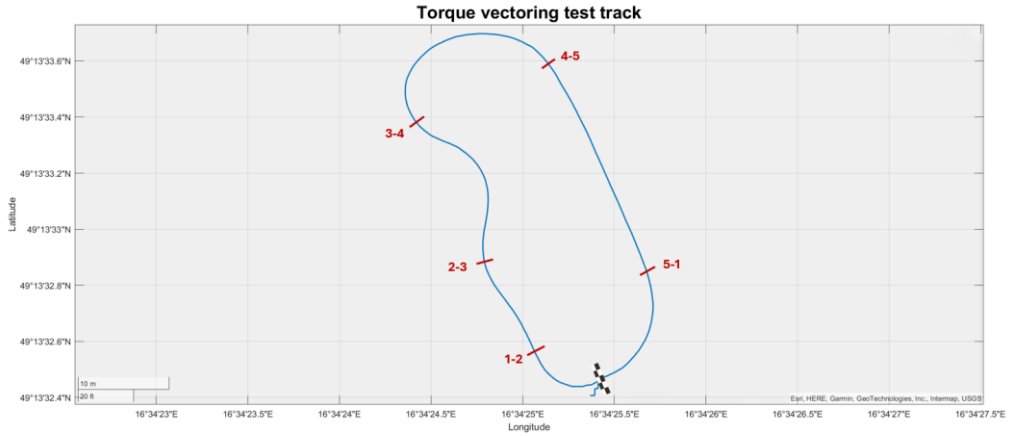

Figure 96 - GPS: vehicle path on the test track

7.2.1 REGULATOR OUTPUT TUNING

The first complication that occurred was that the ideal calculated yaw rate value was smaller than the measured value during the whole drive, which meant that the car oversteered. A slightly oversteering vehicle is beneficial for a racing driver, and it is usually the setup that proved to be most effective. However, in consequence, a higher torque would have been sent to the inner wheel, making the car either fight the driver during corner entry, or spinning the wheel at the middle and exit of the turn due to the wheel not being loaded enough to support the torque.

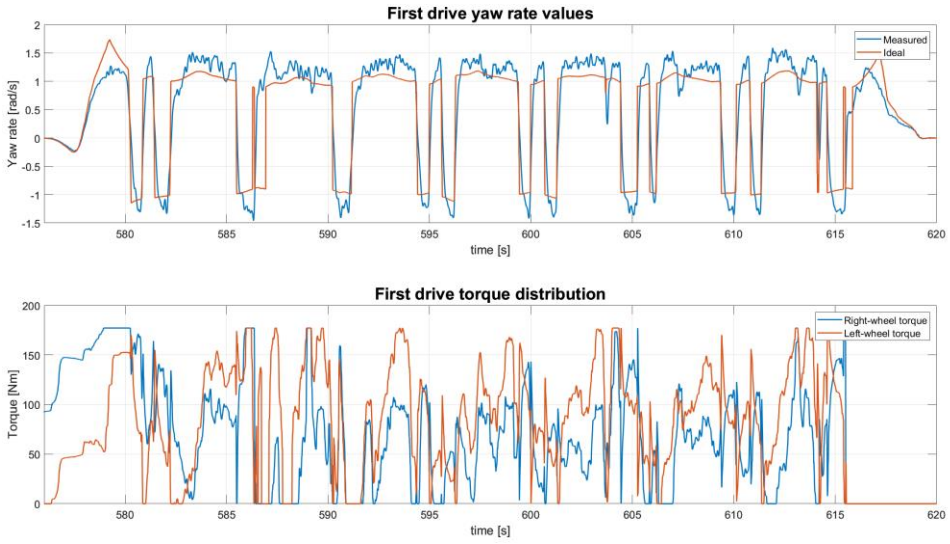

Figure 97 - Regulator output and torque distribution from the first drive

This explained behaviour is illustrated in figure 97. For these reasons, the understeer gradient was implemented back into the torque vectoring system. Although its value being zero proved effective in the virtual environment, it caused issues during testing and proved to be inconvenient for the driver. An oversteering vehicle was defined as the objective for the system. Throughout the testing session, it proved much more important to tailor the aggressivity of the system based on the driver's preference, and not on the theoretical values derived from the simulation. Even though the understeer gradient being zero might be best for exploiting the maximum ideal car potential, it is the imperfect drivers with their individual styles of driving who perform on track. The lap time was improved by adjusting the ideal yaw rate based on the driver's preference of aggressivity and oversteer, in tandem with tuning the PI regulator values.

The understeer gradient proved to be another variable in need of tuning. Nonetheless, it allows to setup the torque vectoring system for different drivers who each drive best at different degrees of oversteer, and so gives the algorithm more flexibility in terms of modifications.

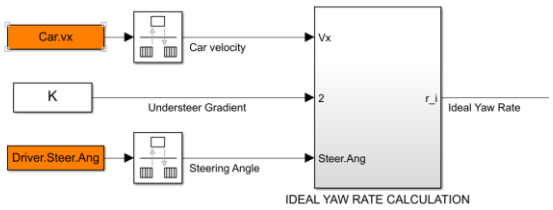

Figure 98 - Including the parameter K

After updating the algorithm, it was possible to observe the ideal calculated yaw rate again. The end data showed that its value is at times above the measured one, meaning the potential improvement by turning on the torque vectoring is possible (view figure 99). Due to a limited amount of testing space the laps were driven in both directions, as most of the turns were oriented in one way (view figure 96), to ensure the system is working correctly.

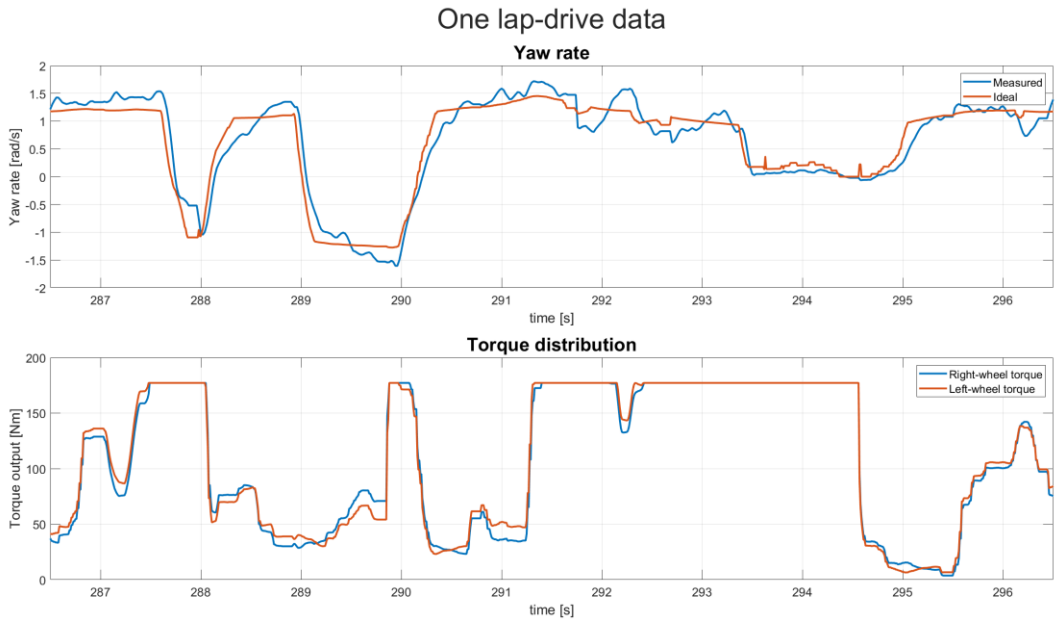

Figure 99 - First yaw rate and torque data after implementing the understeer gradient

Figure 99 shows the ideal and measured yaw rate from which the torques are distributed. The maximum torque value was limited initially to 177 Nm for safety reasons. Based on the criteria of distributing the higher torque to the outside wheel and evening-out the torques on a straight line, the algorithm was working as intended. However, after considering the observed data and getting the driver's feedback, the initial torque distribution was not enough to observe an increase in performance and the driver did not notice any major difference in handling, as there is very little torque difference shown on the figure 99. As this was assumed to be due to a still lower ideal yaw rate value, since the measured yaw rate follows it decently, the *K* value was therefore increased again. Some iterative tuning of the controller's proportional and integral values needed to be done. The impact of changing the controller settings on the torque distribution is shown in figure 100.

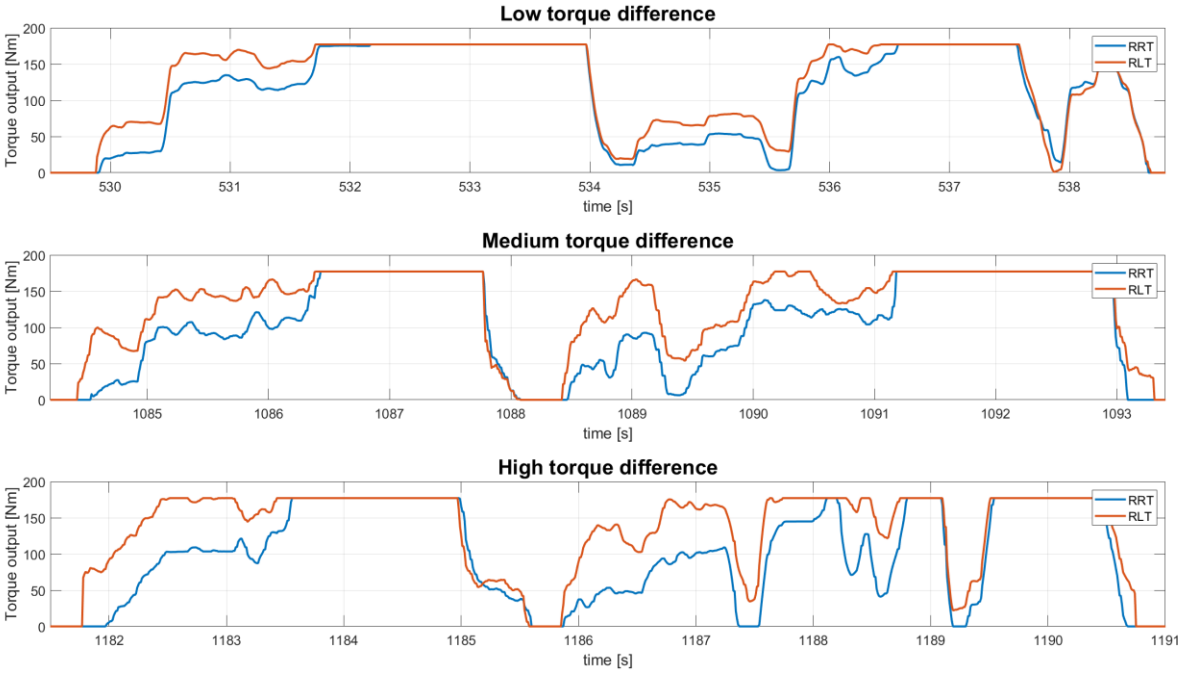

Figure 100 - Grades of torque difference achieved during controller tuning

After tuning the torque distribution based on the most promising results and positive driver feedback, the understeer gradient and PI values were defined to obtain a reasonable and stable output.

The driver was instructed to drive a series of laps with and without the system active, where the significant data together with individual lap times were recorded.

7.2.2 STEERING WHEEL ANGLE

When considering the driver inputs, it is much harder to come to a clear conclusion than it was from the simulation, as each lap is different and as driving conditions change with tire temperature and the track state. To ensure that a coincidence is not mistaken as proof of difference in handling, multiple driven laps were analysed together.

Figure 101 - Steering angle values for a drive without (top) and with (bottom) TV

Figure 101 represents the difference in steering wheel angle. The primary driver feedback from the drive with torque vectoring was that the car felt more agile and responsive to steering inputs. Some key differences can already be seen, however, in order to compare the driver's feedback with measured data properly, a single lap from both drives was taken from the figure 101 for closer analysis. For convenience purposes, the lap starts and ends at the straight-line segment of the track, where the steering wheel angle is zero.

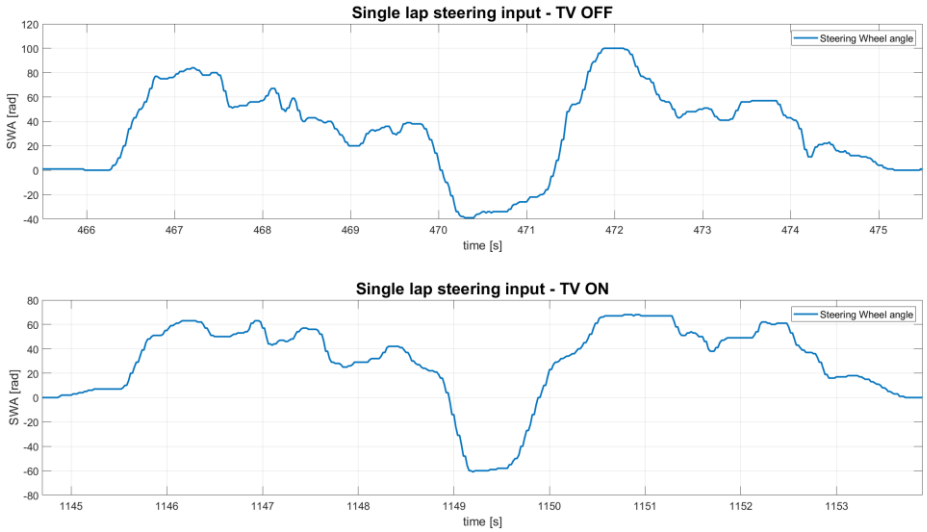

Figure 102 - Steering wheel angle data from a single lap

Looking at the single lap data in figure 102, it's possible to pinpoint the areas of difference in steering wheel angle more accurately. As in the simulation, the data needed to be compared with the driven distance set as the x-axis to make them overlap. The steering wheel values for key track sectors (view figure 96) are displayed in figure 103.

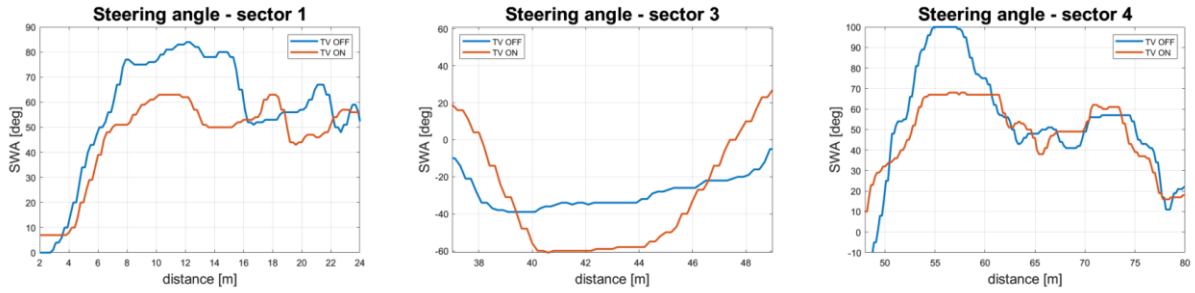

Figure 103 - Steering wheel angle comparison at key track sectors

The most striking difference in the steering input in the steady state sector 4 of the track. When driving without the torque vectoring system, the driver enters the turn with a steering wheel angle of a 100° to a 110°, whereas, when driven with the system on, the steering wheel angle ranges from 60° to 80°. A similar change can be seen in track sector 1, where the value drops from 80° to 60° and starts to even out at corner exit.

However, the opposite seems to be happening in sector 3, which is the only left turn on the track. At first, a wrong torque distribution to the inside wheel was suspected, but when looking at figure 104 comparing the sectors, the driver goes through the corner without requesting any throttle, which means that both the right and the left wheel have a torque value of zero.

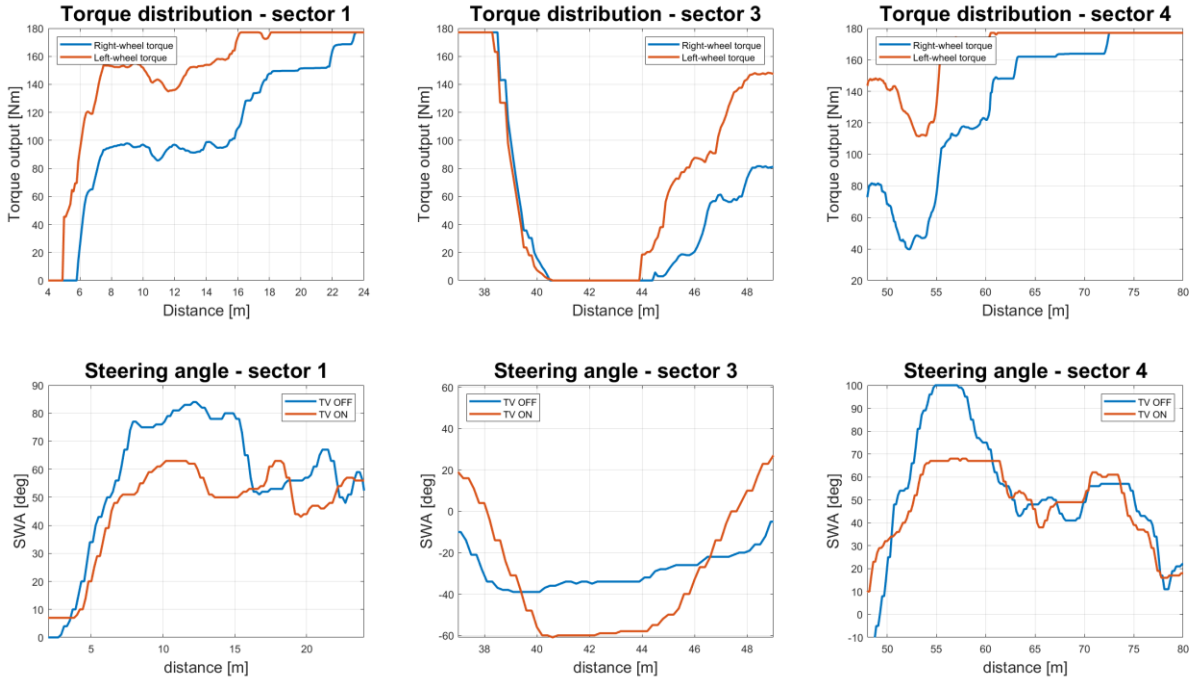

Figure 104 - Comparison of torque distribution and steering angle for key track sectors

The presumed reason for the higher steering wheel angle is a higher yaw moment and velocity the car was under during the previous turn. As the driver didn't request any torque during the left turn, he was fighting more inertia from the preceding turn, to be able to yaw the car in the other direction, hence the higher steering angle value. Figure 104 shows the torques sent to the driven wheels at sectors from figure 96, together with the difference in steering angle from both sessions.

7.2.3 YAW RATE

The ideal and measured yaw rate, as well as torque distribution, were analysed based on the same driven laps as the steering wheel angle. During the drive without torque vectoring, on most of the track's sections, the vehicle's yawing velocity was not capable of reaching its ideal defined value and both wheels were assigned same torque commands through the entire drive (view figure 105).

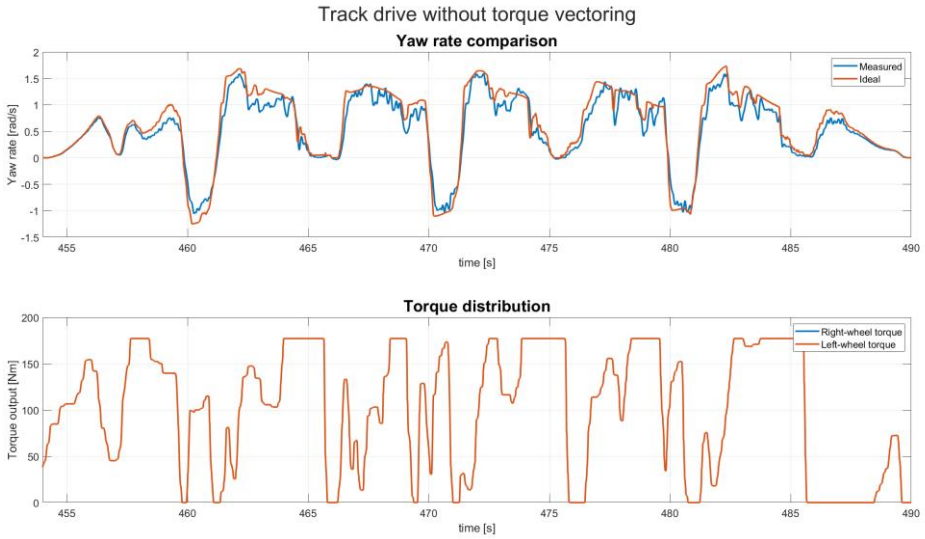

Figure 105 - Yaw rate and wheel torque data from a drive without TV

The data from the drive with the torque vectoring system can be seen in figure 106.

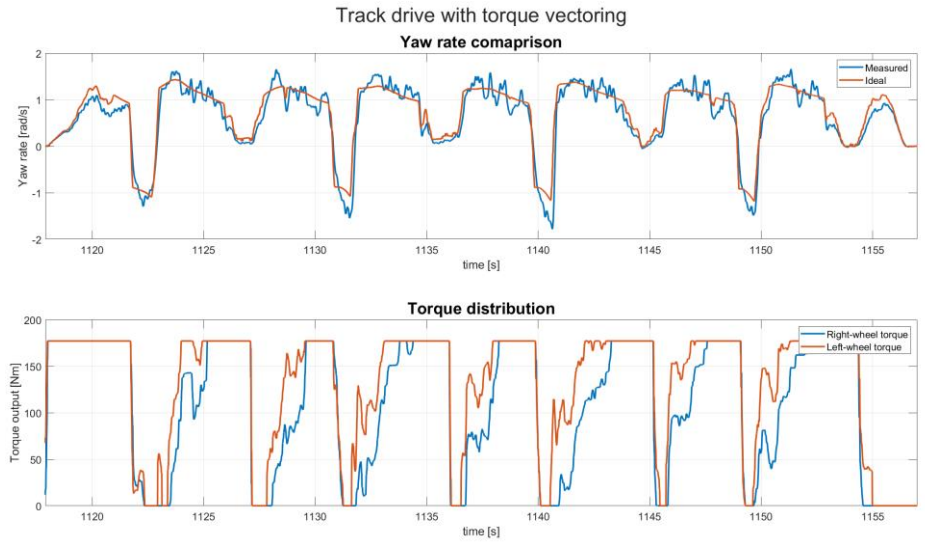

Figure 106 - Yaw rate and wheel torque data from a drive with TV

Comparing figures 105 and 106, the car's yawing velocity overlaps with the ideal one significantly more in the drive with the system activated. Due to the driver's twitching motions with the steering wheel, the measured yaw rate oscillates much more than it did in the simulation, however, a clear improvement in copying the ideal yaw rate value can be observed. The car's yawing velocity surpasses the ideal one even during the previously discussed left turn,

where there are no torques being sent to the wheels. This is due to the substantially higher steering wheel angle, as explained earlier.

As in the simulation, the driver's change in the steering angle affected the ideal yaw rate values. The ideal yaw rate decreases in value at track segments, where a smaller steering wheel angle is applied. The measured yaw rate increases naturally due to having more yawing motion from the torque vectoring system. The ideal and measured yaw rate values for 3 laps of both drives are compared in figure 107.

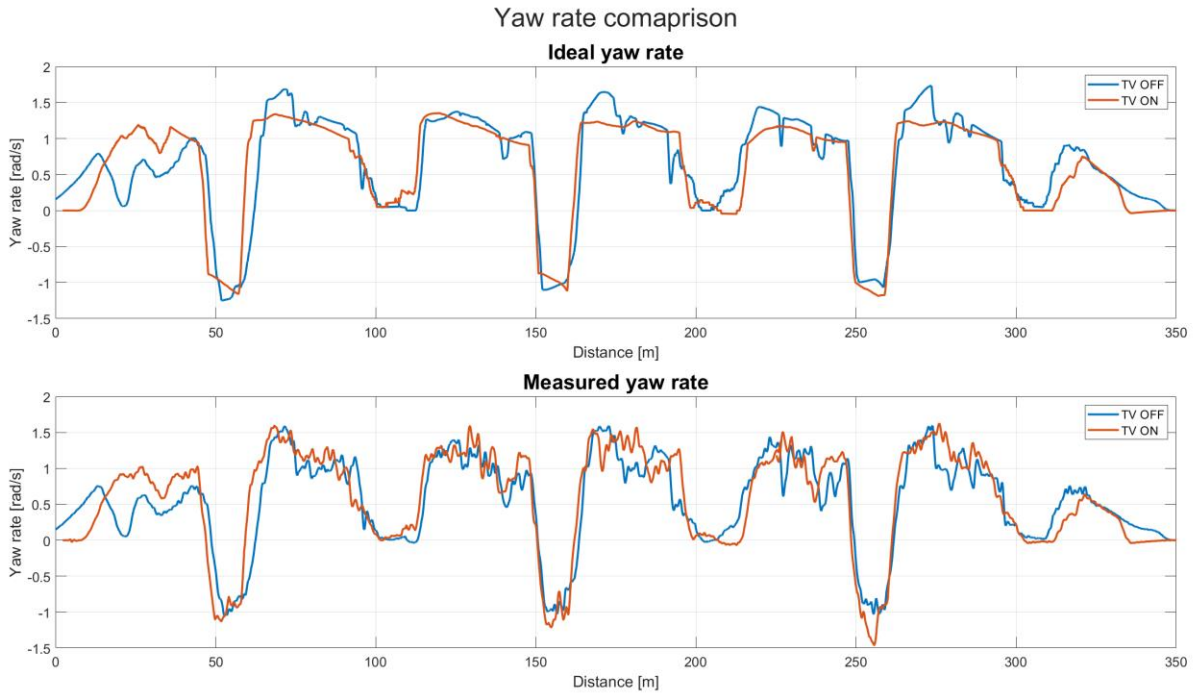

Figure 107 - Ideal and measured yaw rate comparison for both driving sessions

The most significant decrease in the ideal yaw rate happens at the entry to the turn of sector 3, where, as it was analysed before, the driver's steering angle drops by 20-25%. Its value is lower for most of the corner, evening out at the exit. A similar change is seen at the corner of sector 1. The measured yaw rate is harder to derive any conclusion from as the data is more volatile. An overall higher yawing velocity was recorded at sector 3. Nevertheless, some overlapping is present due to the data being less smooth.

In the same way it was done for the steering angle data, the track-sector analysis of the measured and ideal yaw rate from a lap driven with torque vectoring was compared to torque distribution.

As it was presumed, the measured and ideal yaw rate do not overlap perfectly like in the simulation results. Indeed, during the measurement, some parasitic effects, such as steering wheel twitching motion, non-uniform roughness of the track, changing tire behaviour or uneven track driving cause some imprecision in the measurements. Figure 108 shows some of these imprecisions in yaw rate data.

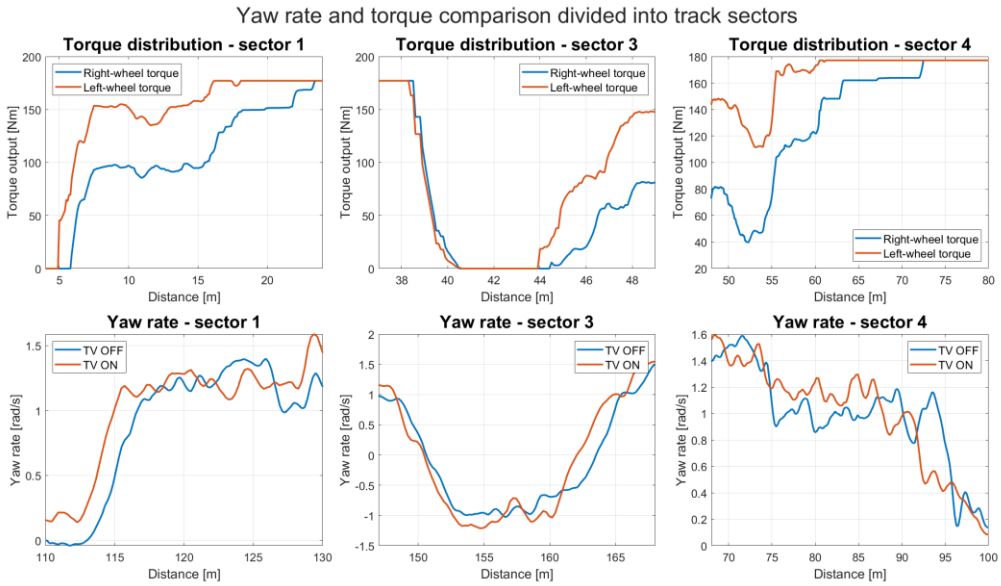

Figure 108 - Comparison of torque distribution and yaw rate for key track sectors

Due to the suboptimal environment and disruptive effects, the measured yaw rate follows the ideal one with significantly more oscillations than in the simulation (compare figures 72 and 106). Nonetheless, the car's yawing velocity does increase at parts of track sectors, as shown in figure 107, where several driven laps can be seen. Figure 108 shows a comparison of yaw velocity of a single lap, where it is easier to see the difference in each track sector and its parts and compare it to torque distribution.

7.2.4 VELOCITY

The forward velocity comparison between both drive sessions is shown in figure 109.

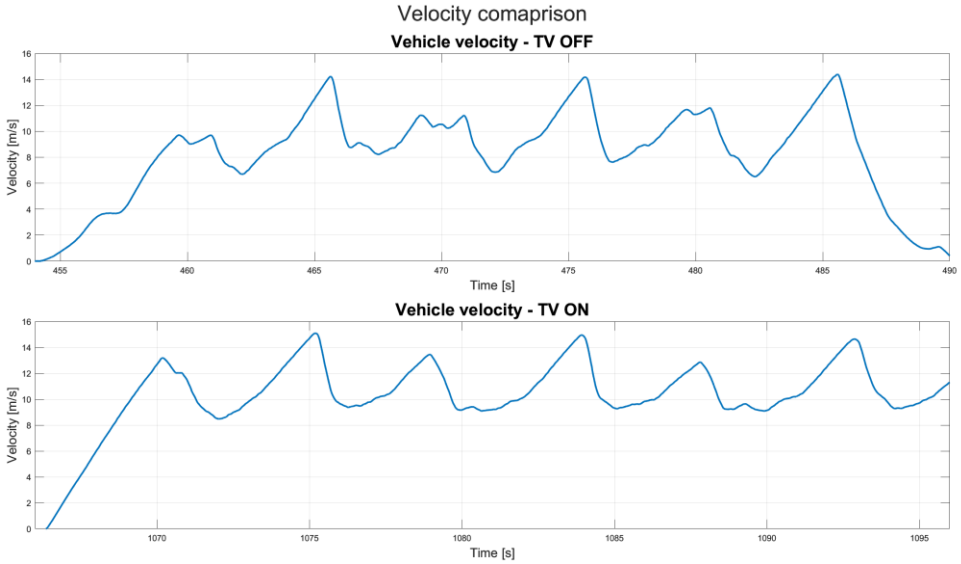

Figure 109 - Comparison of vehicle velocity from both driving sessions

Figure 109 shows the car's forward velocities from both driving sessions. The maximum velocity, which the car reaches at the end of the straight line, is higher for the vehicle with the system on. This is a by-product of a higher velocity at which the car goes through the steady state sector 4 of the track. It is possible to observe that the car without TV goes through the turn at velocities between 6 - 7 m/s, whereas the car with the system active travels faster by 1 m/s through the turn, and therefore accelerates from higher velocities at the straight line. The vehicle also improves at track sector 1, where the velocities of 7 – 8 m/s turn into approximately 9 m/s, and at the exit of sector 4, with an average improvement of 1.5 m/s.

Figure 110 - Vehicle velocity comparison for 2 driven laps

To observe the difference in more detail, figure 110 shows the velocity data of both cars for a drive through 2 laps. There is not enough information to assume that the entire velocity improvement is exclusively due to the torque vectoring system, however, it can still be concluded that the driver is more confident in the car with the system active, that he finds it more responsive to steering inputs and more agile trough the corners, reaching higher velocities as a result.

7.2.5 LAP TIMES

From all the drives with both car settings, the 4 fastest laps were taken and compared to each other. Table 17 shows lap times and the time difference of each lap between both drives.

Table 17 - Lap time improvement made by the car with torque vectoring

Lap	1	2	3	4
TV ON [s]	9.06	8.94	8.86	8.8
TV OFF [s]	9.88	9.42	9.4	9.22
Difference [s]	**-0.82**	**-0.48**	**-0.54**	**-0.42**
Difference [%]	**9.050773**	**5.369128**	**6.094808**	**4.772727**

Table 17 shows, that with torque vectoring, all four fastest laps were driven in shorter time. Lap one has a bigger difference due to a driver error on the track, otherwise the improvement ranges in the window of 0.4s – 0.5s, making it 4.5% – 6% overall faster through the track.

Going back to table 12 with time data from the simulation, the overall testing track improvement was 4.815%, fitting in the middle of the measured track improvement in table 17. The conclusion of a well-defined simulation can be made, as its results are validated by testing data.

It is further clear from the analysed figures and lap data, that the designed torque vectoring provides a clear improvement in track performance.

7.2.6 ACCELERATION

The improvement in performance can be shown by comparing the longitudinal and lateral acceleration from both drives.

Similarly, as in the simulation, the driver achieves higher lateral acceleration at corners. As the track is made mostly from right-turns, more of the data on the G-G plot are concentrated on the right side. Compared to the simulation the drive is not as clean, as it's not an ideal driver that is performing on the track (view figure 111). The data are much more uniformly concentrated, instead of being at the outer limits.

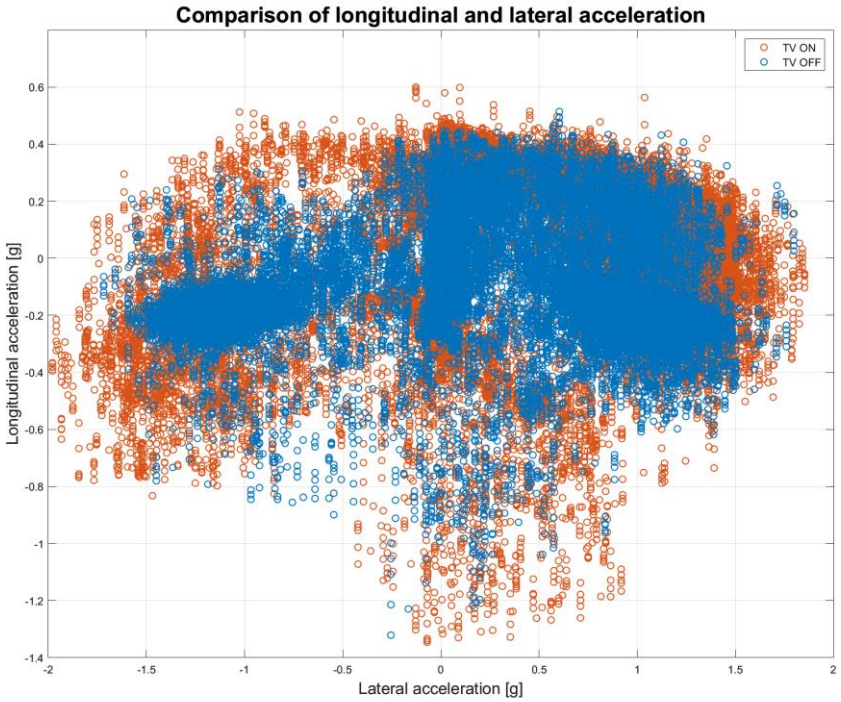

Figure 111 - Comparison of acceleration of cars with and without TV

Figures in this chapter indicate, that there is no apparent loss of longitudinal acceleration like in the simulation, rather the opposite. The system was tailored to the driver's preference for his best performance, which proved most effective to reach better performance, as it has been already reflected in lap times in table 17 and further by figure 111.

7.2.7 TRACK TESTING CONCLUSION

In this chapter, the data from a series of laps driven on a testing track were analysed in order to compare the vehicle handling and behaviour of the car with and without torque vectoring and compare it to the one that resulted from simulations.

After some algorithm modifications, it was possible to achieve a steady and reliable torque distribution between the left and right driven wheels. The vehicle was reaching its ideal yaw rate, although it followed it with more oscillations. The car's velocity was higher during multiple lap drives when driving with torque vectoring, resulting in a shorter lap time.

No loss in corner exit was registered, however, the wheel torque was limited to approximatively half of its potential, making both torque values meet during corner exit at its maximum. A more extensive analysis of corner exits will have to be done with the highest potential torque the motors can safely deliver.

The vehicle with torque vectoring felt more agile and responsive to the driver and data showed that it provided him with higher lateral acceleration limits when driving through corners. The best results were obtained by tuning the system based on the driver's feedback, rather than keeping to calculated values.

The measured data and its behaviour align with those obtained from the algorithm's virtual testing, validating the system design and simulation procedure. The best lap time improvement showed consistent and between 0.4s – 0.5s per lap, making the improvement range from 4.5% to 6%, which correlates with simulation results.

More testing sessions need to be done to test the system on a proper Formula Student track and see, how the car deals with slaloms and different combinations of corners. The drivers will need to get used to the car and its handling, which will then allow them to accelerate through corners through which they normally would not. This could indeed be observed at sector 2 on the test track.

7.3 SKIDPAD TESTING

The driver was instructed to drive some laps in an 8-shaped pattern consisting of two concentric circles. Skidpad is a dynamic discipline that was described earlier in chapter 6 when testing on a virtual skidpad track. A simulation of a steady state drive has been done earlier and it is desirable to compare the simulated data with the measurement. As there was no skidpad track built for this test, it is not reliable to compare the measured data and lap time with those from previous racing events, but an indication of possible improvement can already be derived from it. Figure 112 shows yaw velocities and torque for both circles when driven without TV.

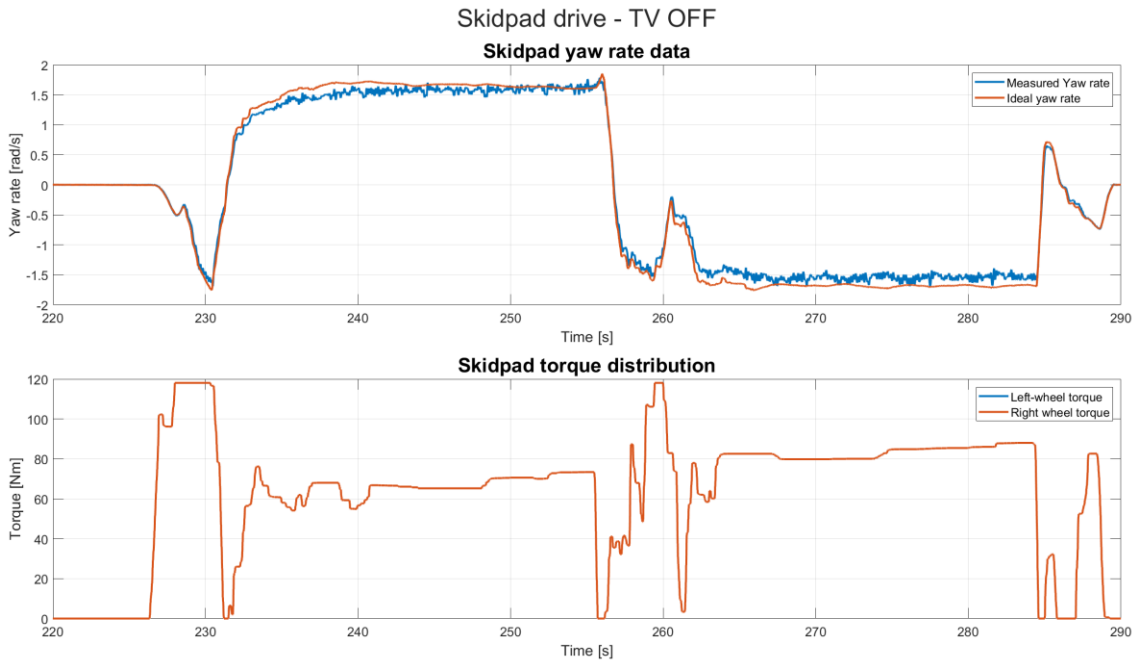

Figure 112 - Yaw rate and torque data from a skidpad-like drive without TV

As on the track drive, the driver going in steady state circles did not reach the ideal yawing velocity. The driver entered the second circle too aggressively and needed to correct the car's course (view figure 112 and 113); otherwise, the drive was clean. The steering wheel angle data in figure 113 shows no major difficulties in handling, and the driver's feedback confirmed it.

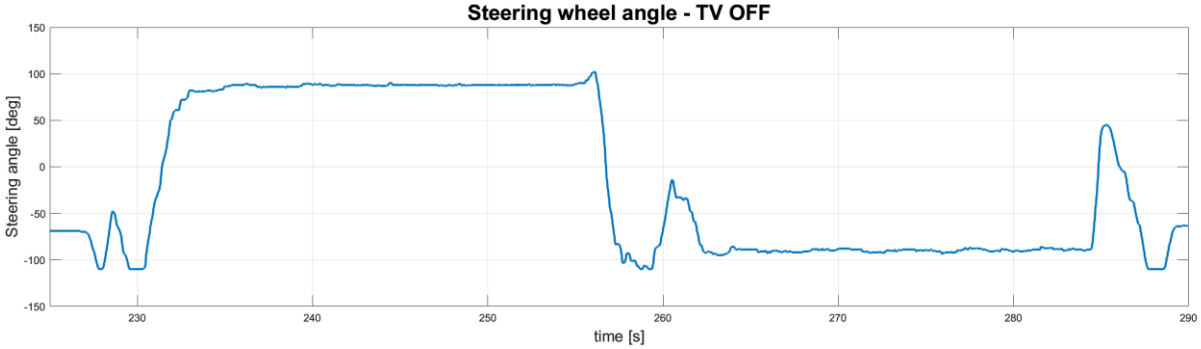

Figure 113 - Steering wheel angle for a skidpad drive without TV

When considering data from a drive with the system active (figure 114), the car's yaw velocity is overlapping the same way it did during the drive on the test track, only this time with much

less oscillations, due to the driver trying to keep a steady steering wheel angle. It is also possible to observe the torque difference changing from one wheel to another when the driver changes circles. This was, however, difficult to observe on the test track.

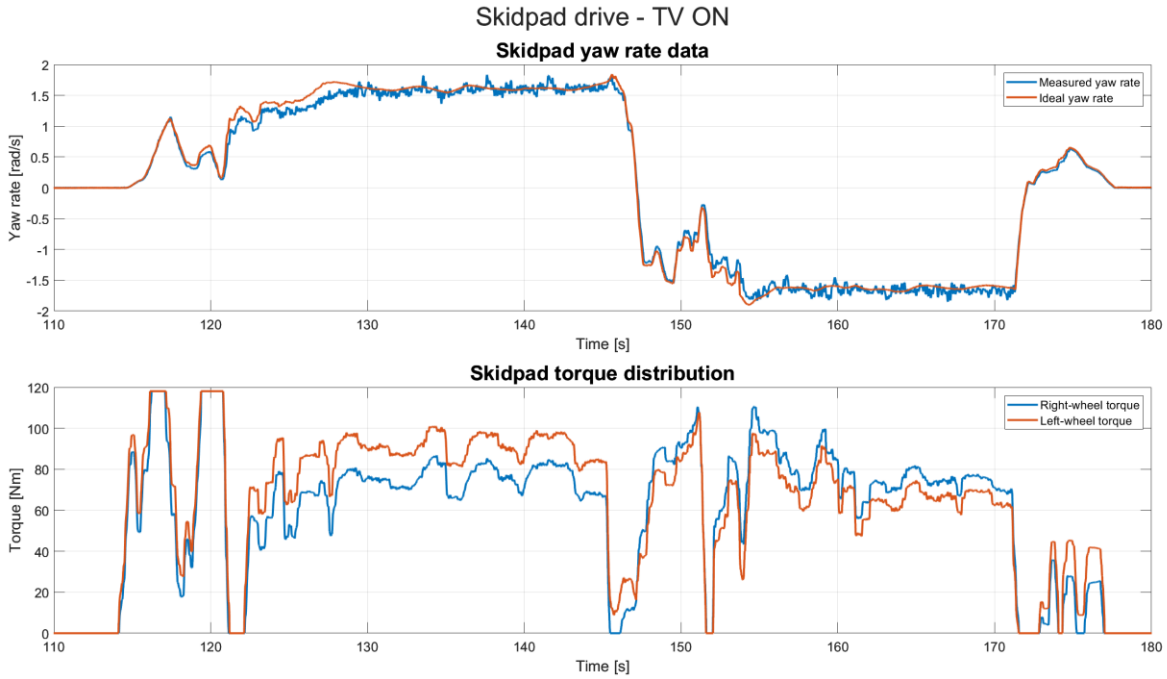

Figure 114 - Yaw rate and torque data from a skidpad-like drive with TV

Figure 115 compares the steering wheel angle and velocities from both drives.

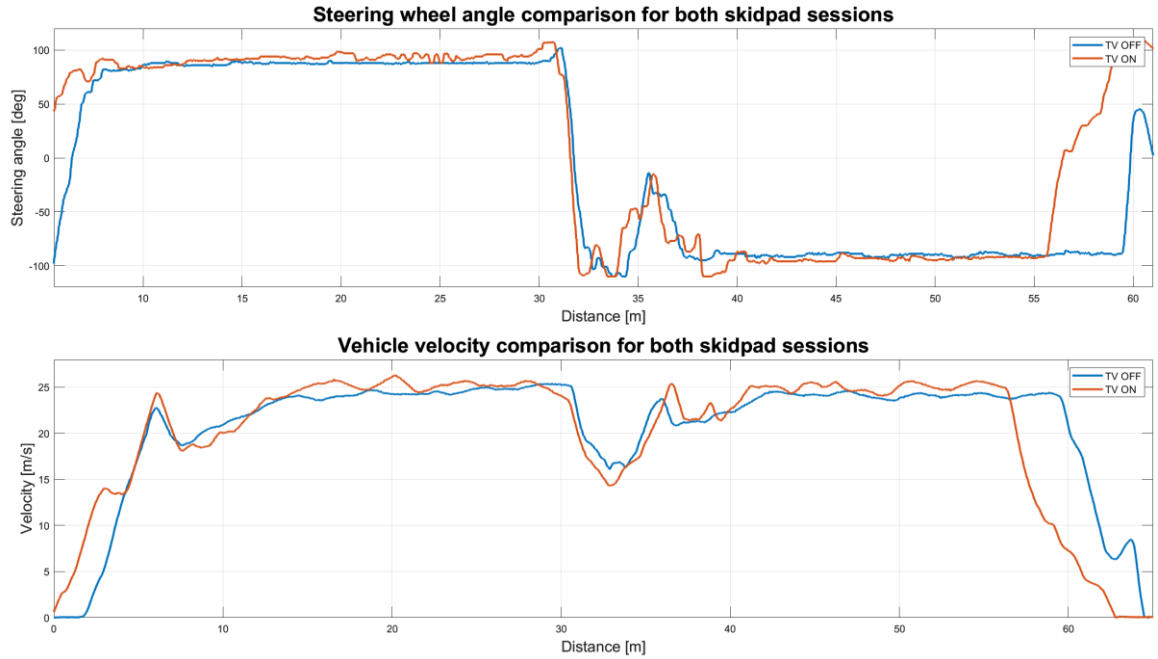

Figure 115 - Steering angle and velocity comparison for both skidpad -like drives

Although figure 115 shows higher velocities during both laps, it also shows a higher steering angle. Following a closer analysis of all figures in this chapter, there is no clear conclusion that can be derived from the Skidpad drive, due to an incorrect testing procedure.

The driver is performing on a free space without any guidance or track limits. This makes him go through the circles of both sessions at different circle radii, the circles getting progressively offset, as seen in figure 116. Considering equations (21) and (22), an increase in velocity must follow a decrease in SWA (and vice versa) to maintain the same track radius when driving an oversteering car. As both velocity and steering angle are higher during the drive with torque vectoring, it is safe to assume that the car was driven on a different circle radius, and the figure below confirms it.

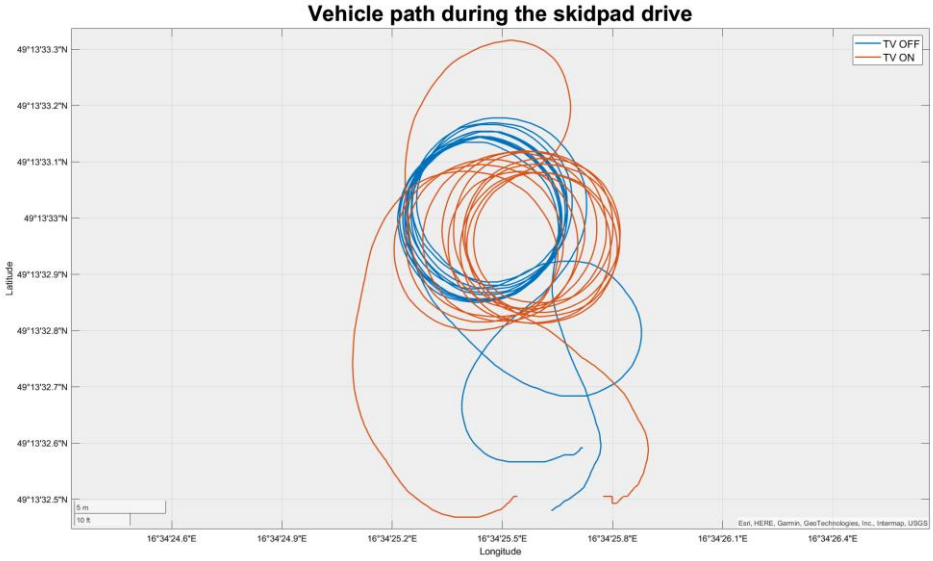

Figure 116 - Vehicle path during the skidpad drive

This reasoning is further supported by the torque distribution data. If the laps were driven on the same turn radius, the torque distribution to the left and right driven wheels should be at both circles of the same magnitude, only switch from left to right. That is not the case and the bottom half of the figure 114 shows that the torque difference is higher during the first circle.

A correctly executed analysis of torque vectoring on a skidpad track will be done in future testing in order to properly compare the drives with and without torque vectoring.

CONCLUSION

The main objective of this thesis was to design a torque vectoring algorithm for a formula student single seater. First, an analysis of vehicle dynamics behaviour on a bicycle model during cornering was done to establish the most effective way of driving through a corner. It was understood that the driving variable influencing good cornering behaviour – especially during steady state – was yaw velocity defined from a neutral steering vehicle. Said vehicle's steering characteristics do not change with increasing velocity, meaning that it goes through the turn the fastest it can. Transient state dynamics proved to be a more complex state to control but have shown potential for further improvements.

After defining the ideal cornering procedure and the key variables that affect it, the effect of torque vectoring was introduced to understand how it can positively influence cornering dynamics. The torque vectoring system provided the option to actively control the vehicle's yawing characteristics by introducing an additional yawing moment. Based on target criteria, said moment worked with or against the already present yaw moment of the vehicle. The yaw moment control was attained by distributing the torque on the left and right driven wheels to create a difference in longitudinal force between both sides, thus generating a turning moment around the vehicle's centre of gravity as the yaw moment is acting at the half-track distance from the CoG.

It became apparent that the driving variable for a good cornering behaviour was yaw velocity of a neutral steering vehicle. Said velocity was defined through equations and set as the target value. The torque vectoring system was designed in MATLAB Simulink. Its objective was to compare the current measured yaw velocity with the ideal one, and based on the resulting difference, allocate the torques appropriately to make the two values align. The vehicle's state space model was defined through equations defining a bicycle model. Those were further used to design the algorithm's PI controller, which is the content of another thesis.

The following step was testing the designed algorithm in a simulated environment. For this purpose, a custom track and a virtual copy of the latest car were created in IPG Carmaker. The drivers of both the car with and without torque vectoring were adapted through driving manoeuvres to be able to perform with both cars at their limit in order to draw a clear conclusion from the difference in car performance. The algorithm was included in the simulation by connecting IPG Carmaker with Simulink.

By successfully computing detailed simulations of track drives with both cars – one having torque vectoring enabled and the other one did not – it was possible to compare them and analyse the difference that the system made on the vehicle's cornering performance. The car with torque vectoring showed higher velocities through corners, with an improvement of 0.5 – 1.5m/s at the corner's apex. Its yawing velocity was higher as well and it aligned with the target ideal yaw rate, thus confirming the hypothesis of improving the car by controlling its yawing motion to be correct. At the same time, the results were proof of a well-designed algorithm with a well-tuned controller for the virtual environment. The lap time was improved by 1.952s, meaning 4.815%. The concluding difference between the car's performance was shown on a friction ellipse from the drive, where the car with the system achieved higher lateral accelerations. A downside of the way the algorithm was designed seemed to be the exit of the corner, where the car was lacking pace due to taking a longer time at the exit. The system distributed the torques based on values defined from the assumption of driving in a steady state,

which, while being slightly inconvenient at the turn exit, still proved to be beneficial in the grand picture.

Moreover, the system was simulated on two types of Formula Student tracks. Firstly, to compare its lap time from those of previous competitions, and secondly to prove that the algorithm would not have any problems with different sequences of corners. No major deviations from the car's handling at the virtual test track were seen and the algorithm showed overall benefits for the driver during the simulation.

Lastly, a design validation of simulation results was in order and so the torque vectoring system was tested on a track. The car was setup for usual racing conditions and the driver instructed to drive the same number of laps with and without the system active, while taking note of the differences in handling. Based on the first testing results, tuning the system based on the combination of measured data and driver feedback proved to be much more effective than keeping to calculated values. Although a neutral steering car proved in theory to be the ideal vehicle behaviour to reach, based on the driver's preference and the measured yaw rate in the car, an oversteering car behaviour was defined as the new objective. After tweaking the system based on the driver's preference and giving him time to get used to the new vehicle handling properties, a clear increase in track performance was recorded. Indeed, the vehicle appeared to be more agile through corner entries and exits, and overall faster at the apexes. Data analysis has shown an increase in both velocity and lateral acceleration as well as a narrowing of the steering angle, leading to the conclusion that the driver was able to drive through a turn of the same radius at a higher velocity and with a smaller steering angle. The car with torque vectoring was faster in each well-driven lap by 0.4s – 0.5s than the var without the system. This translates to an improvement of 4.5% - 6% from the original track time, aligning with the simulation results.

In order to enhance the systems' reliability, further testing sessions on a full-size Formula Student track will be required. The drivers need to get used to the new vehicle handling and a thorough analysis of the car's performance and its behaviour on various tracks will be carried out. The algorithm needs to be tested in a car using its whole potential in order to identify its strengths and weaknesses. Then it becomes possible to decide on the future steps to take to improve on its design. To summarise, the torque vectoring system produced promising performance and handling results in both the virtual and real environments and proved itself to be a solid foundation upon which to build in order to further exploit the vehicle's performance limits.

REFERENCES

[1] *FSG: Concept*, https://www.formulastudent.de/about/concept/. Online. FSG: Formula Student Germany. Dostupné z: https://www.formulastudent.de/about/concept/. [cit. 2023-11-02].

[2] *20230818_13-12-40_0470_maru*, 2023. Online. In: FSG: Formula Student Germany. Dostupné z: https://photos.smugmug.com/2023/Hockenheim/Panoramic-Picture/i-bxD8z3W/0/602eda95/X3/20230818_13-12-40_0470_maru-X3.jpg. [cit. 2023-11-06].

[3] *[Dragon E3 and trophies]*, 2023. Online. In: Facebook. Dostupné z: https://www.facebook.com/photo?fbid=796778302449148&set=pcb.796797499113895. [cit. 2023-11-06].

[4] *Úspěchy - tubrnoracing.cztubrnoracing.cz*, 2023. Online. Úvod - tubrnoracing.cz. Dostupné z: https://tubrnoracing.cz/o-nas/uspechy/. [cit. 2023-11-06].

[5] *History of the electric vehicle - Wikipedia*, 2023. Online. In: Wikipedia: the free encyclopedia. San Francisco (CA): Wikimedia Foundation. Dostupné z: https://en.wikipedia.org/wiki/History_of_the_electric_vehicle. [cit. 2023-11-09].

[6] DE NOVELIS, Leonardo; SORNIOTTI, Aldo; GRUBER, Patrick; SHEAD, Leo; IVANOV, Valentin et al., 2012. Torque Vectoring for Electric Vehicles with Individually Controlled Motors: State-of-the-Art and Future Developments. Online. *World Electric Vehicle Journal 5*. Roč. 2012, č. 2, s. 617-628. ISSN 2032-6653. Dostupné z: https://doi.org/10.3390/wevj5020617. [cit. 2024-01-17].

[7] *Torque-vectoring-64b51e60b58e2*, c2024. Online. In: Car Buying Simplified in the Philippines | AutoDeal. Dostupné z: https://d1hv7ee95zft1i.cloudfront.net/custom/blog-post/original/torque-vectoring-64b51e60b58e2.jpg. [cit. 2024-05-23].

[8] GILLESPIE, Thomas D., 1992. *Fundamentals of Vehicle Dynamics*. Warrendale: SAE International. ISBN 1560911999.

[9] MILLIKEN, W.F. a MILLIKEN, D.L., 1995. *Race Car Vehicle Dynamics*. Warrendale: Society of Automotive Engineers. ISBN 1-56091-526-9.

[10] BALKWILL, James, 2018. *Performance Vehicle Dynamics - Engineering and Applications*. Oxford: Butterworth-Heinemann. ISBN 978-0-12-812693-6.

[11] ROUELLE, Claude, 2018. *OptimumG: Applied Vehicle dynamics seminar*. PDF. 8801 East Hampden Avenue, Suite 210 Denver, Colorado 80231 USA. Dostupné také z: https://optimumg.com/our-seminars/. Str. 37.

[12] ROUELLE, Claude, 2018. *OptimumG: Applied Vehicle dynamics seminar*. PDF. 8801 East Hampden Avenue, Suite 210 Denver, Colorado 80231 USA. Dostupné také z: https://optimumg.com/our-seminars/.

[13] REIMPELL, Jörnsen; STOLL, Helmut a BETZLER, Jürgen, 2001. *The Automotive Chassis: Engineering Principles*. 2nd ed. Oxford: Reed Educational and Professional Publishing. ISBN 0-7506-5054-0.

[14] *Milliken Research Associates, Inc. -- FSAE Tire Test Consortium*, c2001-2024. Online. Milliken Research Associates, Inc. -- FSAE Tire Test Consortium. Dostupné z: https://www.millikenresearch.com/fsaettc.html. [cit. 2024-03-21].

[15] *[Pedal assembly of Dragon e3]*, 2023. Online. In: Fsczech. Dostupné z: https://photos.smugmug.com/Photo/2023/Wednesday/i-5CsxBjg/0/DGL6rzZgBWmBhGr2K8dRLbDh9PRc3DNZDDTc79KzX/X5/09_145148_DSCF1863-X5.jpg. [cit. 2024-03-26].

[16] *VN-300 User Manual: Inertial Navigation Modules*, 2017. 2.22.

[17] *Dragon e3 Design Book*, 2023. Online. Brno.

[18] ŠIMANSKÝ, Sebastian, 2024. *Implementace Torque Vectoring na monopost Formule Student*. Diplomová práce. Brno, Česká Republika: Vysoké Učení Technické v Brně.

[19] RAJAMANI, Rajesh, 2006. *Vehicle Dynamics and Control*. 233 Spring Street, New York, NY 10013, USA: Springer. ISBN 0-387-26396-9.

[20] *CarMaker / TruckMaker / MotorcycleMaker for Simulink*, c2024. Online. MathWorks - Makers of MATLAB and Simulink. Dostupné z: https://www.mathworks.com/products/connections/product_detail/carmaker.html. [cit. 2024-05-23].

[21] *Dragon e3 Design Book: Chassis – Torsional stiffness validation*, 2023. Online. Brno.

[22] *Dragon e3 Design Book: Suspension – Elastokinematics measurement*, 2023. Online. Brno.

[23] GADAS, Petr, 2021. *Měření flexibility komponent podvozku vozidla*. Online, Bakalářská práce, vedoucí Jiří Míša. Brno, Česká Republika: Vysoké Učení Technické v Brně. Dostupné z: https://www.vutbr.cz/studenti/zav-prace/detail/131846. [cit. 2024-05-22].

[24] *Aeromaps*, 2023. Online. Brno.

[25] PORTEŠ, Petr. *QDY: Dynamika vozidel - P03_Vykon*. Online. Brno.

[26] *Contelec_vert_x_13e3_736_221_202_eng_tds*, c2024. Online. Distrelec Česká republika - Distributor Elektronických Komponentú. Dostupné z: https://media.distrelec.com/Web/Downloads/27/71/contelec_vert_x_13e3_736_221_202_eng_tds.pdf. [cit. 2024-05-23].

[27] *FS-Rules 2024 v1.1.pdf*, 2024. Online. In: FSG: Rules & Documents. Dostupné z: https://www.formulastudent.de/fileadmin/user_upload/all/2024/rules/FS-Rules_2024_v1.1.pdf. [cit. 2024-05-24].

ABBREVIATIONS AND SYMBOLS

δ	[rad]	Wheel angle
R	[m]	Turn radius
b	[m]	Distance from the CoG to the front wheel centre
c	[m]	Distance from the CoG to the rear wheel centre
L	[m]	Wheelbase
β	[rad]	Chassis slip angle
v_y	[m·s^{-1}]	Lateral velocity
v_x	[m·s^{-1}]	Longitudinal velocity
V	[m·s^{-1}]	Overall vehicle velocity
α	[rad]	Slip angle
α_F	[rad]	Front tire slip angle
α_R	[rad]	Rear tire slip angle
F_{yF}	[N]	Front lateral force
F_{yR}	[N]	Rear lateral force
r	[rad·s^{-1}]	Yaw rate
C_α	[N/deg]	Tire cornering stiffness
M_z	[N·m]	Yaw moment
F_y	[N]	Lateral force
I_{zz}	[kg·m^{-2}]	Yaw moment inertia
$\dot{r}$	[rad·s^{-2}]	Yaw acceleration
δ_A	[rad]	Ackermann angle
m	[Kg]	Mass
g	[m·s^{-2}]	Gravitational acceleration
F_{zF}	[N]	Front vertical force
F_{zR}	[N]	Rear vertical force
C_F	[N/deg]	Front cornering stiffness
C_R	[N/deg]	Rear cornering stiffness
K	[-]	Understeer gradient
a_y	[m·s^{-2}]	Lateral acceleration
T_W	[N·m]	Wheel torque
F_x	[N]	Longitudinal force
I_w	[kg·m^{-2}]	Wheel moment of inertia

α_w	[rad·s^{-2}]	Wheel angular acceleration
F_{xR}	[N]	Right-wheel longitudinal force
F_{xL}	[N]	Left-wheel longitudinal force
F_{yFR}	[N]	Front right-wheel lateral force
F_{yFL}	[N·m]	Front left-wheel lateral force
M_{TV}	[N·m]	Yaw moment from torque vectoring
$\dot{r}_{TV}$	[rad·s^{-2}]	Yaw acceleration induced by torque vectoring
n	[-]	Numbering
t	[s]	time
SWA	[rad]	Steering wheel angle
r_w	[m]	Wheel radius